Article

Efficient Gene Transfection by Electroporation—In Vitro and In Silico Study of Pulse Parameters

Tjaša Potočnik [ID], Shaurya Sachdev [ID], Tamara Polajžer, Alenka Maček Lebar [ID] and Damijan Miklavčič *[ID]

Faculty of Electrical Engineering, University of Ljubljana, Tržaška 25, 1000 Ljubljana, Slovenia
* Correspondence: damijan.miklavcic@fe.uni-lj.si

Abstract: Gene electrotransfer (GET) is a widely used method for nucleic acids' delivery into cells. We explored, evaluated, and demonstrated the potential use of different pulse durations for introducing plasmid DNA (pDNA) into cells in vitro and compared the efficiency and dynamics of transgene expression after GET. We performed experiments on cell suspensions of 1306 fibroblasts and C2C12 myoblasts with four ranges of pulse durations (nanosecond, high frequency bipolar (HF-BP), and micro- and millisecond). Six different concentrations of pDNA encoding green fluorescent protein were used. We show that GET can be achieved with nanosecond pulses with a low pulse repetition rate (10 Hz). The GET's efficiency depends on the pDNA concentration and cell line. Time dynamics of transgene expression are comparable between millisecond, microsecond, HF-BP, and nanosecond pulses but depend greatly on cell line. Lastly, based on the data obtained in the experiments of pDNA concentration effect on GET the model of the probability of pDNA and cell membrane contact during GET was developed. The model shows that pDNA migration is dominated by diffusion for nanosecond and HF-BP pulses and by electrophoresis for micro- and millisecond pulses. Modeling results can provide valuable guidance for further experiments and interpretations of the results obtained by various pulse protocols.

Keywords: gene electrotransfer; nanosecond pulses; high frequency bipolar pulses; electroporation; plasmid DNA

1. Introduction

Gene electrotransfer (GET), or gene transfection by electroporation, is a widely used method for nucleic acids' delivery into cells based on the phenomenon of electroporation where electric pulses cause temporarily increased cell membrane permeability [1]. GET has been shown to markedly enhance the efficiency of naked plasmid DNA (pDNA) transfer, and has been widely used to introduce nucleic acids into various types of cells in vitro, ex vivo, and in vivo [1,2].

In clinical settings, GET is also considered as a promising method for the delivery of CRISPR/Cas9 gene editing complexes [3]. GET can also be used for vaccination against infectious diseases, with a DNA vaccine currently being developed for vaccination against COVID-19 [4–6]. In oncology, GET is used for the treatment of and vaccination against various cancers [7–10]. GET can also be used for ex vivo genetic engineering. More and more treatments against cancers are based on the ex vivo genetic engineering of T cells to express chimeric antigen receptors (CARs), which bind tumor antigens or tumor-associated antigens in a human leukocyte antigen (HLA)-independent manner [11]. Viral vectors are effective for the genetic engineering of human primary cells but have serious limitations such as high manufacturing cost, long production timelines, and genotoxic risks derived from their semi-random chromosomal integration profiles [12]. In contrast to viral vectors, GET has become the simplest and most appealing nonviral deliver technology with its ability to introduce diverse biomolecules to millions of cells per treatment. The limitation

of most electroporation protocols used for cell therapy is, however, the low transfection efficiency and cell death [13].

The efficiency of GET can be measured in different ways and may depend on the GET application, most often as percentage of transfected cells (referred as GET in our paper), which gives information about the percentage of cells that were successfully transfected among the cells that survived the treatment [14]. This could be useful in applications where cells which can rapidly multiply are used, such as bacteria. For applications of GET in gene therapy, it may be crucial that the majority of cells survive the treatment. In this case, it is important that the results of GET efficiency also include cell survival. GET efficiency representing the percentage of transfected cells based on the number of cells that were exposed to electric pulses is referred to as the overall GET in the paper [15]. Furthermore, GET efficiency, if cells are transfected with fluorescent proteins, can be measured with median fluorescence intensity (MFI), representing the quantity of produced transfected protein [16]. This is important in applications where the goal is the production of high levels of therapeutic proteins such as in DNA vaccination. In this paper, we present results of GET in vitro using all three types of GET efficiency determination, namely, GET, MFI, and overall GET.

In GET applications, pulse parameters (amplitude, duration, repetition frequency, and number) are usually varied to achieve cell membrane permeabilization and at the same time prevent excessive cell damage [17]. The choice of appropriate parameters of electric pulses is one of the most relevant steps of GET. GET can be applied equally to all cell types and at all stages of the cell cycle, but GET efficiency depends on and varies greatly between different cell types. The origins of these differences are not yet well understood. Generally smaller cells require a higher electric field to permeabilize their cell membrane. This is an important consideration for ex vivo gene delivery, especially to hematopoietic cells. Electroporation thresholds for different cells in a heterogeneous tissue thus vary [18,19].

Currently, gene transfer by electroporation is believed to rely on cell membrane permeabilization and electrophoresis of pDNA during pulse delivery. Electrophoresis, which is present during electric field delivery, acts on negatively charged pDNA molecules and enables a higher number of pDNA molecules to come in contact with the cell membrane than would do so solely by diffusion [20]. Small molecules (equal to or smaller than 15 bp [21]) can enter the cell with electrophoresis; however, large pDNA molecules form aggregates on cell membrane during electric field delivery, which later enter the cell with endocytosis [1,22–24]. Because of its role in the formation of pDNA aggregates during electric field delivery, the lack of electrophoresis could represent an important weakness for the use of short pulses in GET [25,26]. The presence of electrophoretic migration of pDNA is the reason why, usually, long millisecond pulses are used for GET. Although leading to efficient GET, these pulses are associated with triggering muscle contractions, pH changes, and electrolysis at the electrode electrolyte interface causing electrochemical reactions [27–33].

Recently suggested high-frequency bipolar pulses (HF-BP), first predominantly used for irreversible electroporation applications–HFIRE [34]—were demonstrated to also enable GET in vitro [15]. One of the characteristics of HF-BP pulses are reduced electrochemical reactions and less metal ions released from the electrodes compared to longer pulses [29,35]. Furthermore, HF-BP pulses induce less muscle contractions and pain during pulse delivery [36–39].

In addition, nanosecond pulses have already been used for GET. When applying 200 ns pulses (10–18 kV/cm) in bursts of ten with a varied pulse repetition rate (up to 1 MHz), it was shown that with the increase in the pulse repetition rate from 100 kHz to 1 MHz, GET increased, resulting in up to 17% GET with a minimal decrease in cell survival [40]. Furthermore, it was shown that with 100×300 ns pulses delivered at 1 MHz and at 5 kV/cm, up to 40% GET can be achieved, which is comparable to an efficiency of 4×100 µs, 1 Hz, 1.5 kV/cm pulse protocol [41].

Interestingly, nanosecond pulses have been suggested to disrupt nuclear envelope which could facilitate delivery of pDNA to the nucleus and thus increase GET [42–44]. Several papers have described using different combinations of nanosecond and milli- or microsecond pulses with the attempt to improve GET. Firstly, it was shown that GET could be increased about four times when cells were exposed to 3.5 ms pulse with 0.3 kV/cm followed by 60 ns pulse at 60 kV/cm after 30 min [45]. However, these results were not reproduced successfully. Later, no effects of nanosecond pulses on GET were observed by applying 8 × 5 ms or 4 × 200 µs pulses delivered at 1 Hz followed by 10, 12, or 15 ns pulses delivered at 10 Hz [46]. However, when the order of pulse delivery was reversed, a more pronounced effect of nanosecond pulses on GET was observed. Using the electroporation approach with a combination of nanosecond (600 ns, 100 kHz, 50 kV/cm) followed immediately by millisecond pulses (1 × 10 ms, 500 V/cm) more than doubled transgene expression; at the same time, cell survival levels were similar as in standard millisecond electroporation [42]. The combination of nanosecond pulses (23 × 60 ns, 1 Hz, 24 kV/cm) and millisecond electric pulses (1 × 5 ms, 50 V) led to a 40-fold increase in GET if nanosecond pulses were applied first followed by millisecond pulse, but not in the reverse order. This effect of nanosecond pulses was time restricted, with the highest efficiency occurring when nanosecond pulses were delivered 5 min before millisecond pulses [47].

Nanosecond pulses can potentially offer a solution to limitations that are present in GET with longer milli- and microsecond pulses. Namely, some cells exposed to GET may lose viability due to excessive heat, pH changes, and ionic imbalance [3]. Nanosecond pulses decrease electrochemical reactions during pulse delivery and in in vivo settings offer more patient-friendly treatment, with reduced muscle contractions [40,48]. Heating is also decreased during nanosecond pulses application, which lowers the thermal effects of treatment [48,49]. Nanosecond pulses widen the use of electroporation while also having an effect on intracellular structures. It has been shown that nanosecond pulses can penetrate the cell interior and permeabilize membranes of internal organelles, such as endosomal vesicles, endoplasmic reticulum, nuclear envelope, and cytoskeleton, leading to the disruption of intracellular vesicles, release of calcium from endoplasmic reticulum, and immediate and prolonged loss of mitochondrial membrane potential [44,50–54]. Successful GET with shorter (i.e., less than 10 µs) pulses in vitro is, however, mostly achieved with high pDNA concentrations, which might be challenging to reach in in vivo settings, at least over a larger volume [2].

Conventional GET, using micro- to millisecond-long pulses, generally relies on electrophoresis to bring the pDNA molecules to the cell membrane for successful transfection [55]. However, for nanosecond duration pulses, electric field/electrophoresis might not be present for sufficient time to ensure a pDNA cell membrane contact. Even with HF-BP pulses, net electrophoretic movement is balanced out due to the bipolar nature of pulses. For these pulses (nanosecond and HF-BP), pDNA molecules then have to rely on diffusion to reach the cell membrane. Moreover, there is only a limited window of time during which the cell membrane is permeable and competent enough to absorb pDNA molecules for successful GET [1,56]. Therefore, depending on how far the pDNA molecule is from the cell membrane, or how concentrated the pDNA solution is, the efficiency of GET for the wide variety of pulse durations (nanosecond to millisecond) can be analyzed using the framework of how electrophoresis and diffusion influence the probability of pDNA molecule reaching the permeabilized cell membrane. A theoretical framework based on the drift-diffusion equation of probability density and the one-dimensional Fokker–Planck equation was used in this work to determine such probabilities [57]. A similar probabilistic framework has also been used earlier to evaluate probabilities of successful pDNA translocation through an electropore in the cell membrane, along with its qualitative comparison to experimental GET efficiencies [58], and has also been compared to experimental pDNA translocation efficiencies in model systems [59].

The purpose of this paper is to explore, evaluate, and demonstrate the potential use of different pulses for introducing pDNA into cells in vitro and to compare GET efficiency and dynamics of gene expression after GET. We performed experiments in vitro, on cell suspensions of immortalized human skin fibroblasts 1306 cell line and on C2C12 myoblasts, covering a range of pulse durations from 200 ns to 5 ms, monopolar and the recently used microsecond bipolar, so-called HFIRE pulses. To clarify the role of electrophoresis in the transport of pDNA in the electroporation medium during GET with different durations of electric pulses, we also developed a simple mathematical model that gives the probability of pDNA contact with the cell membrane during GET and compared experimental results with those calculated by the model.

2. Materials and Methods

2.1. Cells

Immortalized human skin fibroblasts 1306 cell line and C2C12 murine skeletal myoblasts cell line, both from European Collection of Authenticated Cell Cultures (cat no. #90011887 and #91031101, respectively) were used. Cells were grown in 25–150 mm^2 culture flasks (TPP, Trasadingen, Switzerland) for 2–4 days in an incubator (Kambič, Semič, Slovenia) at 37 °C, in a humidified atmosphere of 5% CO_2 in air for 1306 cell line and 10% CO_2 in air for C2C12 cell line. 1306 cells were cultured in Eagle's Minimum Essential Medium (EMEM) growth medium (Sigma Aldrich, Darmstadt, Germany) supplemented with 15% fetal bovine serum (Sigma Aldrich, Darmstadt, Germany), L-glutamine (StemCell, Vancouver, BC, Canada), and antibiotics penicillin/streptomycin (PAA, Vienna, Austria) and gentamycin (Sigma Aldrich, Darmstadt, Germany). C2C12 cells were cultured in Dulbecco's Modified Eagle's Medium (DMEM) growth medium (Sigma Aldrich, Darmstadt, Germany) supplemented with 10% fetal bovine serum (Sigma Aldrich, Darmstadt, Germany), L-glutamine (StemCell, Vancouver, BC, Canada), and antibiotics penicillin/streptomycin (PAA, Vienna, Austria) and gentamycin (Sigma Aldrich, Darmstadt, Germany).

For experiments cells in exponential growth phase were trypsinized using trypsin–EDTA; 5 g trypsin/2 g EDTA in 0.9% NaCl (Sigma Aldrich, Darmstadt, Germany) 10 × diluted in Hanks' Balanced Salt solution (Sigma Aldrich, Darmstadt, Germany). From the obtained cell suspension, trypsin and growth medium were removed by centrifugation at 180× *g* for 5 min at room temperature (Sigma 3–15 K, Welwyn Garden City, UK). The cell pellet was then resuspendend in EMEM growth medium for 1306 cell line or DMEM growth medium for the C2C12 cell line to obtain a final cell density of 2×10^6 cells/mL.

2.2. Cell Size Measurement

Cells in suspension were transferred to Lab-Tek chamber and imaged with inverted Thunder Imager Live Cell system. Moreover, 16-bit images were acquired with a deep-cooled 4.2 MP sCMOS Leica DFC9000 Gt fast camera in the Leica Application Suite X (LAS X) software. Cell diameter was measured using the ImageJ software (accessed on 10 May 2022, http://imagej.nih.gov/ij/). For each cell line 20 cells were measured. Results are presented as mean ± standard deviation. Measured diameters were used in calculating the pDNA to membrane distance.

2.3. Nanosecond Pulses

Pulses of 200 ns or 500 ns duration were delivered by CellFX System electroporator (Pulse Biosciences, Hayward, CA, USA). The electric field strength (E) was calculated from the voltage measured by 1 kΩ resistor and Pearson current monitor model 2877 (1 V/1 A, 200 MHz) (Pearson Electronics, Palo Alto, CA, USA) during the experiment divided by the distance between the electrodes. We also measured the current during each pulse by Pearson current monitor model 2878 (1 V/10 A, 70 MHz) (Pearson Electronics, Palo Alto, CA, USA). Voltage and current measurements were monitored by the oscilloscope WaveSurfer 3024Z, 200 MHz (Teledyne LeCroy, Chestnut Ridge, NY, USA). 25, 100, or

300 pulses were delivered with 5 or 10 Hz pulse repetition frequency at electric field range of 0–19 kV/cm.

2.4. High Frequency Bipolar Pulses

For the delivery of 2 μs high-frequency bipolar pulses, a prototype high-frequency pulse generator L-POR was used (mPOR, Ljubljana, Slovenia). The L-POR electroporator is intended for laboratory use. It enables the generation of high-frequency symmetric and asymmetric bipolar electroporation pulses up to 1400 V and duration of pulses from 500 ns with a pulse repetition rate of up to 1 MHz. It also enables the generation of pulses in bursts. The pulses delivered were monitored by a high-voltage differential probe HVD3605A (Teledyne LeCroy, Chestnut Ridge, NY, USA), current probe CP031 (Teledyne LeCroy, Chestnut Ridge, NY, USA) and HDO6000 High-Definition oscilloscope (Teledyne LeCroy, Chestnut Ridge, NY, USA). In HF-BP pulse protocol, bipolar pulses of 2 μs duration of positive and negative phase were applied. The pause between positive and negative pulse phase and pause between bipolar pulses were 2 μs. 100 bursts were applied, and in each burst, 32 pulses were delivered. Burst repetition rate was 1 Hz [15]. We tested electric field range 0–2.5 kV/cm.

2.5. Micro and Millisecond Pulses

Monopolar rectangular pulses of 100 μs or 5 ms duration were delivered with a laboratory prototype pulse generator (University of Ljubljana), based on H-bridge digital amplifier with 1 kV MOSFETs (DE275-102N06A, IXYS, Milpitas, CA, USA) [60]. Pulse delivery was monitored by the oscilloscope WaveSurfer 422, 200 MHz with high-voltage differential voltage probe ADP305 and current probe CP030 (Teledyne LeCroy, Chestnut Ridge, NY, USA). For microsecond pulses, eight 100 μs pulses with electric fields 0–2 kV/cm and for millisecond pulses eight 5 ms pulses with electric fields 0–1.25 kV/cm were tested.

2.6. Permeabilization

Cell membrane permeabilization of 1306 and C2C12 cells in suspension was expressed as percentage of propidium iodide (PI) fluorescent cells. First, 5 μL of 1.5 mM PI was added to 200 μL of cells in growth medium at concentration 2×10^6 cells/mL in electroporation cuvette with 2 mm gap (VWR International, Radnor, PA, USA). Emission of PI fluorescence was detected by flow cytometry (Attune NxT, Carlsbad, CA, USA) using a blue laser excitation at 488 nm and detecting the emitted fluorescence through a 574/26 nm band-pass filter, 3 min after exposure of cells to electric pulses. Data for percentage of permeabilized cells and their median fluorescence intensity were collected. At every measurement 10,000 events were recorded. Data obtained were analyzed with the Attune NxT software (version 3.1.2).

2.7. Temperature Measurement during Pulse Delivery

The temperature of the cell sample was monitored during pulse delivery for all five pulse protocols and for both cell lines. The fiber optic sensor system (opSens, Québec, QC, Canada), which consisted of ProSens signal conditioner and a fiber optic temperature sensor OTG-M170, was used. The fiber optic sensor was carefully placed in the cell suspension in the middle of the gap between the electrodes in the cuvette. Sampling frequency was 1000 Hz. Two measurements were taken for each of the five pulse protocols and for both cell lines.

2.8. Cell Survival after Permeabilization

For cell survival experiments, 200 μL of cells in suspension in growth medium at concentration 2×10^6 cells/mL was pipetted in a 2 mm gap electroporation cuvette (VWR International, Radnor, PA, USA) and exposed to electric pulses. After pulse application, 50 μL of fetal bovine serum (Sigma Aldrich, Darmstadt, Germany) was added to cell suspension. Cells were incubated for 5 min at 37 °C [61]; afterwards, 1×10^4 C2C12

myoblasts or 2×10^4 1306 fibroblasts from cuvette were seeded in 100 μL of growth medium in a 96-well plate (TPP, Trasadingen, Switzerland). Cells were seeded in triplicates. The plate was then incubated for 24 h (37 °C, 10% CO_2 for C2C12 and 37 °C, 5% CO_2 for 1306). Cell survival was determined with the MTS-based Cell Titer 96 AQueous One Solution Cell Proliferation Assay (Promega, Madison, WI, USA). After incubation, 20 μL of MTS reagent were added to each well and cells were incubated for additional 2 h in the incubator (37 °C, 10% CO_2 for C2C12 and 37 °C, 5% CO_2 for 1306). Absorption at 490 nm wavelength was measured with a Tecan Infinite M200 spectrophotometer (Tecan, Männedorf, Switzerland). An average absorption obtained in the samples containing only growth medium was subtracted from the absorption measured in cell samples. To calculate the percentage of viable cells the absorption of each cell sample was divided by an average absorption of the control cell samples, where cells were treated as described but not exposed to electric pulses.

2.9. Plasmids

A 4.7 kb plasmid pEGFP-N1 (Clontech Laboratories Inc., Mountain View, CA, USA) and a 3.5 kb plasmid pmaxGFP (Lonza, Basel, Switzerland) both encoding green fluorescent protein (GFP) under the control of CMV promotor were used. pDNA was amplified using Escherichia coli and isolated with HiSpeed Plasmid Maxi Kit (Qiagen, Hilden, Germany). pDNA concentration was spectrophotometrically determined at 260 nm. We tested six different pDNA concentrations, namely, 40, 60, 80, 100, 250, and 500 μg/mL.

2.10. Gene Electrotransfer and Cell Survival after Gene Electrotransfer

A volume of 200 μL of cell suspension with different concentrations of pDNA was exposed to electric pulses in electroporation cuvettes with a 2 mm gap (VWR International, Radnor, PA, USA). After pulse delivery, 50 μL of fetal bovine serum (Sigma Aldrich, Darmstadt, Germany) was added to each cuvette, and cells were incubated 5 min at 37 °C [61,62]. After incubation, 1×10^5 1306 cells and 5×10^4 C2C12 cells from cuvette were transferred to a 24-well plate (TPP, Trasadingen, Switzerland) and seeded in growth medium for gene electrotransfer determination. From the rest of the cell sample in cuvette, 1×10^4 C2C12 myoblasts or 2×10^4 1306 fibroblasts were seeded in triplicates in 100 μL of growth medium in a 96-well plate (TPP, Trasadingen, Switzerland) to determine cell survival. Both plates were incubated for 24 h (37 °C, 10% CO_2 for C2C12 and 37 °C, 5% CO_2 for 1306).

After incubation, cells in 24-well plates were trypsinized and resuspended in 200 μL of PBS. Percentage of GFP-positive cells and median fluorescence intensity (MFI) of GFP-positive cells were detected using flow cytometer (Attune NxT, Carlsbad, CA, USA) with a blue laser at 488 nm and a 530/30 nm bandpass filter. At every measurement, 10,000 events were recorded. Data obtained were analyzed with the Attune NxT software (version 3.1.2).

Cell survival was determined with the MTS-based Cell Titer 96 AQueous One Solution Cell Proliferation Assay (Promega, Madison, WI, USA). After incubation, 20 μL of MTS reagent was added to each well, and cells were incubated for an additional 2 h in the incubator (37 °C, 10% CO_2 for C2C12 and 37 °C, 5% CO_2 for 1306). Absorption at 490 nm wavelength was measured with a Tecan Infinite M200 spectrophotometer (Tecan, Switzerland). An average absorption obtained in the samples containing only growth medium was subtracted from the absorption measured in cell samples. To calculate the percentage of viable cells the absorption of each sample was divided by an average absorption of the control samples.

2.11. Overall Gene Electrotransfer

When reporting GET efficiency, we distinguish between percentage of transfected cells among cells that survived the treatment and overall gene electrotransfer (overall GET), which represents the percentage of transfected cells relative to the initial population, which

considers both the efficiency of transfection and cell survival. Overall, GET was calculated as: overall GET (%) = GET (%) × cell survival (%)/100.

2.12. The Time Dynamics of Transgene Expression

Cells were electrotransfected with 500 µg/mL of pEGFP-N1 plasmid as described in point gene electrotransfer and cell survival after gene electrotransfer. After incubation, sample was divided into 14 parts, and cells were seeded in different numbers (1×10^5–5×10^3) to a 24-well plate (TPP, Trasadingen, Switzerland) and placed in the incubator (37 °C, 5% CO_2). For the next 5 days, every 8 h, cells from one well of the 24-well plate (TPP, Trasadingen, Switzerland) were trypsinized and resuspended in 200 µL of PBS and percentage of GFP-positive cells and median fluorescence intensity of GFP-positive cells were detected using flow cytometer (Attune NxT, Carlsbad, CA, USA) with a blue laser at 488 nm and a 530/30 nm bandpass filter. At every measurement 10,000 events were recorded. Data obtained were analyzed with the Attune NxT software (version 3.1.2).

2.13. Statistical Analysis

All results are reported as a mean value of 3 or 4 experiments. The spread of the data is given by standard deviation. The significance between the experimental groups was analyzed in SigmaPlot 11.0 (Systat Software Inc., Chicago, IL, USA) and determined using One-way ANOVA test followed by Tukey's multiple comparison test. Statistically significant difference was assumed at $p < 0.05$.

2.14. Modeling the Probability of pDNA and Cell Membrane Contact during GET

To determine the probability of pDNA and cell membrane contact, the distance of a pDNA molecule from the cell membrane needs to be determined. This pDNA–cell membrane distance depends on the concentration of pDNA. To determine the pDNA–cell membrane distance, we followed [16,55].

The radius of the cell is R_{cell}, and there is a total of N_{cells} in the suspension. The total volume occupied by the cells in suspension is thus $V_{cells} = N_{cells} \cdot \left(\frac{4}{3}\pi R_{cell}^3\right)$. For a solution volume (V_{sol}), the volume space left to be occupied by pDNA molecules is:

$$V_{DNA} = V_{sol} - N_{cells} \cdot \left(\frac{4}{3}\pi R_{cell}^3\right) \tag{1}$$

For pDNA molecules at a concentration (c_{DNA}) and with molecular weight (M_w), the total number of pDNA molecules in the solution is $N_{DNA} = \frac{c_{DNA} \cdot V_{sol} \cdot N_A}{M_w}$, where N_A is the Avogadro's number. Assuming the space available to a single pDNA molecule is defined by a sphere of radius of R_{DNA} (Figure 1), the volume occupied by pDNA molecules in the solution is $V_{DNA} = N_{DNA} \cdot \frac{4}{3}\pi R_{DNA}^3$ or:

$$V_{DNA} = \left(\frac{c_{DNA} \cdot V_{sol} \cdot N_A}{M_w}\right) \cdot \frac{4}{3}\pi R_{DNA}^3 \tag{2}$$

Thus, equating (1) and (2), we obtain $\left(\frac{c_{DNA} \cdot V_{sol} \cdot N_A}{M_w}\right) \cdot \frac{4}{3}\pi R_{DNA}^3 = V_{sol} - N_{cells} \cdot \left(\frac{4}{3}\pi R_{cell}^3\right)$, or the space available to a single pDNA molecule in a sphere, is defined by radius R_{DNA} as follows:

$$R_{DNA} = \left(\frac{1 - \rho_{cell} \cdot \left(\frac{4}{3}\pi R_{cell}^3\right)}{\frac{4}{3}\pi \cdot \left(\frac{c_{DNA} \cdot N_A}{M_w}\right)}\right)^{1/3} \tag{3}$$

where $\rho_{cell} = \frac{N_{cells}}{V_{sol}}$. R_{DNA} was then calculated using Equation (3) for different values of c_{DNA} and is shown in Supplementary Table S1. The following set of parameters were used—cell density (ρ_{cell}) = 2×10^6 cells/mL, molecular weight of pDNA (M_w) = 660 g/mol/bp ×

4700 bp = 3,102,000 g/mol for pEGFP-N1 pDNA, Avogadro's constant (N_A) = 6.023 × 10^{23}, R_{cell}(C2C12) = 8.4 μm, and R_{cell}(1306) = 7.15 μm.
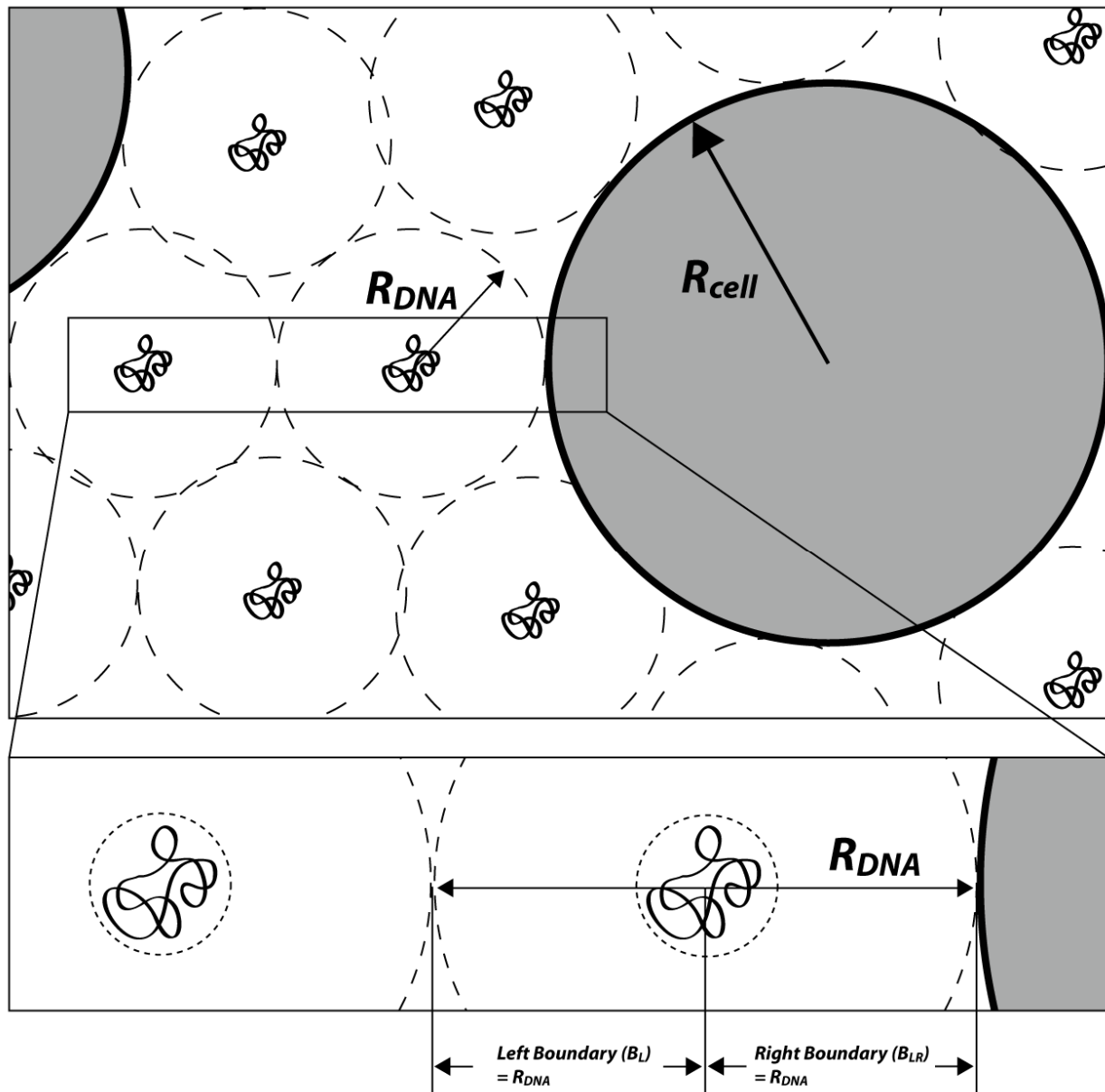

Figure 1. Schematic of distribution of pDNA molecules and cells in suspension. R_{cell} represents the radius of the cell, R_{DNA} represents the radius of the (nominal/free) spherical space available to the pDNA molecule. Subset in figure shows the boundaries within which a pDNA molecule close the cell membrane is allowed to move.

R_{DNA} can be considered as an estimate for the distance between a pDNA molecule and the nearest cell membrane. Furthermore, the boundaries within which a pDNA molecule can move needs to be defined for the model which determines the probability of pDNA molecule coming in contact with the cell membrane. Based on Figure 1, a natural choice for the right boundary (B_R), which constitutes the cell membrane, is R_{DNA}. Since R_{DNA} is the radius of spherical space available to the pDNA in the solution, the left boundary (B_L) is also considered as R_{DNA}. Other estimates of B_L and B_R can be considered, such as R_{DNA}, $R_{DNA} - R_g$ and $2R_{DNA} - 2R_g$, where R_g is the radius of gyration of the pDNA molecule. These are explained in the Supplementary Figure S1.

To determine the probability that a pDNA molecule reaches the permeabilized cell membrane, we assume a 1D case where a pDNA molecule can only move along the one axis (direction of applied electric field) bounded by the left and the right boundaries (Figure 2). The fundamental contribution of electrophoresis and diffusion to the probability of a pDNA molecule reaching the permeabilized cell membrane can be captured in 1D (in the direction of the electric field). We expect that the addition of extra dimensions will not contribute significantly to a more detailed picture of the process with the probabilistic framework described below.
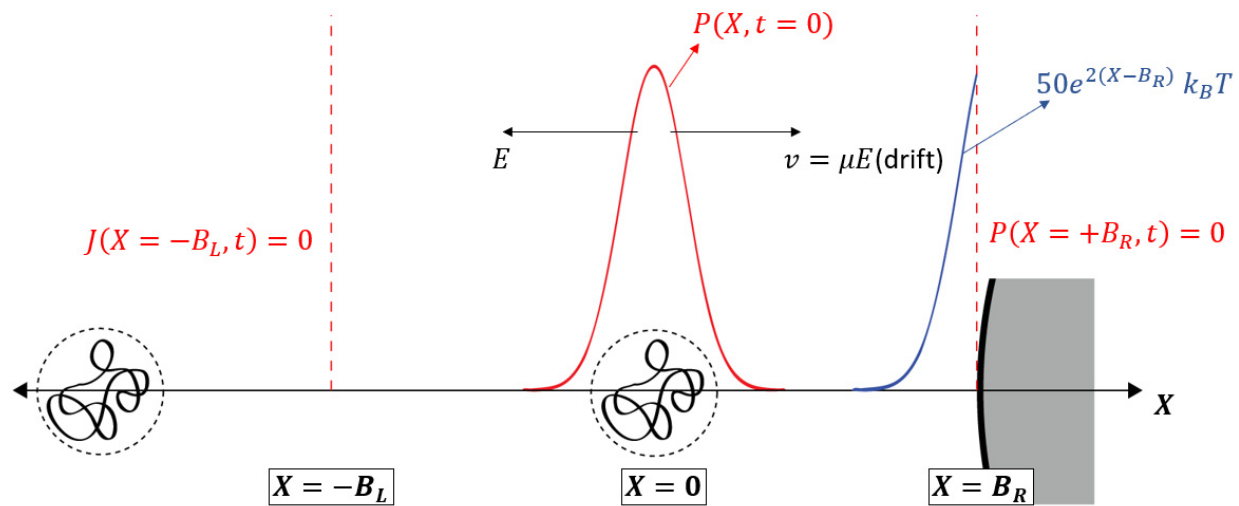

Figure 2. Schematic of the biased random walk of pDNA molecule along the X-axis due to drift (electrophoresis), diffusion, and a free energy barrier. Electric field acts along the negative X-axis, which creates a drift in the pDNA molecule along the positive X-axis. The pDNA molecule is initially centered at $X = 0$ with the initial condition defined by a narrow-band Gaussian distribution. The boundary conditions at the right ($X = +B_R$) and left ($X = -B_L$) of the domain are the absorbing and reflecting boundary conditions, respectively. A free energy barrier between the pDNA molecule and the cell membrane is present at the right boundary ($X = +B_R$).

The simplicity of such a 1D assumption enhances the pedagogical aspect of inferring the role of diffusion and electrophoresis in bringing the pDNA molecule to the permeabilized membrane (a prerequisite for GET) for a wide variety of experimental conditions used (e.g., pulse durations ranging from nanosecond to millisecond and concentrations ranging from 40 µg/mL to 500 µg/mL). The purpose of the model is not an estimation and/or prediction of experimental outcomes such as GET efficiency or MFI.

The probability density ($P(X,t)$) of finding the pDNA molecule at particular location along the X-axis at time t can be described using the following drift–diffusion equation of probability density [57]:

$$\frac{\partial P(X,t)}{\partial t} = -v\frac{\partial P(X,t)}{\partial X} + D\frac{\partial^2 P(X,t)}{\partial X^2} \tag{4}$$

Equation (4) does not assume any interaction between the pDNA molecule and the cell membrane. However, a pDNA and cell membrane interaction free energy $F(X)$ can be assumed between the pDNA molecule and the cell membrane. In this case, the probability density of finding a particle at a particular location along the X-axis at time t can be described using the one-dimensional Fokker–Planck equation [57]:

$$\frac{\partial P(X,t)}{\partial t} = \frac{D}{k_B T}\frac{\partial}{\partial X}\left[\frac{\partial F(X)}{\partial X}P(X,t)\right] - v\frac{\partial P(X,t)}{\partial X} + D\frac{\partial^2 P(X,t)}{\partial X^2} \tag{5}$$

The free energy barrier $F(X)$ is assumed to be $F(X) = 50e^{2(X-B_R)} k_B T$, i.e., a barrier with a height of 50 $k_B T$ that steeply decays exponentially away from the cell membrane at $X = +B_R$ (Figure 2). Such a barrier is inspired from [63]. The drift term in Equations (4) and (5) is due to the electrophoresis of the pDNA molecule and is given by $v = \mu E$, where μ is the electrophoretic mobility of the pDNA molecule ($\mu = -3.75 \times 10^{-8}$ m^{2}V^{-1}s^{-1}) [59,64,65] and E is the electric field intensity. The diffusion coefficient of pDNA is taken as $D = 10^{-12}$ m^{2}s^{-1} [65]. Equation (4) describes the process of finding pDNA at a particular location along the X-axis as a biased random walk, where the bias is due to electrophoresis of pDNA molecule. Equation (5) describes the same process of finding pDNA at a particular location along the X-axis based on a bias (electrophoresis), diffusion, and free energy interaction (barrier) with the cell membrane. The drift term in Equations (4) and (5) is non-zero only when the electric field pulse is present and is zero otherwise.

Equations (4) and (5) are solved for the probability density function $P(X,t)$ in the domain $X \in [B_L, B_R]$ with appropriate boundary and initial conditions using the pdepe() function in MATLAB® (R2021b). The initial condition for the pDNA molecule is considered as a narrow-band Gaussian/normal distribution with zero mean (centered at $X = 0$, Figure 2) and a standard deviation of 10 nm. The boundary at the right (positive end of the domain), i.e., the cell membrane, is considered an absorbing boundary condition, implying that once pDNA reaches the cell membrane, it is absorbed into the cell membrane, i.e., it is internalized and expressed by the cell. The resulting boundary condition at $X = +B_R$ is thus $P(X = +B_R, t) = 0$. The left boundary is considered to be a reflective barrier, implying that once the pDNA molecule reaches the left boundary, it is reflected back into the domain, i.e., the flux in the probability density function is zero. Flux for Equation (4) is given by $J(X,t) = vP(X,t) - D\frac{\partial P}{\partial X}(X,t)$ and for Equation (5) by $J(X,t) = \frac{D}{k_B T}\left[-\frac{\partial F(X)}{\partial X}\right]P(X,t) + vP(X,t) - D\frac{\partial P}{\partial X}(X,t)$. Thus, the resulting left boundary condition for Equation (4) is $vP(X = -B_L, t) - D\frac{\partial P}{\partial X}(X = -B_L, t) = 0$ and for Equation (5) is $\frac{D}{k_B T}\left[-\frac{\partial F(X=-B_L)}{\partial X}\right]P(X = -B_L, t) + vP(X = -B_L, t) - D\frac{\partial P}{\partial X}(X = -B_L, t) = 0$.

The concentration dependance of the experimental results is modeled by varying the location of the right (B_R) and the left (B_L) boundaries. These boundaries are defined by the free sphereical space (R_{DNA} in Figure 1) available to the pDNA molecule which shrinks or expands depending upon high or low concentration, respectively. Various estimates of R_{DNA} are given in Supplementary Table S1 for different concentrations. Since concentrations in the experiments in the current work vary from 40 μg/mL to 500 μg/mL, $B_L, B_R = R_{DNA}$ is varied from 312 nm to 134 nm, respectively. However, values of R_{DNA} as small as 77 nm (corresponding to 2500 μg/mL) and as high as 433 nm (corresponding to 15 μg/mL) are also considered to analyse a larger spectrum of concentrations that could be commonly found in GET experiments. It should be noted that boundaries of the domain $X \in [B_L, B_R]$ are defined using $B_L, B_R = R_{DNA}$ (Figure 1), the values for which are given in Supplementary Table S1 for different concentrations. However, other definitions of B_L, B_R can be used (see Figure S1), the values for which are given in Supplementary Table S2. Finally, Equations (4) and (5) are solved for the probability density function $P(X,t)$ in the domain $X \in [B_L, B_R]$.

3. Results

In this paper, different electric pulses were used to introduce pDNA into cells in vitro. We compared GET efficiency and the time dynamics of transgene expression after GET performed by using different pulses. The experiments were performed on cell suspensions of 1306 fibroblasts and on C2C12 myoblasts with a range of pulse durations from 200 ns to 5 ms, monopolar and bipolar pulses. The results are presented as the percentage of transfected cells (GET), quantity of produced transgene measured as median fluorescence intensity (MFI) and as the percentage of transfected cells considering cell survival (overall GET).

We first determined the optimal electric field amplitudes used in GET for each pulse protocol based on permeabilization and survival curves. After determining optimal electric field amplitude, the effect of pDNA concentration on GET, MFI, cell survival, and overall GET was determined. We compared the overall GET and MFI of all pulse durations at the highest pDNA concentration. Furthermore, with a subset of pulses, we explored the effect of different pDNA sizes on GET, MFI, cell survival, and overall GET. We also monitored the time dynamics of pDNA expression after GET with different pulse durations. Lastly, based on the data obtained in the experiments of the pDNA concentration effect on GET, the model of the probability of pDNA and cell membrane contact during GET was developed. The model was compared to GET efficiency using different pulse durations, with the aim to determine the importance of diffusive and electrophoretic movement of pDNA.

3.1. Determining Optimal Electric Field Amplitude for GET

In order to determine the optimal parameters for GET (intersections of permeabilization and survival curves) for C2C12 myoblast and 1306 fibroblast cell lines, we varied the nanosecond pulse parameters—pulse duration: 200 or 500 ns; pulse number: 25, 100, or 300 pulses; pulse repetition frequency: 5 or 10 Hz, and delivered electric field: 0–19 kV/cm.

In both cell lines, C2C12 myoblasts and 1306 fibroblasts, we achieved >90% cell membrane permeabilization, with different pulse durations of 200 ns and 500 ns and different tested pulse numbers, 25, 100, and 300 pulses (Supplementary Figures S2 and S3). No significant difference in permeabilization, survival, and PI MFI curves was observed when changing pulse repetition frequency (5 or 10 Hz) for 200 ns and 500 ns pulses for all three pulse numbers tested in C2C12 myoblasts (data not shown). Based on this, we decided to use only a 10 Hz pulse repetition frequency for experiments with 1306 fibroblasts.

Intersections of permeabilization and survival curves were observed at similar electric fields for C2C12 myoblasts and 1306 fibroblasts, except for 25 × 200 ns pulses, where the intersection of permeabilization and survival curves was observed at a lower electric field in 1306 cells—12–14 kV/cm compared to 15–18 kV/cm for C2C12 myoblasts (Supplementary Figure S2). Since cell size can influence the permeabilization threshold, we measured the diameters of cells in suspension, which were 16.8 ± 1.8 μm for C2C12 myoblasts and 14.3 ± 1.4 μm for 1306 fibroblasts.

A higher MFI of PI-positive cells was observed with 500 ns pulses compared to 200 ns duration pulses; additionally, the MFI increased with the increasing number of pulses from 25 to 300 in both pulse durations tested. Comparing MFI between C2C12 myoblasts and 1306 fibroblasts, lower MFI was observed in 1306 fibroblasts with both 200 ns and 500 ns pulses but only at high electric field amplitudes (Supplementary Figure S4).

The HF-BP pulse protocol consisted of bipolar pulses of 2 μs duration of positive and negative phase, 2 μs pause between positive and negative pulse phase, and pause between bipolar pulses. We applied 100 bursts, each containing 32 pulses. The burst repetition rate was 1 Hz, and the applied electric field was 0–2.5 kV/cm. For microsecond pulses we delivered: 8 × 100 μs, 1 Hz pulse repetition frequency, with the applied electric filed, 0–2 kV/cm and for millisecond pulses; 8 × 5 ms, 1 Hz pulse repetition frequency and applied electric filed, 0–1.25 kV/cm.

Permeabilization and survival curves for HF-BP pulse protocol behave similarly as permeabilization and survival curves of 8 × 100 μs pulse protocol for both cell lines. Permeabilization was achieved at lower values of electric field for 8 × 5 ms compared to 8 × 100 μs pulse protocol and survival deceased at lower values of electric field for 8 × 5 ms compared to 8 × 100 μs pulse protocol in both cell lines. MFI of permeabilized cells was higher at lower values of electric field when longer millisecond pulses were applied. Similarly, as for nanosecond pulses permeabilization, the MFI of permeabilized cells with a high electric field with HF-BP, micro-, and millisecond pulses was lower in 1306 cells compared to C2C12 myoblasts (Supplementary Figures S5 and S6).

After the initial parameters were determined, based on the permeabilization and survival curve, further optimization for every pulse protocol was performed. Performing

GET, we tested three different electric field amplitudes in the range of slightly below to slightly above the intersection of permeabilization and survival curve to determine the electric field at which the overall GET was the best (data not shown). Pulse protocols with chosen electric fields used to determine the effect of pDNA concentration and the time dynamics of transgene expression are given Table 1.

Table 1. Pulse protocols used to determine the effect of pDNA concentration.

C2C12 (16.8 ± 1.8 μm)	1306 (14.3 ± 1.4 μm)
25 × 200 ns, 10 Hz, 15.8 kV/cm	25 × 200 ns, 10 Hz, 12.8 kV/cm
100 × 500 ns, 10 Hz, 4.1 kV/cm	25 × 500 ns, 10 Hz, 6.5 kV/cm
2-2-2-2, 32 p, 100 b, 1 Hz, 1.25 kV/cm	2-2-2-2, 32 p, 100 b, 1 Hz, 1 kV/cm
8 × 100 μs, 1 Hz, 1.25 kV/cm	8 × 100 μs, 1 Hz, 1.25 kV/cm
8 × 5 ms, 1 Hz, 0.4 kV/cm	8 × 5 ms, 1 Hz, 0.6 kV/cm

For each cell line, only one 200 ns and one 500 ns pulse protocol were used to determine the effect of the pDNA concentration on GET. We chose pulse protocols with which the best overall GET of 500 μg/mL of pEGFP-N1 was obtained (Table 1).

3.2. Effect of pDNA Concentration on GET, MFI, Cell Survival, and Overall GET

In determining the effect of pDNA concentration on GET, MFI, cell survival, and overall GET, six different concentrations of pEGFP-N1 were tested, namely, 0, 40, 80, 100, 250, and 500 μg/mL.

The GET in C2C12 myotubes was significantly higher with HF-BP, 8 × 100 μs, and 8 × 5 ms pulses compared to nanosecond pulses for all pDNA concentrations tested (Figure 3A). Interestingly, in 1306 fibroblasts, the GET was higher with HF-BP, 8 × 100 μs, and 8 × 5 ms pulses compared to nanosecond pulses up to 250 μg/mL of pDNA. However, at the highest pDNA concentration in 1306 fibroblast, there were no significant differences in the GET between all pulse protocols (Figure 3C).

The effect of the pDNA concentration on GET depends on the cell line. However, the efficiency of nanosecond pulses depends more on the pDNA concentration compared to HF-BP, 8 × 100 μs, and 8 × 5 ms pulses in both cell lines.

The MFI of cells is indicative of how many pDNA copies were successfully transcribed and translated into fluorescent protein. The MFI of GFP-positive cells was higher in 1306 fibroblasts at all pDNA concentrations when compared to C2C12 myoblasts for all pulse protocols. The MFI of C2C12 myoblast was the highest with 8 × 5 ms pulse protocol followed by 8 × 100 μs, HF-BP, and the lowest with nanosecond pulse protocols. Interestingly, the MFI of C2C12 myoblasts slowly increased up to 250 μg/mL of pDNA and then reached a plateau. For pulse protocols 8 × 5 ms and 8 × 100 μs, there was a small increase in MFI from 250 μg/mL to 500 μg/mL pDNA concentration, but not statistically significant (Figure 3B).

Similarly, MFI of 1306 fibroblasts was also different compared to C2C12 myoblasts. At the highest pDNA concentration, the MFI of 1306 fibroblasts was the highest with the 8 × 100 μs pulse protocol followed by the nanosecond, HF-BP, and 8 × 5 ms pulse protocols. The MFI after the HF-BP and 8 × 5 ms pulse protocols increased gradually with increasing pDNA concentration. With the 8 × 100 μs pulse protocol, a significant increase was observed between 100 μg/mL and 250 μg/mL pDNA concentration. Interestingly, the MFI of 1306 fibroblasts increased significantly from 250 μg/mL to of 500 μg/mL pDNA concentration with both 200 ns and 500 ns pulse protocols (Figure 3D). The MFI of GFP-positive cells is cell-line-dependent and increases with increasing pDNA concentration.
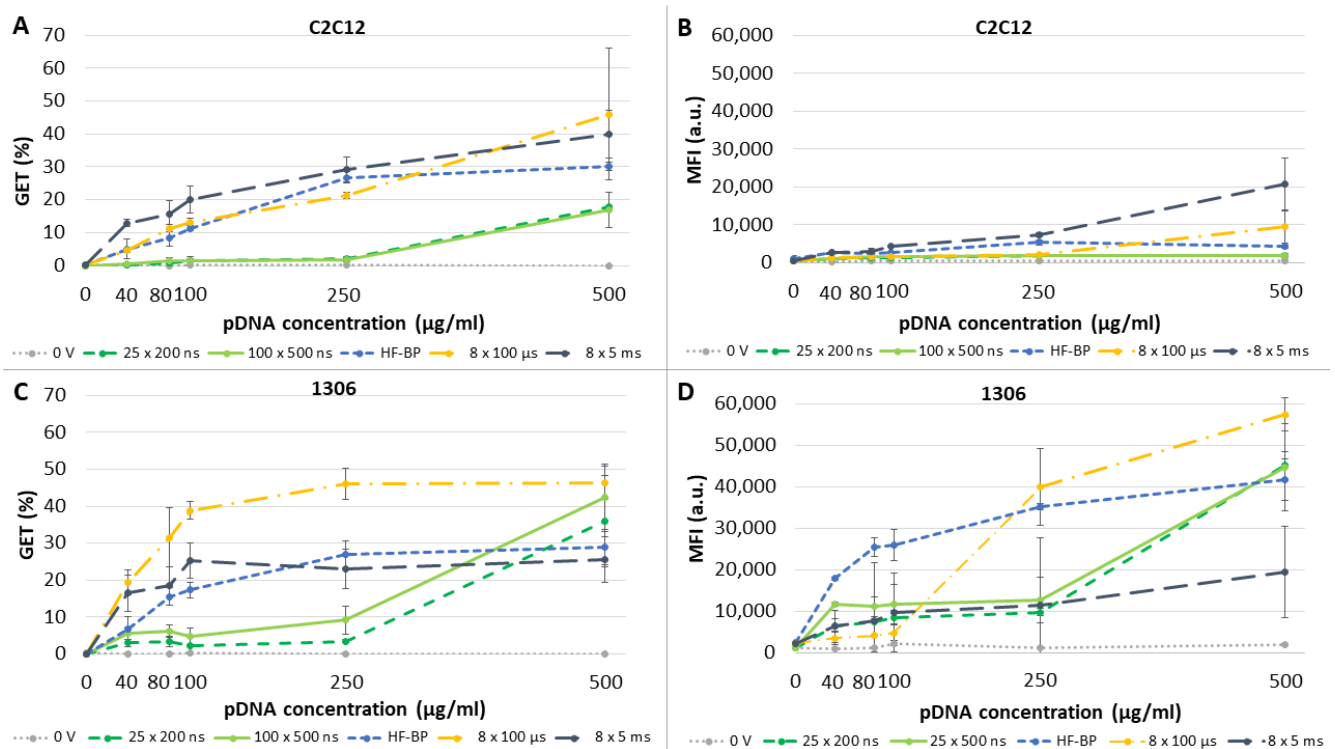
Figure 3. GET and median fluorescence intensity (MFI) of GFP-positive cells with different concentrations of pEGFP-N1 pDNA. (**A**) GET of C2C12 myoblasts, pulses: 25 × 200 ns: 25 × 200 ns, 10 Hz, 15.8 kV/cm; 100 × 500 ns: 100 × 500 ns, 10 Hz, 4.1 kV/cm; HF-BP: 2-2-2-2, 32p, 100b, 1 Hz, 1.25 kV/cm; 8 × 100 µs: 8 × 100 µs, 1 Hz, 1.25 kV/cm; and 8 × 5 ms: 8 × 5 ms, 1 Hz, 0.4 kV/cm. (**B**) MFI of C2C12 myoblasts, pulses: 25 × 200 ns: 25 × 200 ns, 10 Hz, 15.8 kV/cm; 100 × 500 ns: 100 × 500 ns, 10 Hz, 4.1 kV/cm; HF-BP: 2-2-2-2, 32p, 100b, 1 Hz, 1.25 kV/cm; 8 × 100 µs: 8 × 100 µs, 1 Hz, 1.25 kV/cm; and 8 × 5 ms: 8 × 5 ms, 1 Hz, 0.4 kV/cm. (**C**) GET of 1306 fibroblasts, pulses: 25 × 200 ns: 25 × 200 ns, 10 Hz, 12.8 kV/cm; 25 × 500 ns: 25 × 500 ns, 10 Hz, 6.5 kV/cm; HF-BP: 2-2-2-2, 32p, 100b, 1 Hz, 1 kV/cm; 8 × 100 µs: 8 × 100 µs, 1 Hz, 1.25 kV/cm; and 8 × 5 ms: 8 × 5 ms, 1 Hz, 0.6 kV/cm. (**D**) MFI of 1306 fibroblasts, pulses: 25 × 200 ns: 25 × 200 ns, 10 Hz, 12.8 kV/cm; 25 × 500 ns: 25 × 500 ns, 10 Hz, 6.5 kV/cm; HF-BP: 2-2-2-2, 32p, 100b, 1 Hz, 1 kV/cm; 8 × 100 µs: 8 × 100 µs, 1 Hz, 1.25 kV/cm; and 8 × 5 ms: 8 × 5 ms, 1 Hz, 0.6 kV/cm. 0 V represents control where cells were not exposed to electric pulses. Results are represented as an average of 3 repetitions. Statistical differences are given in the text. Bars represent standard deviation.

High concentration of pDNA used for GET was reported to affect cell survival [16]. In our study, however, with 8 × 5 ms pulses, we did not observe any decrease in cell survival with increasing pDNA concentrations compared to cells that were exposed just to electric pulses in both cell lines. In addition, in C2C12 myoblasts, pDNA concentration did not have any effect on cell survival after GET with 500 ns and 200 ns pulse protocols. With the 8 × 100 µs pulse protocol in C2C12, survival was significantly lower, with 500 µg/mL of pDNA. Interestingly, with HF-BP pulses in C2C12 myoblasts, a significant decrease in cell survival was observed already with the lowest pDNA concentration (40 µg/mL). In 1306 fibroblasts with the 500 ns and 200 ns pulse protocols, survival was significantly lower, with 500 µg/mL of pDNA. With HF-BP pulses with concentrations higher than 100 µg/mL and with the 8 × 100 µs pulse protocol, survival was significantly lower with 250 µg/mL and 500 µg/mL of pDNA (Figure 4). Our results suggest that the decrease in survival after GET with high pDNA concentrations is cell-line-dependent.
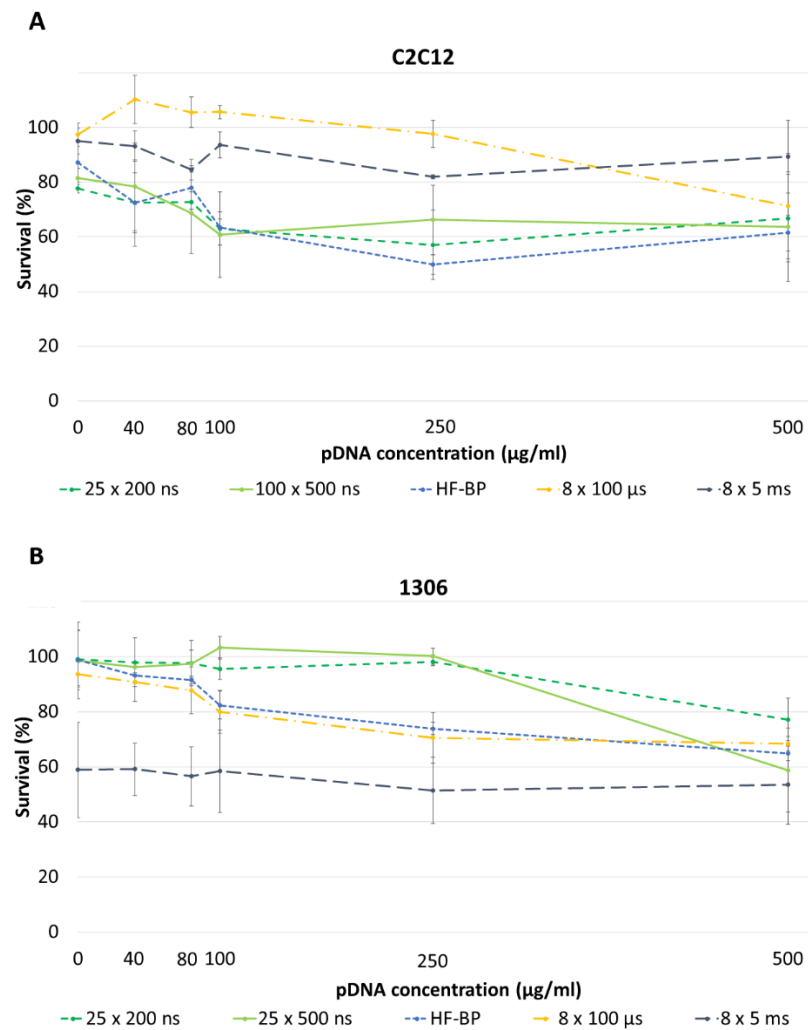
Figure 4. Cell survival with different concentrations of pEGFP-N1 pDNA. (**A**) C2C12 myoblasts, pulses: 25 × 200 ns: 25 × 200 ns, 10 Hz, 15.8 kV/cm; 100 × 500 ns: 100 × 500 ns, 10 Hz, 4.1 kV/cm; HF-BP: 2-2-2-2, 32p, 100b, 1 Hz, 1.25 kV/cm; 8 × 100 μs: 8 × 100 μs, 1 Hz, 1.25 kV/cm; and 8 × 5 ms: 8 × 5 ms, 1 Hz, 0.4 kV/cm; and (**B**) 1306 fibroblasts, pulses: 25 × 200 ns: 25 × 200 ns, 10 Hz, 12.8 kV/cm; 25 × 500 ns: 25 × 500 ns, 10 Hz, 6.5 kV/cm; HF-BP: 2-2-2-2, 32p, 100b, 1 Hz, 1 kV/cm; 8 × 100 μs: 8 × 100 μs, 1 Hz, 1.25 kV/cm; and 8 × 5 ms: 8 × 5 ms, 1 Hz, 0.6 kV/cm. 0 V represents control where cells were not exposed to electric pulses. Results are represented as an average of 3 repetitions. Statistical differences are given in the text. Bars represent standard deviation.

When also considering cell survival, i.e., calculating overall GET, we obtained the results presented in Figure 5. The overall GET increased with the increasing pDNA concentration for all pulse protocols and both cell lines. In C2C12 myoblasts, the highest overall GET was reached with 8 × 5 ms and 8 × 100 μs pulse protocols, followed by HF-BP, 500 ns, and 200 ns protocols. With all five pulse protocols, the overall GET increased up to the highest pDNA concentration used, i.e., 500 μg/mL. In C2C12 myoblasts, the overall GET with 40, 80, and 100 μg/mL pDNA concentrations was, however, below 1% with both 200 ns and 500 ns pulses (Figure 5A).

In 1306 fibroblasts, the highest overall GET was observed with 8 × 100 μs pulse protocol regardless of pDNA concentration used. Interestingly, with the highest pDNA concentration, i.e., 500 μg/mL, using the 8 × 5 ms pulse protocol, we achieved the lowest overall GET, even lower than the nanosecond and HF-BP pulse protocols. In addition, the overall GET increase with the increasing pDNA concentration was different compared to C2C12 myoblasts. In 1306 fibroblasts with the 8 × 100 μs, 8 × 5 ms, and HF-BP

pulse protocols, a plateau in the overall GET was observed between 100 μg/mL and 500 μg/mL pDNA concentrations, where the overall GET did not increase significantly with the increasing pDNA concentration. In contrast, with nanosecond pulse protocols, a significant increase in overall GET was observed between 250 μg/mL and 500 μg/mL pDNA concentration (Figure 5B).
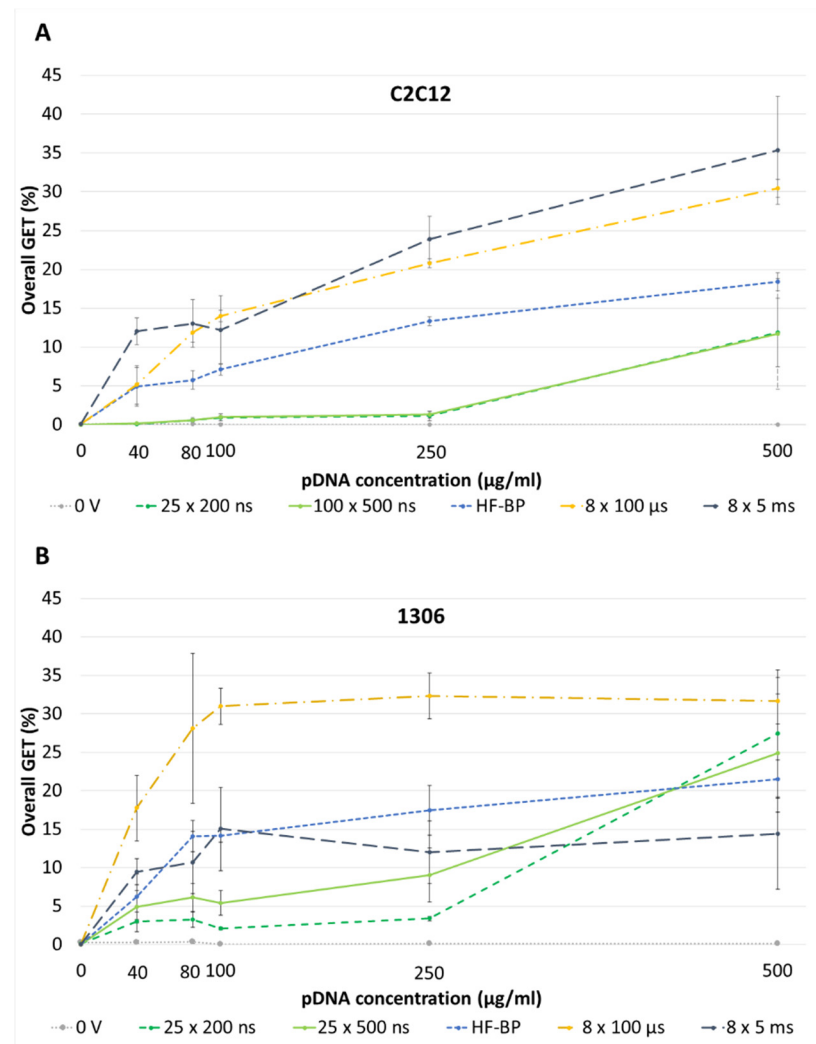

Figure 5. Overall GET with different concentrations of pEGFP-N1 pDNA. (**A**) C2C12 myoblasts, pulses: 25×200 ns: 25×200 ns, 10 Hz, 15.8 kV/cm; 100×500 ns: 100×500 ns, 10 Hz, 4.1 kV/cm; HF-BP: 2-2-2-2, 32p, 100b, 1 Hz, 1.25 kV/cm; 8×100 μs: 8×100 μs, 1 Hz, 1.25 kV/cm; and 8×5 ms: 8×5 ms, 1 Hz, 0.4 kV/cm; and (**B**) 1306 fibroblasts, pulses: 25×200 ns: 25×200 ns, 10 Hz, 12.8 kV/cm; 25×500 ns: 25×500 ns, 10 Hz, 6.5 kV/cm; HF-BP: 2-2-2-2, 32p, 100b, 1 Hz, 1 kV/cm; 8×100 μs: 8×100 μs, 1 Hz, 1.25 kV/cm; and 8×5 ms: 8×5 ms, 1 Hz, 0.6 kV/cm. 0 V represents control where cells were not exposed to electric pulses. Results are represented as an average of 3 repetitions. Statistical differences are given in the text. Bars represent standard deviation.

The importance of pDNA concentration is most noticeable with nanosecond pulses, where overall GET is less than a half in both cell lines already at pDNA concentration 250 μg/mL. With the lowest pDNA concentration, 40 μg/mL, overall GET in 1306 fibroblast was 3% and 5% for 200 and 500 ns pulses, respectively. In C2C12 myoblasts, the overall GET with 40, 80, and 100 μg/mL pDNA concentrations was below 1% with both 200 ns and 500 ns pulses (Figure 5). Based on these results, a pDNA concentration of 500 μg/mL was chosen to achieve robust overall GET.

3.3. Effect of Different pDNA Size on GET

Since pDNA size is reported to have an effect on GET efficiency, we performed experiments using two different size pDNA, comparing a 3.5 kb plasmid pmaxGFP and a 4.7 kb plasmid pEGFP-N1, both encoding GFP under the control of a CMV promotor. The concentrations of both plasmids in all experiments were 500 μg/mL, meaning that the number of pDNA copies added was 1.34 × higher for the smaller pDNA. We performed experiments with pmaxGFP for both cell lines for pulse protocols which gave the highest GET with pEGFP-N1 plasmid (Table 1).

As we can observe in Figure 6A, in C2C12 myoblasts with smaller pDNA, significantly higher overall GET was observed only for 8 × 100 μs pulse protocol. Overall GET with 200 ns, 500 ns and HF-BP protocol was comparable. Interestingly, overall GET with 8 × 5 ms was lower with smaller pDNA compared to larger pDNA.
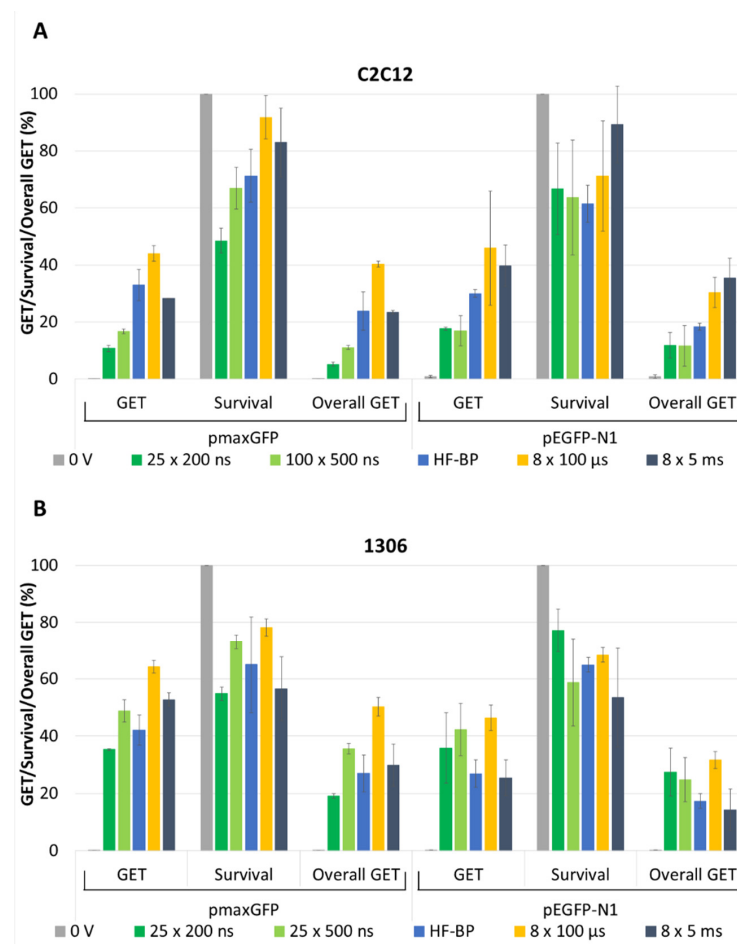

Figure 6. GET, cell survival, and overall GET with 500 μg/mL of pmaxGFP and pEGFP-N1 pDNA with different pulse protocols for (**A**) C2C12 myoblasts, 25 × 200 ns: 25 × 200 ns, 10 Hz, 15.8 kV/cm; 100 × 500 ns: 100 × 500 ns, 10 Hz, 4.1 kV/cm; HF-BP: 2-2-2-2, 32 pulses, 100 bursts, 1 Hz, 1.25 kV/cm; 8 × 100 μs: 8 × 100 μs, 1 Hz, 1.25 kV/cm; 8 × 5 ms: 8 × 5 ms, 1 Hz, 0.4 kV/cm; and (**B**) 1306 fibroblasts, 25 × 200 ns: 25 × 200 ns 10 Hz, 12.8 kV/cm;, 25 × 500 ns: 25 × 500 ns, 10 Hz, 6.5 kV/cm; HF-BP: 2-2-2-2, 32 pulses, 100 bursts, 1 Hz, 1. kV/cm; 8 × 100 μs: 8 × 100 μs, 1 Hz, 1.25 kV/cm; 8 × 5 ms: 8 × 5 ms, 1 Hz, 0.6 kV/cm. 0 V represents cells not exposed to electric pulses. Results are represented as an average of 3 repetitions. Bars represent standard deviation.

Similar results were obtained for 1306 fibroblasts (Figure 6B). Overall GET was significantly higher with smaller pDNA only for 8 × 100 μs protocol when compared to larger pDNA. With the 200 ns, 500 ns, HF-BP, and 8 × 5 ms protocols, comparable overall GET was observed with both pDNA sizes.

When comparing MFI of all pulse protocols between different pDNA sizes a marked difference was observed between the two cell lines. In C2C12 myoblasts, the MFI of the GFP-positive cells was significantly higher with smaller pDNA (pmaxGFP) after GET with the 200 ns, 500 ns, and HF-BP protocols (Figure 7A), while 1306 fibroblasts exhibited significantly higher MFI with smaller pDNA after 8×100 μs and 8×5 ms protocols (Figure 7B).

A

B

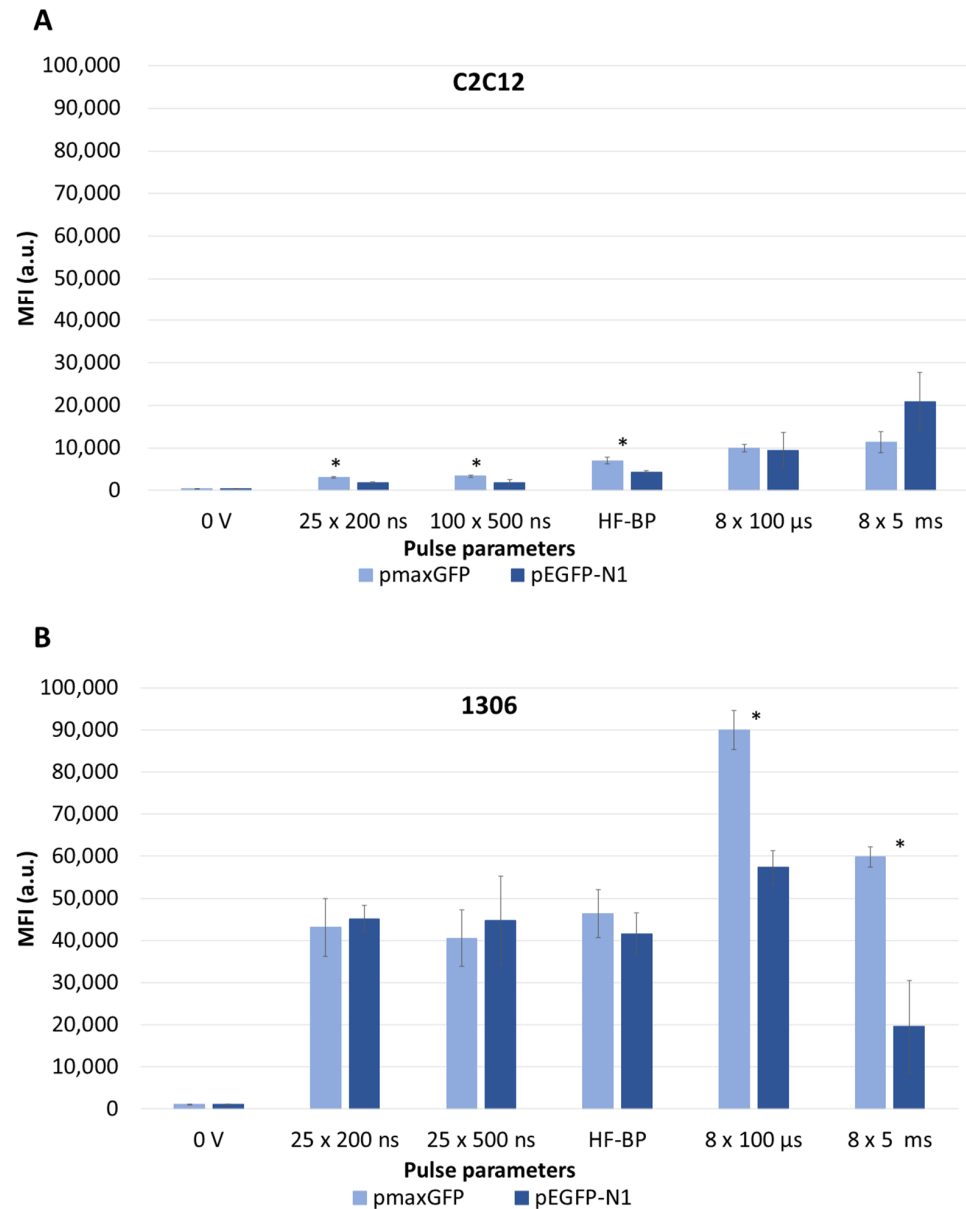**Figure 7.** Median fluorescence (MFI) of GFP-positive cells with 500 μg/mL of pmaxGFP and pEGFP-N1 pDNA with different pulse protocols for (**A**) C2C12 myoblasts, 25×200 ns: 25×200 ns, 10 Hz, 15.8 kV/cm; 100×500 ns: 100×500 ns, 10 Hz, 4.1 kV/cm; HF-BP: 2-2-2-2, 32 pulses, 100 bursts, 1 Hz, 1.25 kV/cm; 8×100 μs: 8×100 μs, 1 Hz, 1.25 kV/cm; 8×5 ms: 8×5 ms, 1 Hz, 0.4 kV/cm; and (**B**) 1306 fibroblasts, 25×200 ns: 25×200 ns, 10 Hz, 12.8 kV/cm; 25×500 ns: 25×500 ns, 10 Hz, 6.5 kV/cm; HF-BP: 2-2-2-2, 32 pulses, 100 bursts, 1 Hz, 1. kV/cm; 8×100 μs: 8×100 μs, 1 Hz, 1.25 kV/cm; 8×5 ms: 8×5 ms, 1 Hz, 0.6 kV/cm. 0 V represents cells not exposed to electric pulses. Results are represented as an average of 3 repetitions. Bars represent standard deviation. Asterisk * represents statistically significant ($p < 0.05$) difference between pmaxGFP and pEGFP-N1 for the same pulse protocol.

3.4. Effect of Pulse Parameters on Overall GET and MFI

We compared overall GET of different pulse protocols after GET with 500 µg/mL of pEGFP-N1 since this were the conditions which led to the highest overall GET.

As we can observe in Figure 8, we achieved around a 35% overall GET with the 8×5 ms pulse protocol in C2C12 myoblast. The overall GET with the 8×5 ms pulse protocol was, however, significantly lower in 1306 fibroblast, 15%. The overall GET with the 8×100 µs pulses was comparable in both cell lines, at approximately 30%, as well as for the HF-BP pulse protocol, at 20%. On the contrary, the overall GET with nanosecond pulses was interestingly higher in 1306 fibroblasts compared to C2C12 myoblasts, with the overall GET using the 25×500 ns and 300×200 ns pulse protocols being significantly higher.
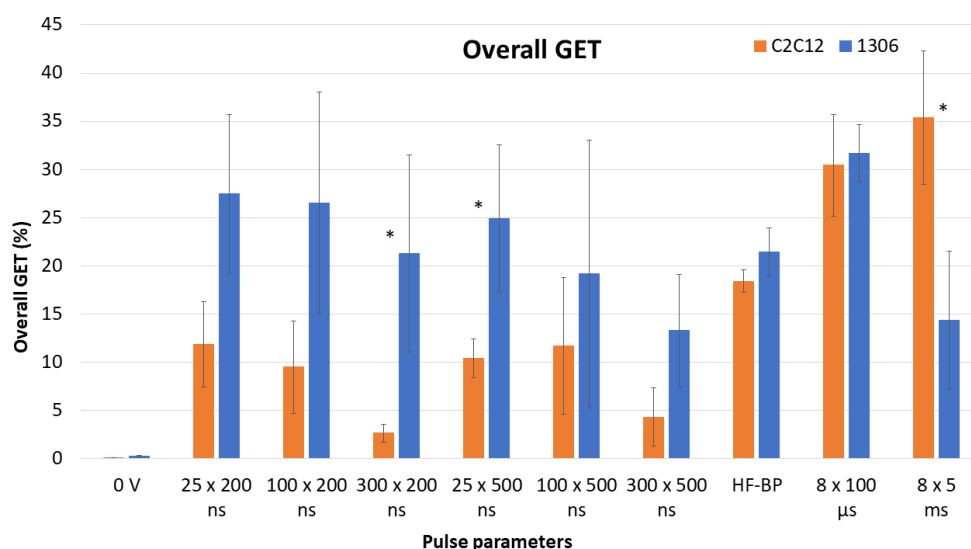

Figure 8. Overall GET with different pulse protocols for C2C12 myoblasts and 1306 fibroblasts with 500 µg/mL of pEGFP-N1. **C2C12:** 25×200 ns: 25×200 ns, 10 Hz, 15.8 kV/cm; 100×200 ns: 100×200 ns, 10 Hz, 6.9 kV/cm; 300×200 ns: 300×200 ns, 10 Hz, 6.3 kV/cm; 25×500 ns: 25×500 ns, 10 Hz, 6.9 kV/cm; 100×500 ns: 100×500 ns, 10 Hz, 4.1 kV/cm; 300×500 ns: 300×500 ns, 10 Hz, 2.4 kV/cm; HF-BP: 2-2-2-2, 32 pulses, 100 bursts, 1 Hz, 1.25 kV/cm; 8×100 µs: 8×100 µs, 1 Hz, 1.25 kV/cm; 8×5 ms; 8×5 ms, 1 Hz, 0.4 kV/cm. **1306:** 25×200 ns: 25×200 ns, 10 Hz, 12.8 kV/cm; 100×200 ns: 100×200 ns, 10 Hz, 6.9 kV/cm; 300×200 ns: 300×200 ns, 10 Hz, 4.2 kV/cm; 25×500 ns: 25×500 ns, 10 Hz, 6.5 kV/cm; 100×500 ns: 100×500 ns, 10 Hz, 3.5 kV/cm; 300×500 ns: 300×500 ns, 10 Hz, 2.7 kV/cm; HF-BP: 2-2-2-2, 32 pulses, 100 bursts, 1 Hz, 1 kV/cm; 8×100 µs: 8×100 µs, 1 Hz, 1.25 kV/cm; 8×5 ms; 8×5 ms, 1 Hz, 0.6 kV/cm. 0 V represents cells not exposed to electric pulses. Results are represented as an average of 3 repetitions. Bars represent standard deviation. Asterisk * represents statistically significant ($p < 0.05$) difference between cell lines for the same pulse protocol.

With respect to pulse parameters, overall GET with the highest pDNA concentration tested in C2C12 myoblasts was significantly higher with 8×5 ms compared to HF-BP and nanosecond pulse protocols. In addition, overall GET with 8×100 µs protocol was significantly higher compared to nanosecond pulse protocols. The overall GET in C2C12 myoblasts was significantly higher with HF-BP pulses compared to the 300×500 ns and 300×200 ns pulse protocols. However, due to the high variability, in 1306 fibroblasts, there was no significant difference in the overall GET when comparing 8×5 ms, 8×100 µs, HF-BP, and nanosecond pulse protocols.

With 8×100 µs pulses, the overall GET was comparable between both cell lines. The overall GET was significantly lower in 1306 fibroblasts for the 8×5 ms protocol and significantly higher for the 300×200 ns and 25×500 ns pulse protocols compared to the overall GET in C2C12 myoblasts. In addition, overall GET with 8×100 µs and

nanosecond pulses in 1306 fibroblasts, although not significantly, was higher as overall GET with 8 × 5 ms pulses (Supplementary Tables S3 and S4).

The MFI of GFP-positive cells was significantly higher in 1306 fibroblast with all pulse protocols, except for the 8 × 5 ms pulse protocol. The MFI of C2C12 myoblasts was up to 20,000 a.u. and was significantly different only between 8 × 5 ms and 300 × 500 ns pulse protocols. MFI of 1306 fibroblast was up to 60,000 a.u. There was no significant difference in MFI between different pulse protocols in 1306 fibroblasts (Figure 9).
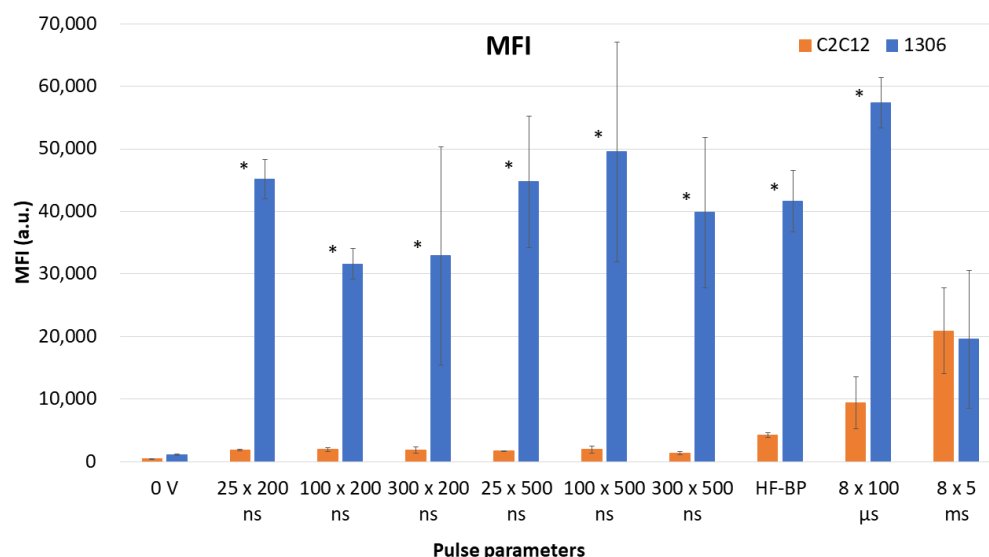

Figure 9. Median fluorescence intensity (MFI) of GFP-positive cells with different pulse protocols for C2C12 myoblasts and 1306 fibroblasts with 500 μg/mL of pEGFP-N1. **C2C12:** 25 × 200 ns: 25 × 200 ns, 10 Hz, 15.8 kV/cm; 100 × 200 ns: 100 × 200 ns, 10 Hz, 6.9 kV/cm; 300 × 200 ns: 300 × 200 ns, 10 Hz, 6.3 kV/cm; 25 × 500 ns: 25 × 500 ns, 10 Hz, 6.9 kV/cm; 100 × 500 ns: 100 × 500 ns, 10 Hz, 4.1 kV/cm; 300 × 500 ns: 300 × 500 ns, 10 Hz, 2.4 kV/cm; HF-BP: 2-2-2-2, 32 pulses, 100 bursts, 1 Hz, 1.25 kV/cm; 8 × 100 μs: 8 × 100 μs, 1 Hz, 1.25 kV/cm; 8 × 5 ms; 8 × 5 ms, 1 Hz, 0.4 kV/cm. **1306:** 25 × 200 ns: 25 × 200 ns, 10 Hz, 12.8 kV/cm; 100 × 200 ns: 100 × 200 ns, 10 Hz, 6.9 kV/cm; 300 × 200 ns: 300 × 200 ns, 10 Hz, 4.2 kV/cm; 25 × 500 ns: 25 × 500 ns, 10 Hz, 6.5 kV/cm; 100 × 500 ns: 100 × 500 ns, 10 Hz, 3.5 kV/cm; 300 × 500 ns: 300 × 500 ns, 10 Hz, 2.7 kV/cm; HF-BP: 2-2-2-2, 32 pulses, 100 bursts, 1 Hz, 1 kV/cm; 8 × 100 μs: 8 × 100 μs, 1 Hz, 1.25 kV/cm; 8 × 5 ms; 8 × 5 ms, 1 Hz, 0.6 kV/cm. 0 V represents cells not exposed to electric pulses. Results are represented as an average of 3 repetitions. Bars represent standard deviation. Asterisk * represents statistically significant ($p < 0.05$) difference between cell lines for the same pulse protocol.

3.5. Time Dynamics of pDNA Expression

The time dynamics of pDNA expression was also monitored for both cell lines for those pulse protocols with which we obtained the best overall GET with 500 μg/mL of pEGFP-N1 plasmid (Table 1). The percentage of GFP-positive cells and their MFI were measured every 8 h for 6 days. Since we did not measure cell survival at each time point, the results for time dynamics of pDNA expression are presented as GET (not overall GET).

Our results show that the dynamics of the onset of GFP expression (both percentage of GFP-positive cells and their MFI) are comparable for all pulse protocols tested (i.e., from 200 ns up to 5 ms pulse durations) but varied greatly between the two cell lines (Figures 10 and 11).
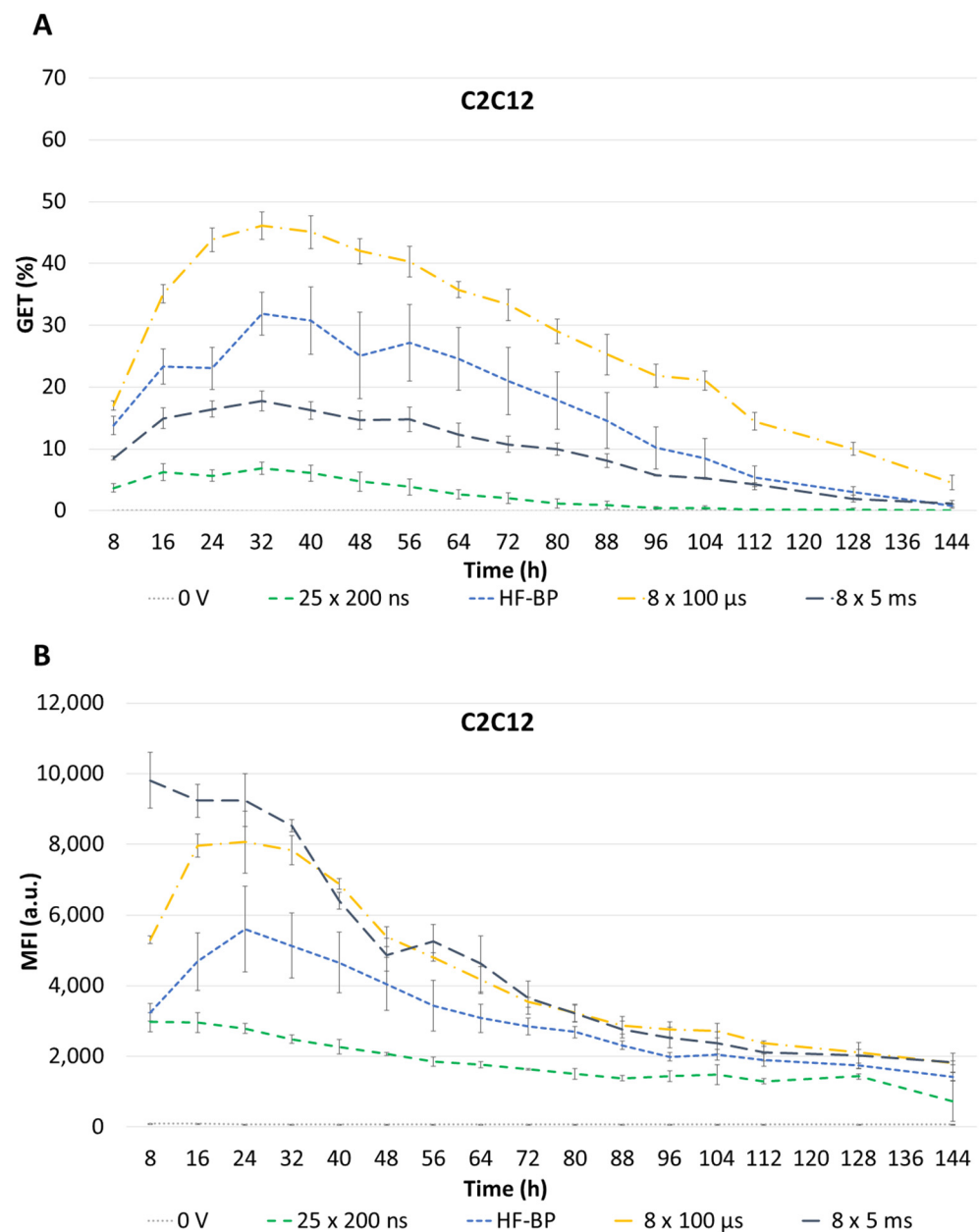
A

B

Figure 10. (**A**) GET and (**B**) median fluorescence intensity (MFI) of GFP-positive C2C12 myoblasts with 500 µg/mL pEGFP-N1 pDNA with different pulse protocols on 1306 fibroblasts, 25×200 ns: 25×200 ns, 10 Hz, 12.8 kV/cm; HF-BP: 2-2-2-2, 32 pulses, 100 bursts, 1 Hz, 1.25 kV/cm; 8×100 µs: 8×100 µs, 1 Hz, 1.25 kV/cm; 8×5 ms: 8×5 ms, 1 Hz, 0.6 kV/cm, 0 V represents control where cells were not exposed to electric pulses. Results are represented as an average of 3 repetitions. Bars represent standard deviation.

In C2C12 myoblasts, the GET increased with all pulse protocols reaching a maximum at 32 h after GET. The best GET was achieved with the 8×100 µs pulse protocol (46.2%), followed by HF-BP (31.9%), 8×5 ms (17.8%) and 25×200 ns (6.9%). Afterwards the GET started to decline and after 144 h (i.e., 6 days) decreased below 10% for all pulse protocols reaching 4.5%, 0.7%, 1.1%, and 0.02% for the 8×100 µs, HF-BP, 8×5 ms, and 25×200 ns pulse protocols, respectively (Figure 10A).
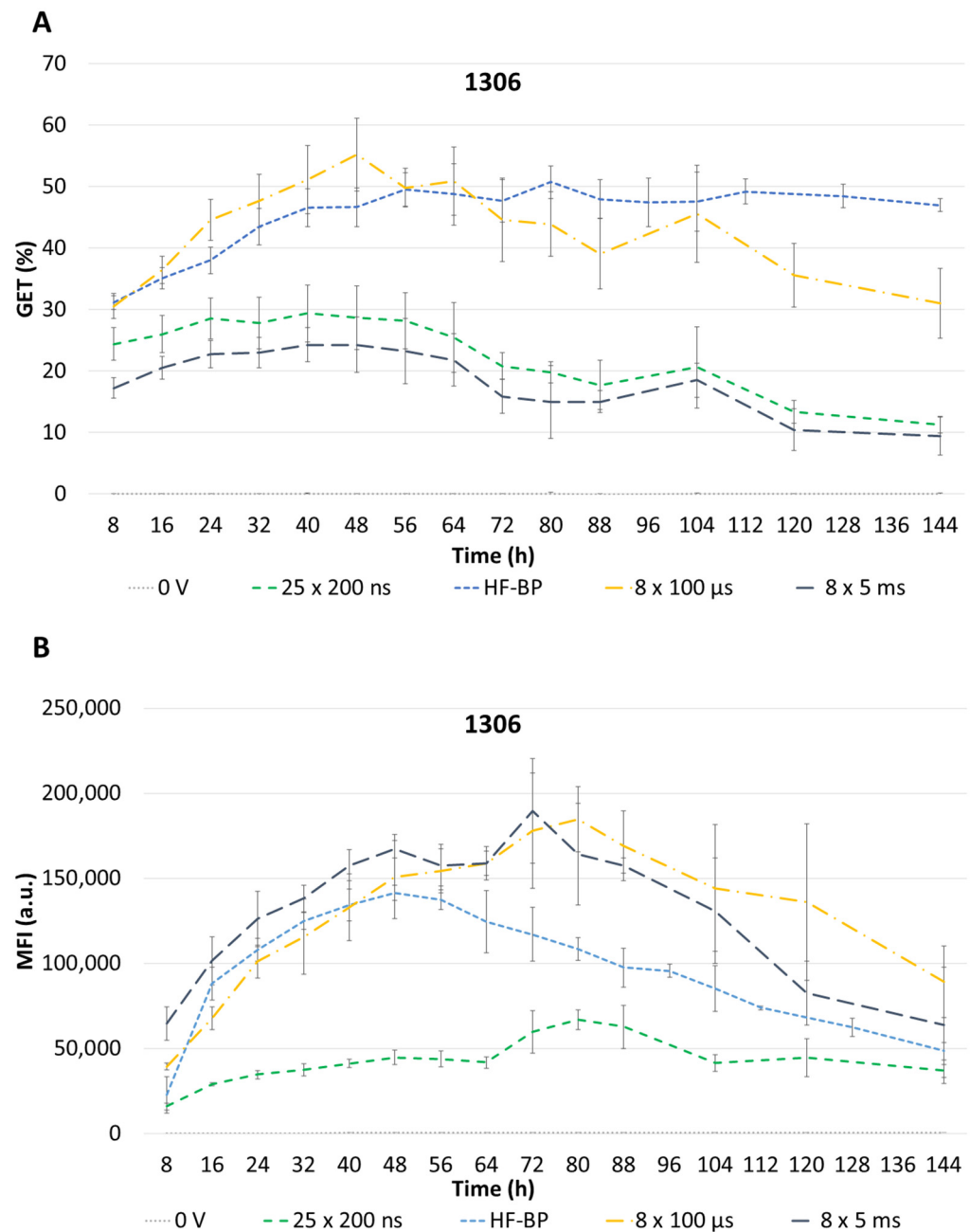
Figure 11. (**A**) GET and (**B**) median fluorescence intensity (MFI) of GFP-positive 1306 fibroblasts with 500 μg/mL pEGFP-N1 pDNA with different pulse protocols on 1306 fibroblasts, 25 × 200 ns: 25 × 200 ns, 10 Hz, 12.8 kV/cm; HF-BP: 2-2-2-2, 32 pulses, 100 bursts, 1 Hz, 1 kV/cm; 8 × 100 μs: 8 × 100 μs, 1 Hz, 1.25 kV/cm; 8 × 5 ms: 8 × 5 ms, 1 Hz, 0.6 kV/cm. 0 V represents control where cells were not exposed to electric pulses. Results are represented as an average of 3 repetitions. Bars represent standard deviation.

A similar dynamic was observed for MFI of GFP positive in C2C12 myoblasts. MFI reached the peak at 24 h after GET with 8 × 100 μs and HF-BP protocols and then stated to decline. Interestingly, MFI after the 8 × 5 ms and 25 × 200 ns protocols peaked already at 8 h after GET, after which it declined steadily (Figure 10B).

Contrary to C2C12 myoblasts, broad peaks in GET were observed in 1306 fibroblasts for all pulse protocols tested. The maximum percentage of GFP-positive cells was reached between 8 and 64 h for the 8 × 5 ms and 25 × 200 ns pulse protocols, between 24 and 104 h after GET with the 8 × 100 μs pulse protocol, and between 40 and 112 h after GET with

the HF-BP pulse protocol. The best GET was achieved with the 8×100 µs pulse protocol (max at 48 h, 55.2%), followed by the HF-BP (max at 80 h, 50.8%), 25×200 ns (max at 40 h, 29.2%) and 8×5 ms protocols (max at 40 h, 24.3%). Interestingly, higher GET was achieved with 25×200 ns compared to 8×5 ms protocol. After reaching a peak, the percentage of GFP-positive cells started to decrease slowly, except for the HF-BP protocol, where it remained at the same level for the entire time of observation. On day 6 (i.e., 144 h) after GET, 31.1%, 47.0%, 11.3%, and 9.5% of cells were still GFP-positive for the 8×100 µs, HF-BP, 25×200 ns, and 8×5 ms pulse protocols, respectively (Figure 11A).

In addition, in MFI, broad peaks were observed for all pulse protocols in 1306 fibroblasts. The MFI reached a peak later than the maximum percentage of GFP-positive cells between 24 and 104 h after GET with the 25×200 ns pulse protocol, between 40 and 104 h after GET with the 8×100 µs and 8×5 ms pulse protocols, and between 32 and 72 h after GET with the HF-BP pulse protocol. Comparable MFIs were observed between the 8×5 ms, 8×100 µs, and HF-BP protocols, which were higher compared to the 25×200 ns protocol (Figure 11B).

3.6. Modeling the Probability of pDNA and Cell Membrane Contact during GET

3.6.1. 200 ns and 500 ns Pulses

Equation (4) is first solved for a single pulse of 200 ns at an electric field intensity of 15.8 kV/cm. These were the conditions used in the experiments for C2C12 cells (Table 1). The results of the solution of Equation (4) are shown in Figure 12A below for $B_L, B_R = 134$ nm, representing 500 µg/mL pDNA solution concentration. The solid lines represent the evolution of $P(X,t)$ during the pulse, and the dashed lines represent the evolution of $P(X,t)$ after the pulse. Equation (4) is solved for $t = 100$ ms since the ns pulses are applied at a frequency of 10 Hz (implying 100 ms between pulses). During the pulse ($t = 0$ ns to $t = 200$ ns), the initial narrow band normal/Gaussian distribution drifts towards the right by electrophoresis and spreads only a little by diffusion. After the pulse, there is no drift, and the distribution spreads purely by diffusion. The time between two successive pulses is long enough for $P(X,t)$ to become almost flat before the onset of the second pulse ($t = 100$ ms).

To calculate the Probability of Successful Contact $PSC(t)$, the flux $P(X,t)$ is collected at the cell membrane, i.e., at $X = B_R$. $PSC(t)$ is calculated as $PSC(t) = 1 - \int_{-B_L}^{+B_R} P(X,t)dX$. This represents the probability that a pDNA molecule will successfully establish contact with, and be absorbed by, the cell membrane, which is pre-requisite for a successful GET. As observed from Figure 12B, $PSC(t)$ remains negligibly small during and after the 200 ns pulse, implying a negligible probability of pDNA establishing contact with the cell membrane. Only from around $t\sim1$ ms does $PSC(t)$ start to rise (due to diffusion), attaining a non-negligible probability.

To determine the influence of concentration (i.e., of the distance between the pDNA and the cell membrane (in Figure 1)), another simulation using $B_L, B_R = 433$ nm, representing 15 µg/mL pDNA solution concentration, is shown in Figure 12C,D. Due to the lower concentration (or a larger distance between the pDNA and the cell membrane), the domain has expanded (Figure 12C), and the pDNA molecule has to travel a larger distance before it can reach the cell membrane. Due to insufficient electrophoresis, the pDNA molecule relies on diffusion after the cessation of pulse to cover this large distance and reach the cell membrane. For $B_L, B_R = 433$ nm, $PSC(t)$ starts to rise at a much later time and attains a lower $PSC(t)$ at $t = 100$ ms (Figure 12D), compared to $B_L, B_R = 134$ nm (Figure 12B).
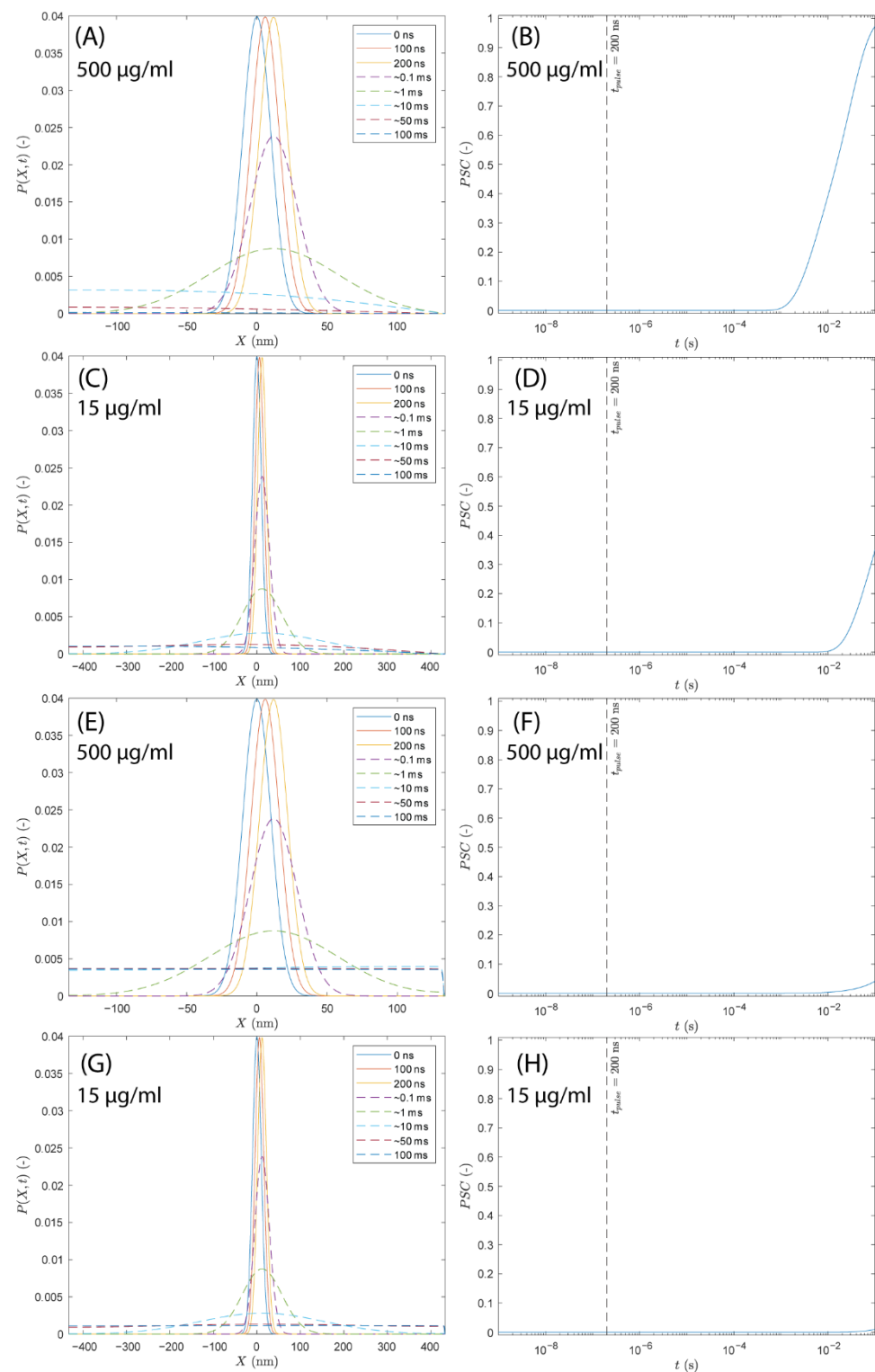
Figure 12. The 200 ns pulse: Evolution of $P(X, t)$ and the corresponding Probability of Successful Contact $PSC(t) = 1 - \int_{-B_L}^{+B_R} P(X, t) dX$ for $B_L, B_R = 134$ nm in (**A**,**B**,**E**,**F**) and for $B_L, B_R = 433$ nm in (**C**,**D**,**G**,**H**); (**A**–**D**) represent cases without free energy barrier and (**E**–**H**) represent cases with free energy barrier. Solid lines in (**A**,**C**,**E**,**G**) correspond to times during the pulse, and dashed lines in (**A**,**C**,**E**,**G**) correspond to times after the pulse. The dashed lines in (**B**,**D**,**F**,**H**) represent the time at which the 200 ns pulse ends.

Evolution of $P(X, t)$, as calculated using Equation (5), i.e., in the presence of a free energy barrier between the pDNA and the cell membrane, is shown in Figure 12E for

B_L, B_R = 134 nm (500 µg/mL) and in Figure 12G for B_L, B_R = 433 nm (15 µg/mL); the corresponding $PSC(t)$ values are shown in Figure 12F,H, respectively. The presence of a high free energy barrier (barrier height of 50 $k_B T$) signficantly reduces the probability of pDNA reaching the cell membrane. For a 200 ns pulse, electrophoresis acts for an insufficient amount of time to bring the pDNA molecule close to the cell membrane and for it to influence the pDNA molecule in overcoming the free energy barrier. Due to the nature of the free energy barrier considered in this study ($50e^{2(X-B_R)} k_B T$), the free energy is negligibly small at distance greater than ∼2 nm away from the cell membrane, and it rises sharply as we approach the cell membrane. Therefore, for the electric field (and electrophoresis) to overcome this barrier, the pDNA molecule must already be present very close to the cell membrane, or the electric field should be applied for a longer duration such that electrophoresis first drags the pDNA molecule close to the cell membrane and then subsequently helps the pDNA molecule in overcoming this barrier. Thus, the pDNA molecule which relies on diffusion to reach the cell membrane is also repulsed by the free energy barrier, resulting in lower $PSC(t)$ compared to the case when no free energy barrier was present (comparing Figure 12B,D vs. Figure 12F,H). Since the probability of pDNA being absorbed by the cell membrane is low in the presence of a free energy barrier, the probability of finding the pDNA molecule in the domain $X \in [-B_L, B_R]$ at t=100 ms is higher (comparing Figure 12A,C vs. Figure 12E,G at t=100 ms). For 200 ns pulses, the time between pulses (t = 100 ms) is large enough for $P(X, t)$ to become almost flat (by diffusion) before the onset of the second pulse. This is the case for both – without the free energy barrier (Figure 12A,C) and the with free energy barrier (Figure 12E,G). This implies that it is almost equally probable to find the pDNA molecule at any X for $X \in [-B_L, B_R]$. Thus, for both cases, a uniform distribution of $P(X, t)$ in $X \in [-B_L, B_R]$ can be considered as an initial condition for the second pulse. For a uniform distribution, there is a higher probabilty of pDNA being close to the cell membrane compared to the narrow-band Gaussian distribution with a standard deviation of 10 nm centered around $X = 0$, the tail of which is neglibly small at $X = -B_L, +B_R$. Therefore, we expect that electrophoresis provided by the second pulse would contribute more to the rise in $PSC(t)$ during the second pulse compared to the first pulse for which the rise in $PSC(t)$ was negligible during the pulse (Figure 12B,D,F,H). However, since the pulse duration is small, we further expect that the rise in $PSC(t)$ will still not be significant to completely ensure the absorption of pDNA at the cell membrane. $PSC(t)$ will still have to rely on the diffusion post-second pulse. We expect this process to continue in the subsequent pulses until diffusion increases $PSC(t)$ to a value of 1. The role of any additional pulses after $PSC(t)$ reaches 1 is not accounted for by the model since the pDNA is absorbed by the cell membrane and $P(X, t) = 0$ in $X \in [-B_L, B_R]$. In such cases, additional pulses can be thought to add more pDNA molecules to the cell membrane.

To illustrate the point that ns pulses can be analysed in isolation, we can look at the Peclet number defined as the ratio of distance covered during electrophoresis to the distance covered during diffusion post pulse ($Pe = \frac{\mu E t_p}{\sqrt{2Dt_{bp}}}$, where t_p is the pulse duration and t_{bp} is the duration between pulses). For the 200 ns pulse, E = 15.8 kV/cm, t_p = 200 ns, and t_{bp} = 100 ms, which gives a Pe = 0.03 (< 1), indicating that $P(X, t)$ would spread more by diffusion and reach the cell membrane while becoming flat than it would be drifted towards the cell membrane by electrophoresis over a single phase (during pulse and post-pulse). As a result, the role of electric field pulses can be studied in isolation without the confounding/compounding effects of multiple pulses.

Furthermore, for pedagogical purposes, and to study the effect of concentration on pDNA being absorbed by the cell membrane (a pre-requisite for GET) in isolation as a function different pulse durations and electric field intensities, we have decided to simulate only one pulse. Such an analysis effectivly allows us to infer and isolate the roles of electropohoresis and diffusion for different kinds of pulses/pulse durations used for GET as a function of concentration and will allow us to draw more general conclusions.

$PSC(t)$ is evaluated for the 200 ns pulse and 500 ns pulse at the corresponding electric field intensities (Table 1 for C2C12 cells) using (B_L, B_R) ranging from 77 nm to 433 nm (corresponding to concentrations ranging from 2500 µg/mL to 15 µg/mL, respectively) and is shown in Figure 13A–D. For all ranges of (B_L, B_R) tested, $PSC(t)$ rises post pulse termination (for both 200 ns and 500 ns pulses) through the diffusive process. As seen from Figure 13A,C (without the free energy barrier), $PSC(t)$ starts to rise from $t \sim 0.2$ ms for the lowest $(B_L, B_R) = 77$ nm. The time at which $PSC(t)$ begins to rise depends on (B_L, B_R), and $PSC(t)$ starts to rise earlier for lower (B_L, B_R), since the pDNA molecule is initially located close to the cell membrane and thus has a higher probability of reaching the cell membrane (through diffusion) first. Similar profiles (rise times) of $PSC(t)$ can be seen for 200 ns and 500 ns pulses as $PSC(t)$ rises predominantly by diffusion with little contribution from electrophoresis. For the case with free energy barrier (Figure 13B,D), the rise in $PSC(t)$ is delayed. $PSC(t)$ starts to rise from $t \sim 10$ ms for the lowest $((B_L, B_R) = 77$ nm) and attains a lower final $PSC(t)$ at $t = 100$ ms compared to the case without a free energy barrier. Similar profiles of $PSC(t)$ were obtained for both the 200 ns and 500 ns pulse in the presence of the free energy barrier as well, further indicating the dominating effect of the diffusive process with little contribution from electrophoresis.
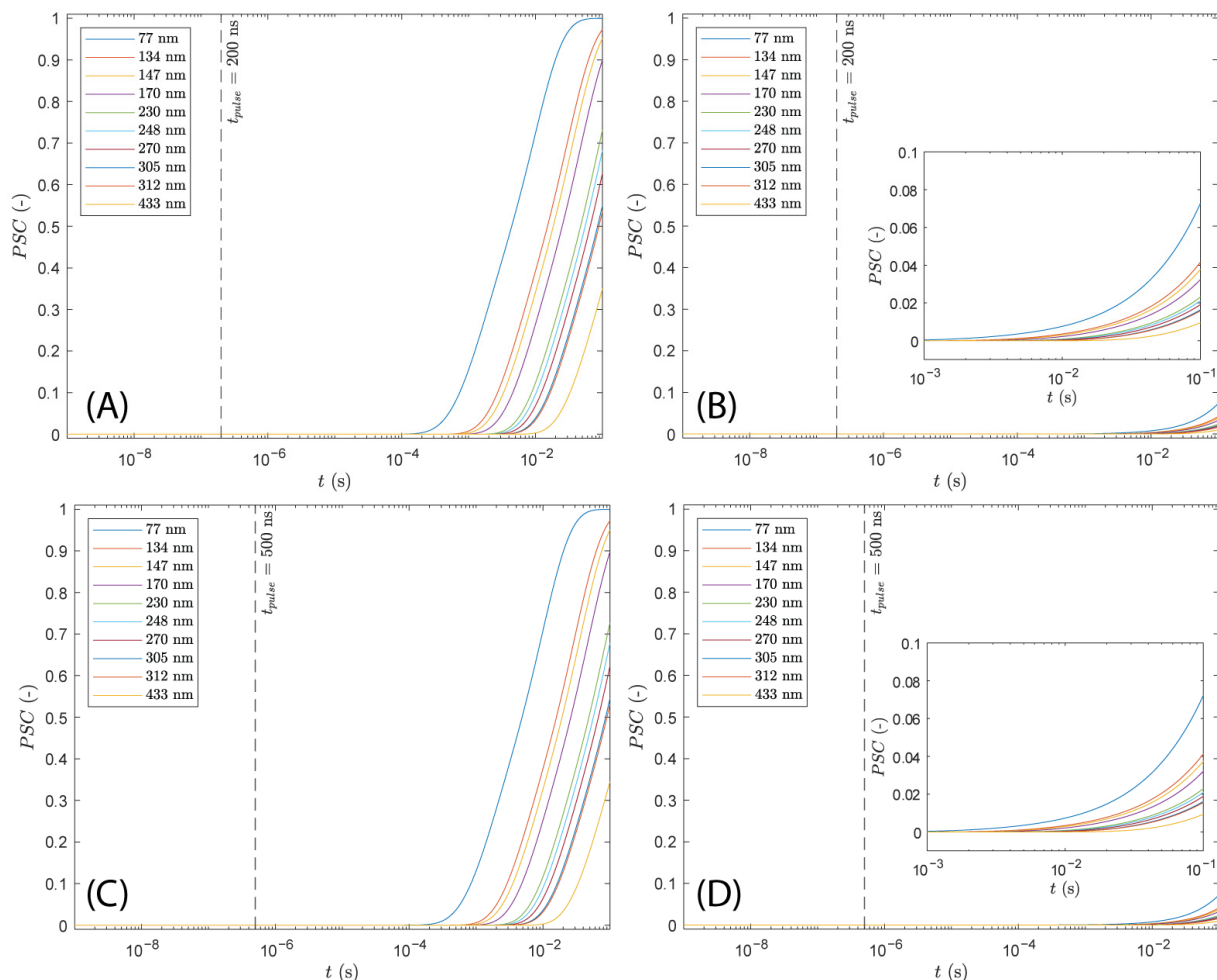

Figure 13. Evolution of $PSC(t)$ for different (B_L, B_R) ranging from 77 nm to 433 nm, corresponding to concentrations ranging from 2500 µg/mL to 15 µg/mL, respectively. (**A,B**) The 200 ns pulse at 15.8 kV/cm: (**A**) without free energy barrier, (**B**) with free energy barrier. (**C,D**) The 500 ns pulse at 4.1 kV/cm: (**C**) without free energy barrier, (**D**) with free energy barrier. Dashed lines represent the time at which nanosecond pulse ends. Insets in (**B,D**) show zoomed-in plots for rise in $PSC(t)$ from 1 ms.

For the 200 ns and 500 ns pulses, and for both – without and with free energy barrier, the final $PSC(t)$, i.e., $PSC(t = 100 \text{ ms})$ depends upon (B_L, B_R); thus, we can expect GET to depend on concentrations ranging from 2500 µg/mL to 15 µg/mL.

3.6.2. HF-BP Pulses

Equation (4) is solved using $B_L, B_R = 134$ nm (representing 500 µg/mL pDNA solution concentration) for 32 bipolar pulses (constituting 1 burst out of a 100 bursts) as described by the protocol given in Table 1 for C2C12 cells. Figure 14A–C show the evolution of $P(X, t)$ during the 32 pulses, whereas Figure 14D shows shows the evolution of $P(X, t)$ after termination of 32 pulses, i.e., 1 burst. The domain length considered was $B_L, B_R = 134$ nm, corresponding to 500 µg/mL.

Figure 14A shows the evolution of $P(X, t)$ during the first bipolar pulse. During the first 2 µs of the pulse, when the electric field is applied in the negative X direction, $P(X, t)$ moves to the right due to electrophoresis and only spreads slightly due to diffusion. During the next 2 µs, when the electric field is absent, the peak of $P(X, t)$ remains at the same X location, and $P(X, t)$ spreads slightly by diffusion. During the next 2 µs, the electric field is applied in the positive X direction and the peak of $P(X, t)$ moves to the left due to electrophoresis and spreads slightly by diffusion. During the last 2 µs of the pulse, the electric field is absent again, and the peak of $P(X, t)$ remains at the same location, spreading slightly by diffusion. The same pattern is repeated for 32 such bipolar pulses. Figure 14B shows the evolution of $P(X, t)$ during pulse number 15 and Figure 14C shows the evolution of $P(X, t)$ during pulse number 32. It can be seen from Figure 14B,C that the peak $P(X, t)$ remains close to $X = 0$ nm during the 32 pulses, as there is a net zero drift in $P(X, t)$ due to the bipolar nature of the pulses. $P(X, t)$, however, spreads by diffusion during the 32 pulses. Finally, after the cessation of 32 bipolar pulses (i.e., after 1 burst), or after $t = 256$ µs, $P(X, t)$ only spreads by diffusion and becomes almost flat until the onset of the next burst (at $t = 1$ s).

The Probability of Successful Contact, $PSC(t)$, is calculated as $PSC(t) = 1 - \int_{-B_L}^{+B_R} P(X, t) dX$ and is shown in Figure 14E. $PSC(t)$ remains negligibly small during the burst of 32 bipolar pulses, i.e., until $t = 256$ µs, as indicated by the dotted vertical line. Only from around $t \sim 1$ ms does $PSC(t)$ start to rise (due to diffusion), attaining a non-negligible probability. $PSC(t)$ reaches a final probability of 1 before the onset of the next burst of bipolar pulses (at $t = 1$ s).

To see the influence of the free energy barrier, Equation (5) is solved using $B_L, B_R = 134$ nm (representing 500 µg/mL pDNA solution concentration) for 32 bipolar pulses, and the the evolution of $P(X, t)$ is shown in Figure 14F–H during the 32 pulses and in Figure 14I after the termination of the 32 pulses. Similar to the case with no free energy barrier, the domain length considered was $B_L, B_R = 134$ nm, corresponding to 500 µg/mL. The evolution of $P(X, t)$ during 32 pulses for the case with the free energy barrier (Figure 14F–H) was similar to the the evolution of $P(X, t)$ during the 32 pulses without the free energy barrier (Figure 14A–C). This could be due to the fact that $P(X, t)$ is not able to spread enough by diffusion during the burst (and net electrophoresis is also negligible due to the bipolar nature of the pulses) to have a signficant portion other than the thin tail of $P(X, t)$ close to the cell membrane where the free energy barrier is present. Therefore, the evolution of $P(X, t)$ with the free energy barrier would be simlar to the case without the free energy barrier for the large enough domain considered here ($B_L, B_R = 134$ nm, corresponding to 500 µg/mL). For smaller domain lengths (or concentrations > 500 µg/mL), this might not be the case.
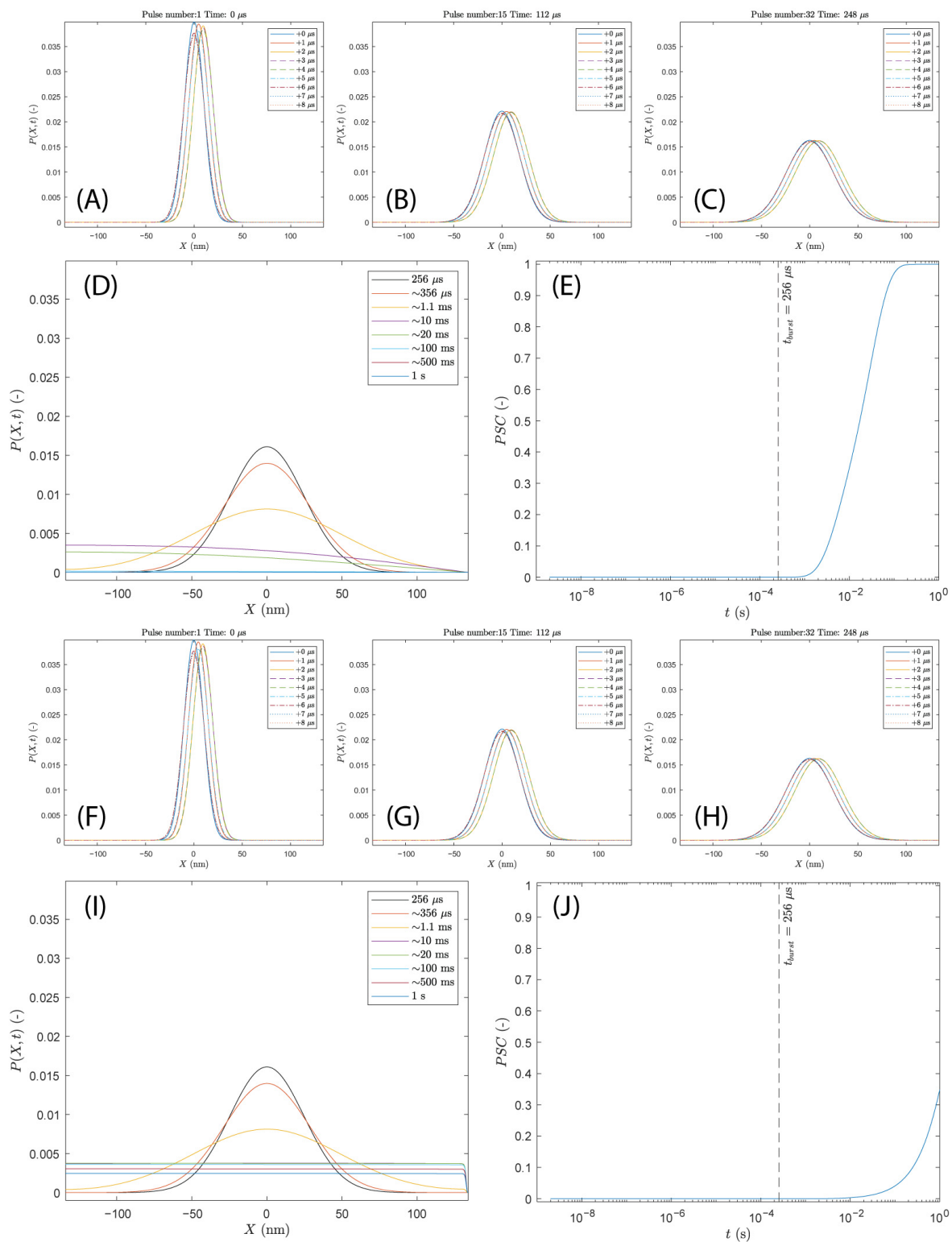
Figure 14. HF-BP pulses: Evolution of $P(X, t)$ and the corresponding Probability of Successful Contact $PSC(t) = 1 - \int_{-B_L}^{+B_R} P(X, t)dX$ for $B_L, B_R = 134$ nm (corresponding to 500 µg/mL) during a sequence of 32 bipolar pulses (1 burst) at an electric field intensity of 1.25 kV/cm (Table 1 for C2C12 cells). (**A**–**E**) represent cases without free energy barrier and (**F**–**J**) represent cases with free energy barrier. The dashed lines in (**E**,**J**) represent the time at which the sequence of 32 pulses (i.e., 1 burst) ends.

The difference between the cases without and with the free energy barrier can be seen in the evolution of $P(X, t)$ after the burst (comparing Figure 14D with Figure 14I). Similar to ns pulses, it is less probable for the pDNA molecule to come in contact with the cell membrane by diffusion only in the presence of the free energy barrier. As a result, there is higher probability for the pDNA molecule to stay within the domain $X \in [-B_L, B_R]$. Correspondingly, $PSC(t)$ begins to rise at a much later time in the presence of the free energy barrier (Figure 14J) compared to the case without the free energy barrier (Figure 14E). $PSC(t)$ also reaches a lower final value of only silightly greater than 0.3 at the end of the burst.

$PSC(t)$ is evaluated using (B_L, B_R) ranging from 77 nm to 433 nm, corresponding to concentrations ranging from 2500 µg/mL to 15 µg/mL, respectively, and is shown in Figure 15A for the case without the free energy barrier and in Figure 15B for the case with the free energy barrier. For all ranges of (B_L, B_R) tested, $PSC(t)$ rises post-burst termination (32 bipolar pulses) through the diffusive process. As seen from Figure 15A, and similar to nanosecond pulses, $PSC(t)$ starts to rise from $t \sim 0.2$ ms for the lowest $(B_L, B_R) = 77$ nm. Furthermore, the time at which $PSC(t)$ begins to rise depends on (B_L, B_R), and $PSC(t)$ starts to rise earlier for lower (B_L, B_R). A similar trend was observed for the case with the free energy barrier; however, the rise in $PSC(t)$ was delayed (to $t \sim 10$ ms for the lowest $(B_L, B_R) = 77$ nm) and $PSC(t)$ attains a lower final value (at = 1 s) compared to the case without the free energy barrier.
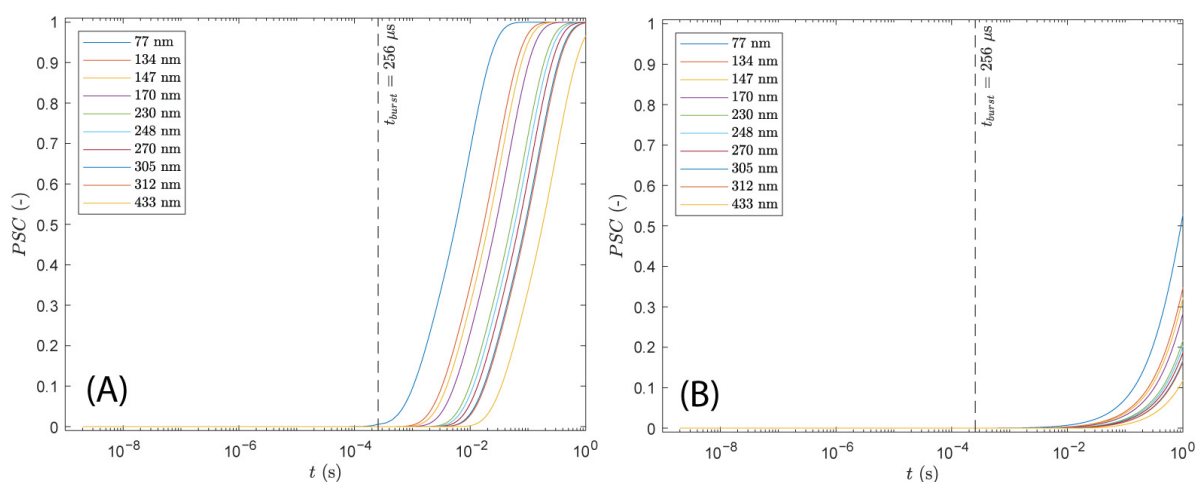

Figure 15. Evolution of $PSC(t)$ for different (B_L, B_R) ranging from 77 nm to 433 nm, corresponding to concentrations ranging from 2500 µg/mL to 15 µg/mL, respectively, for a sequence of 32 bipolar pulses (1 burst) at an electric field intensity of 1.25 kV/cm (Table 1 for C2C12 cells): (**A**) without free energy barrier and (**B**) with free energy barrier. Dashed lines represent the time at which the sequence of 32 pulses (i.e., 1 burst) ends.

The evolution of $PSC(t)$ is similar for nanosecond and HF-BP pulses. Figure 16 shows $PSC(t)$ using $B_L, B_R = 134$ nm (500 µg/mL) for a 200 ns pulse, a 500 ns pulse, and a bipolar burst. Irrespective of the pulse duration (200 ns, 500 ns, or a burst of 2 µs bipolar pulses), $PSC(t)$ starts to rise post-pulse/burst termination from around $t \sim 1$ ms (for the case without the free energy barrier Figure 16A) and $t \sim 20$ ms (for the case with the free energy barrier Figure 16B) and rises at the same rate. This indicates that the electrophoresis provided by these nanosecond and HF-BP pulses is insufficient to establish a pDNA contact with the cell membrane, and $PSC(t)$ rises due to diffusion. The solid vertical line in Figure 16A,B represents the onset of the next 200 ns or 500 ns pulse (pulse repition rate for ns pulses is 10 Hz).
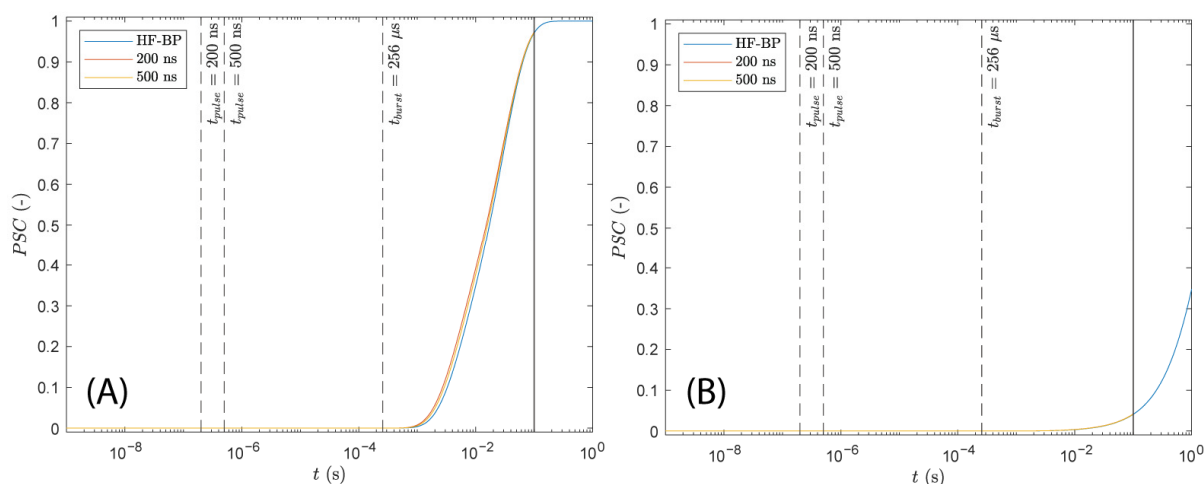
Figure 16. Evolution of $PSC(t)$ for a single 200 ns pulse, a single 500 ns pulse and a single burst (32 bipolar pulses) for (B_L, B_R) = 134 nm, corresponding to 500 µg/mL: (**A**) without free energy barrier and (**B**) with free energy barrier. Dashed lines represent the time at which the ns pulses end or the sequence of 32 pulses (i.e., 1 burst) ends. The solid vertical line represents the onset of the next 200 ns or 500 ns pulse (pulse repetition rate for ns pulses is 10 Hz). The next burst of HF-BP pulses starts at 1 s (burst repetition frequency is 1 Hz).

It is worthwhile to note that for ns pulses, a single pulse was considered, whereas for HF-BP pulses, 32 bipolar pulses (or 1 burst) were considered. As mentioned previously, the Peclet number ($Pe = \frac{\mu E t_p}{\sqrt{2D t_{bp}}}$) during a single phase (pulse + post pulse) of the 200 ns pulse was $Pe = 0.03$ (< 1), indicating that diffusion dominated the process during the phase and that the initial narrow-band Gaussian distribution drifts very little due to electrophoresis and becomes nearly flat by spreading due to diffusion by the end of the phase. As a result, ns pulses can be studied in isolation. However, for a sequence of 32 bipolar pulses, pulse duration t_p = 2 µs and time between pulses t_{bp} = 2 µs is not large. For an electric field intensity of 1.25 kV/cm, the Peclet number for HF-BP pulses is $Pe = 4.69$ (> 1), indicating the electrophoresis during the pulse dominates the diffusion in between pulses, and there is very little time for diffusion to spread the distribution. As a result, there could be a compounding effect of subsequent pulses due to which the entire sequence of 32 pulses was considered. However, if we consider pulse duration t_p = 2 µs and the time between bursts t_{bp} = 1 s, the Peclet number for a single burst is $Pe = 0.01$ (< 1), indicating that diffusion dominates over electrophoresis and spreads the distribution, making it almost flat by the end of the burst. As a result, the individual bursts can be studied in isolation. The assumption of t_p = 2 µs as opposed to t_p = 32 × 2 µs is valid, as there is net zero electrophoresis/drift during the 32 pulses.

For HF-BP pulses, the time between bursts (t = 1 s) is large enough for $P(X, t)$ to become almost flat (by diffusion) before the onset of the second burst. For the case without the free energy barrier, $PSC(t)$ for (B_L, B_R) ranging from 77 nm to 433 nm reaches 1 before the onset of the second burst (Figure 15A). This should imply that without the free energy barrier, GET should be independent of concentration. This is unlike the 200 ns pulse and 500 ns pulse protocols, where, although the time between pulses was large (t = 100 ms), it was not large enough to esnure $PSC(t)$ reaches 1 for (B_L, B_R) ranging from 77 nm to 433 nm (Figure 13A,C), thus implying GET dependance on concentration even without the free energy barrier for 200 and 500 ns pulses. Furthermore, since $PSC(t)$ reaches 1 before the onset of the second burst, the model does not account for the second burst since $P(X, t) \sim 0$ in $X \in [-B_L, B_R]$. In this case, additional bursts can be thought to add more pDNA molecules to the cell membrane.

For the case with free energy barrier, $PSC(t)$ does not reach a value of 1, and the final value depends on (B_L, B_R) ranging from 77 nm to 433 nm (Figure 15B). This implies that

GET should depend on concentration when the free energy barrier is present. However, since the time between bursts is large (t = 1 s), $P(X, t)$ becomes almost flat (but non-zero) before the onset of the second burst (Figure 14I at t = 1 s). Therefore, as with 200 ns pulses, a uniform distribution of $P(X, t)$ in $X \in [-B_L, B_R]$ can be considered as an initial condition for the second burst. For a uniform distribution, there is a higher probabilty of pDNA being close to the cell membrane compared to the narrow-band Gaussian distribution with a standard deviation of 10 nm centered around $X = 0$, the tail of which is neglibly small at $X = -B_L, +B_R$. Therefore, we expect that electrophoresis provided by the second burst pulses would contribute more to the rise of $PSC(t)$ during burst compared to the first burst for which the rise in $PSC(t)$ was negligible during burst. However, due to the bipolar nature of the pulses and due to the free energy barrier, we further expect that the rise in $PSC(t)$ will not be significant during the sequence of 32 bipolar pulses of the second burst. $PSC(t)$ will still have to rely on diffusion post-second pulse. We expect this process to continue in the subsequent bursts till diffusion rises $PSC(t)$ to a value of 1. The role of any additional bursts after $PSC(t)$ reaches 1 is not accounted for by the model since the pDNA is absorbed by the cell membrane and $P(X, t) = 0$ in $X \in [-B_L, B_R]$. In such cases, additional pulses can be thought to add more pDNA molecules to the cell membrane.

3.6.3. 100 μs Pulses

Equations (4) and (5) were solved using B_L, B_R = 134 nm (representing 500 μg/mL pDNA solution concentration) for a 100 μs (monopolar) pulse at an electric field intensity of 1.25 kV/cm, corresponding to experimental conditions for C2C12 cells (Table 1). The evolution of $P(X, t)$ is shown in Figure 17A for the case without the free energy barrier and in Figure 17C for the case with free energy barrier. For the case without the free energy barrier, electophoresis shifts the peak of $P(X, t)$ towards the cell membrane and acts for a sufficient amount of time to ensure that the pDNA molecule reaches the cell membrane during the pulse. This is further evident from the evolution of $PSC(t)$ in Figure 17B, where $PSC(t)$ remains negligibly small until around $t \sim 20$ μs and then suddenly increases to a final value of 1 well before the pulse terminates at t = 100 μs. This is further evident from $P(X, t) = 0$ in $X \in [B_L, B_R]$ for times $t > 20$ μs in Figure 17A, indicating that the pDNA has been absorbed by the cell membrane by this time.

For the case with the free energy barrier, similar to the case without the free energy barrier, electrophoresis drives the peak of $P(X, t)$ towards the cell membrane during the pulse (Figure 17C). When nearing the cell membrane, and while electrophoresis is still present, electrophoresis is driving the pDNA molecule to establish a contact with the cell membrane, and at the same time, it is facing the free energy barrier preventing the pDNA molecule from being absorbed at the cell membrane. As a result of this, there is a high probability of finding the pDNA molecule close to the cell membrane (see the peak at $t \sim 50$ μs in Figure 17C, also notice the change in scale of the Y-axis between Figure 17A,C) Eventually, with electrophoresis acting on the pDNA molecule, the probability of pDNA overcoming the free energy barrier and establishing a contact with the cell membrane increases. Simultaneously, the probability of the pDNA molecule being located close to the cell membrane decreases, as is evident in the decrease in the peak of $P(X, t)$ from $t \sim 50$ μs to $t \sim 100$ μs (Figure 17C).

Similar inferences can be made from the evolution of $PSC(t)$ in Figure 17D. Similar to the case without the free energy barrier (Figure 17B), $PSC(t)$ begins to rise at $t \sim 20$ μs in Figure 17D; however, the rise is not as steep as was with the case without the free energy barrier. The free energy barrier slows down the rise in $PSC(t)$. Furthermore, it also prevents $PSC(t)$ from attaining a vlaue of 1 during the pulse. Once the pulse is terminated, $PSC(t)$ begins to rise by diffusion. However, the rise is negligibly small since the free energy barrier is too strong/high to be overcome by diffusion.
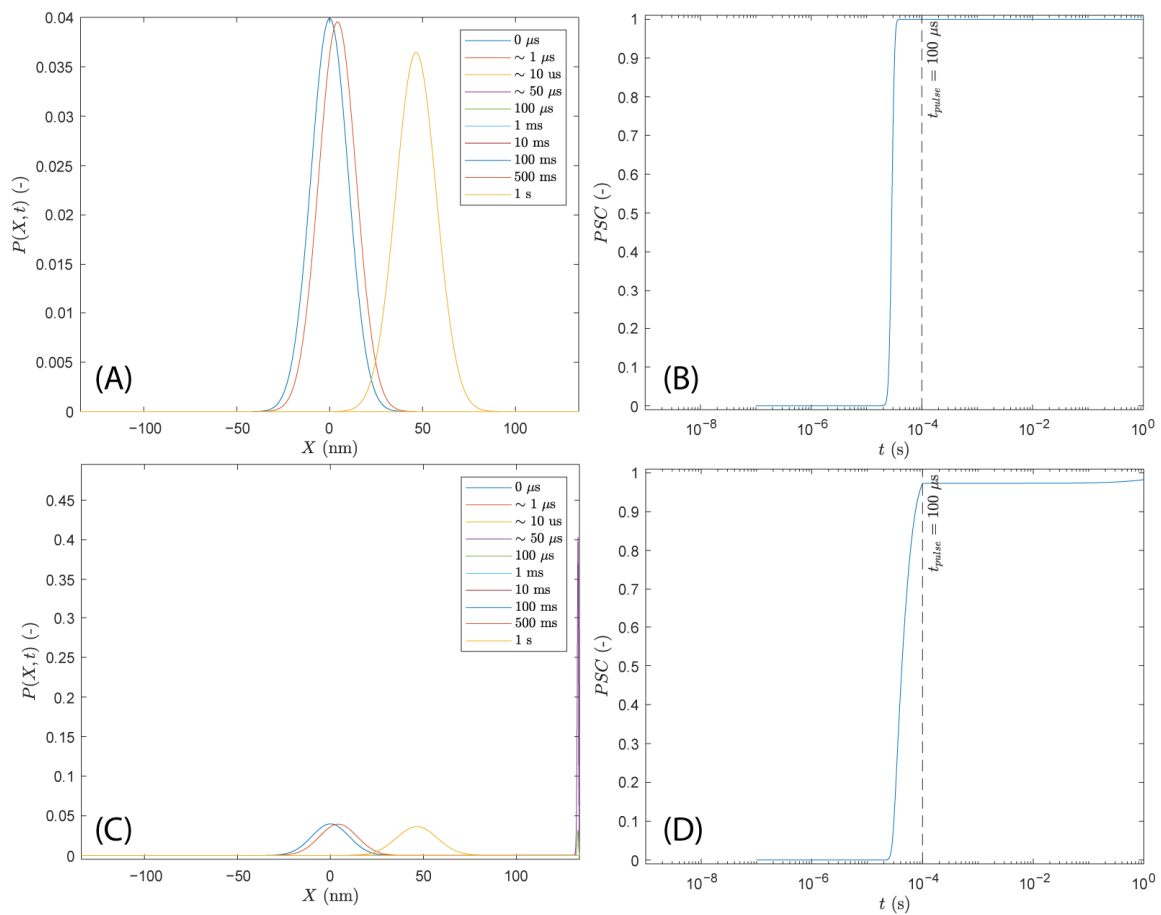
Figure 17. The 100 µs pulses: Evolution of $P(X, t)$ and the corresponding Probability of Successful Contact $PSC(t) = 1 - \int_{-B_L}^{+B_R} P(X, t)dX$ for B_L, B_R = 134 nm (500 µg/mL) for a 100 µs pulse at an electric field intensity of 1.25 kV/cm (Table 1 for C2C12 cells). (**A,B**) represent cases without free energy barrier and (**C,D**) represent cases with free energy barrier. The dashed lines in (**B,D**) represent the time at which the 100 µs pulse ends. For (A), $P(X, t) = 0$ in $X \in [B_L, B_R]$ for legends in $t \geq 50$ µs, as a result of which $P(X, t)$ is not visible in (A) for these values of t. For (C), $P(X, t) \sim 0$ in $X \in [B_L, B_R]$ for legends in $t \geq 1$ ms, as a result of which $P(X, t)$ is not visible in (C) for these values of t.

$PSC(t)$ is evaluated for (B_L, B_R) ranging from 77 nm to 433 nm, corresponding to concentrations ranging from 2500 µg/mL to 15 µg/mL, respectively, and is shown in Figure 18A for the case without the free energy barrier. For most ranges of (B_L, B_R) tested, $PSC(t)$ rises steeply through electrophoresis and attains a final value of 1 before the 100 µs pulse. For (B_L, B_R) = 433 nm (corresponding to the lowest concentration of 15 µg/mL), $PSC(t)$ just falls short of reaching a value of 1 before the 100 µs pulse's termination; however, $PSC(t)$ reaches a value of 1 post-pulse termination. The time at which $PSC(t)$ begins to rise depends on (B_L, B_R), and $PSC(t)$ starts to rise earlier for lower (B_L, B_R), i.e., for higher concentrations. For the 100 µs pulse, the rise in $PSC(t)$ happens before the termination of the pulse, unlike nanosecond and HF-BP pulses, where $PSC(t)$ rises post-pulse/burst termination through the diffusive process.
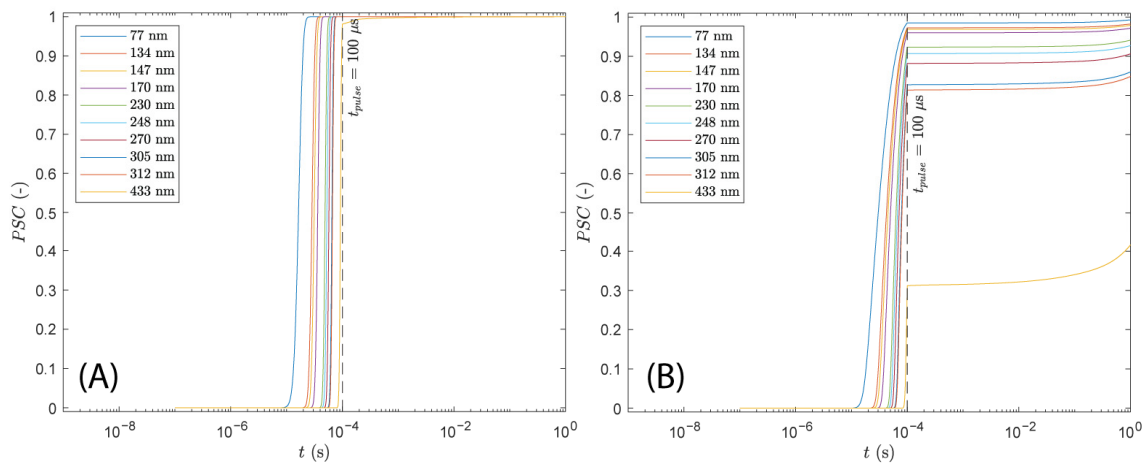
Figure 18. Evolution of $PSC(t)$ for different (B_L, B_R) ranging from 77 nm to 433 nm, corresponding to concentrations ranging from 2500 µg/mL to 15 µg/mL, for a 100 µs pulse at an electric field intensity of 1.25 kV/cm (Table 1 for C2C12 cells): (**A**) without free energy barrier and (**B**) with free energy barrier. Dashed lines represent the time at which the 100 µs pulse ends.

For the case with the free energy barrier (Figure 18B), $PSC(t)$ begins to rise before $t = 100$ µs and continues to rise until $t = 100$ µs (due to electrophoresis) for all (B_L, B_R) ranging from 77 nm to 433 nm, corresponding to concentrations ranging from 2500 µg/mL to 15 µg/mL, respectively. The rise is not as steep as it is for the case without the free energy barrier. Moreover, $PSC(t)$ does not attain a value of 1 at $t = 100$ µs, and the value of $PSC(t)$ at $t = 100$ µs depends on (B_L, B_R). After $t = 100$ µs (pulse termination), $PSC(t)$ increases slowly through the diffusive process. However, the post-pulse diffusive rise is small since diffusion is not strong enough to efficiently overcome the high free energy barrier.

These results indicate that even though the electrophoresis provided by the 100 µs pulse aids in overcoming the free energy barrier (as indicated by the higher $PSC(t)$ observed compared to the nanosecond and HF-BP pulses), they are not entirely sufficient to completely ensure that the pDNA molecule comes in contact with the cell membrane during pulse.

It is interesting to note that the final $PSC(t)$ before the onset of the second pulse, i.e., $PSC(t = 1 \text{ s})$ does not depend upon (B_L, B_R)/concentration for no free energy barrier (Figure 18A), whereas it depends on the (B_L, B_R)/concentration with the free energy barrier (Figure 18B). Therefore, similar to HF-BP pulses, depending on the presence of a free energy barrier and its strength/height, the results for the 100 µs pulse at an electric field strength of 1.25 kV/cm may depend on the concentration.

Furthermore, the Peclet number during a single phase (pulse + post-pulse) is $Pe = \dfrac{\mu E t_p}{\sqrt{2D t_{bp}}} = 0.33$, considering $t_p = 100$ µs, time between pulses $t_{bp} = 1$ s, and $E = 1.25$ kV/cm. Such a value of Peclet number, although < 1, does not convince us entirely of either electrophoresis or of diffusion dominating the process during the single phase (pulse + post-pulse). Therefore, there could be a confounding role of subsequent pulses, and individual pulses cannot be inferred in isolation. For the case with the free energy barrier, we expect the additional pulses to increase the probability of pDNA reaching the cell membrane and contribute to the further rise in $PSC(t)$. For the case without the free energy barrier, $PSC(t)$ already reaches 1 before 100 µs pulse termination, and $P(X, t) = 0$ in $X \in [-B_L, B_R]$ before the onset of the second pulse. As mentioned previously, the model does not account for the second (or additional) pulse. Therefore, additional pulses can be thought to add additional pDNA molecules to the cell membrane.

3.6.4. 5 ms Pulses

Equations (4) and (5) were solved using $B_L, B_R = 134$ nm (representing 500 µg/mL pDNA solution concentration) for a 5 ms pulse at an electric field intensity of 0.6 KV/cm

corresponding to experimental conditions for C2C12 cells (Table 1), and the results are shown in Figure 19A,B for the case without the free energy barrier and in Figure 19C,D for the case with the free energy barrier. For the case in which no free energy barrier is present, the evolution of $P(X,t)$ is shown in Figure 19A. Similar to a 100 µs pulse without a free energy barrier, electrophoresis with a 5 ms pulse drives the peak of $P(X,t)$ towards the cell membrane. The 5 ms pulse is long enough to ensure that the pDNA molecule is able to reach the cell membrane. This is also evident from the evolution of $PSC(t)$ in Figure 19B. $PSC(t)$ remains negligibly small until $t \sim 40$ µs and then suddenly rises to attain a final value of 1 well before the 5 ms pulse ends. For a 100 µs pulse without free energy barrier Figure 17B, $PSC(t)$ remains negligibly small until $t \sim 20$ µs, then rising suddenly to reach a final of 1. The difference in the time when $PSC(t)$ begins to rise can be explained by the difference in the electric field intensities used. For the 100 µs pulse, the electric field was 1.25 kV/cm, whereas for the 5 ms pulse, the electric field was 0.6 kV/cm. As a result, it takes approximately twice the amount of time for $PSC(t)$ to become non-negligible and then rise suddenly (steeply) for the 5 ms pulse conditions. $P(X,t) = 0$ in $X \in [B_L, B_R]$ for times $t > 50$ µs in Figure 19A, indicating that the pDNA has been absorbed by the cell membrane by this time.
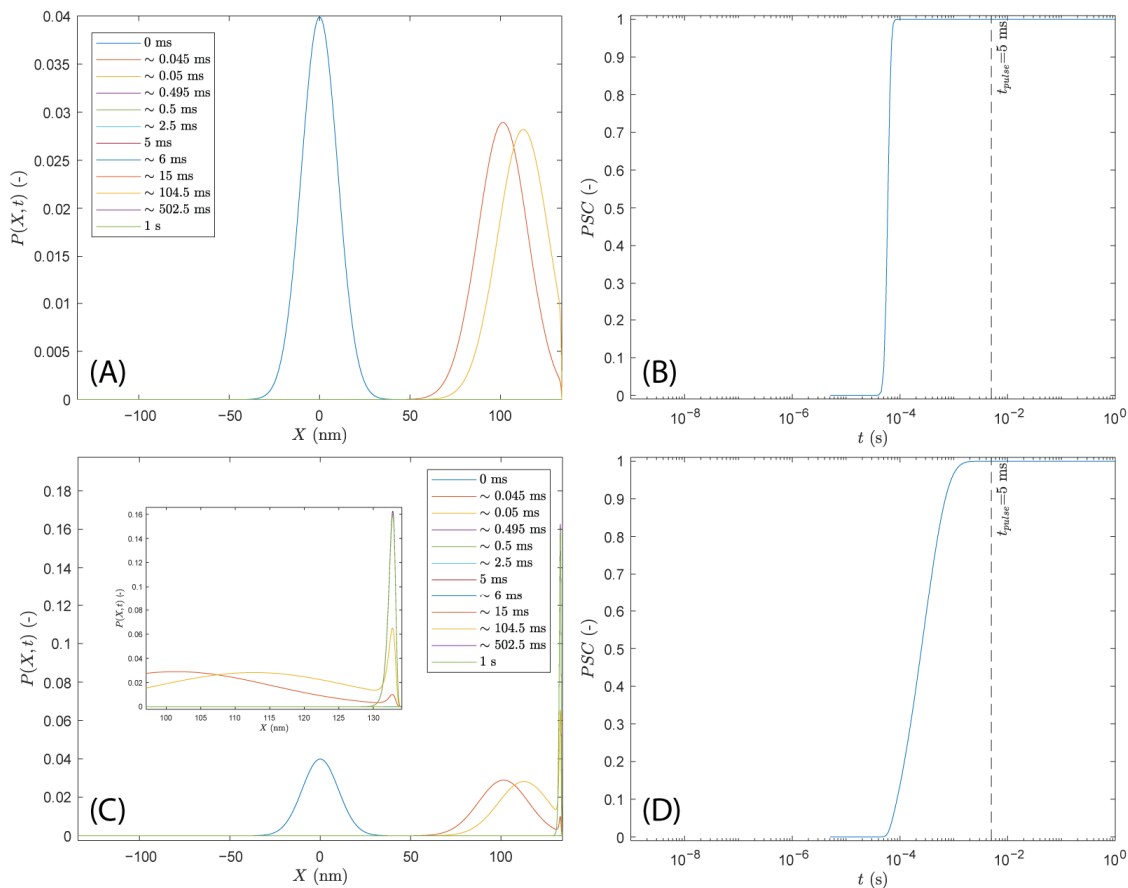

Figure 19. The 5 ms pulses: Evolution of $P(X,t)$ and the corresponding Probability of Successful Contact $PSC(t) = 1 - \int_{-B_L}^{+B_R} P(X,t)dX$ for $B_L, B_R = 134$ nm (500 µg/mL) for a 5 ms pulse at an electric field intensity of 0.6 kV/cm (Table 1 for C2C12 cells). (**A**,**B**) represent cases without free energy barrier and (**C**,**D**) represent cases with free energy barrier. The dashed lines in (**B**,**D**) represent the time at which the 5 ms pulse ends. For (**A**), $P(X,t) = 0$ in $X \in [B_L, B_R]$ for legends in $t \geq 0.495$ ms, as a result of which $P(X,t)$ is not visible in (**A**) for these values of t. For (**C**), $P(X,t) = 0$ in $X \in [B_L, B_R]$ for legends in $t \geq 2.5$ ms, as a result of which $P(X,t)$ is not visible in (**C**) for these values of t.

When a free energy barrier is present between the pDNA molecule and the cell membrane, similar to the 100 µs pulse, electrophoresis from the 5 ms pulses drives the

peak towards the cell membrane (Figure 19C). However, in the presence of the free energy barrier, when the $P(X,t)$ distribution reaches the cell membrane, electrophoresis is driving the probability for the pDNA to be absorbed at the cell membrane and, at the same time, the free energy barrier is preventing pDNA from being absorbed. This competition between electrophoresis and the free energy barrier leads to another peak of $P(X,t)$ being formed close to the cell membrane, which rises with time (Figure 19C at $t \sim 0.045$ ms and $t \sim 0.05$ ms, also note the difference in the scale of the Y-axis between Figure 19A,C). Eventually, the distribution of $P(X,t)$ becomes concentrated to a single peak with a narrow distribution (Figure 19C at $t \sim 0.495$ ms and inset). As electrophoresis continues to act, the probability of pDNA overcoming the free energy barrier and of pDNA being absorbed by the cell membrane increases, reducing the peak of narrow band $P(X,t)$ (Figure 19C at $t \sim 0.495$ ms and $t \sim 0.5$ ms and inset). Eventually, electrophoresis acts long enough to ensure that the pDNA molecule is absorbed by the cell membrane.

Similar inferences can be made from the evolution of $PSC(t)$ for the case with the free energy barrier (Figure 19D). $PSC(t)$ remains negligibly small until $t \sim 40$ μs and then begins to rise. Compared to the case without the free energy barrier (Figure 19B), the rise in $PSC(t)$ is slower, owing to the competing effect of electrophoresis and free energy barrier. Eventually, electrophoresis is able to overcome the free energy barrier, and $PSC(t)$ reaches a final value of 1 before the end of the pulse.

$PSC(t)$ is also evaluated for (B_L, B_R) ranging from 77 nm to 433 nm (representing 2500 μg/mL to 15 μg/mL pDNA solution concentration, respectively) and is shown in Figure 20A for the case without the free energy barrier. For all ranges of (B_L, B_R) tested, $PSC(t)$ rises steeply and attains a final value of 1 before pulse termination through electrophoresis. The time at which $PSC(t)$ begins to rise depends on (B_L, B_R), and $PSC(t)$ starts to rise earlier for lower (B_L, B_R) (i.e., higher concentrations). These observations are similar to the case without the free energy barrier for a 100 μs pulse (Figure 18A) and unlike for nanosecond pulses and HF-BP pulses, where $PSC(t)$ rises post-pulse/burst termination through the diffusive process (Figure 13A,C, Figures 15A and 16A).
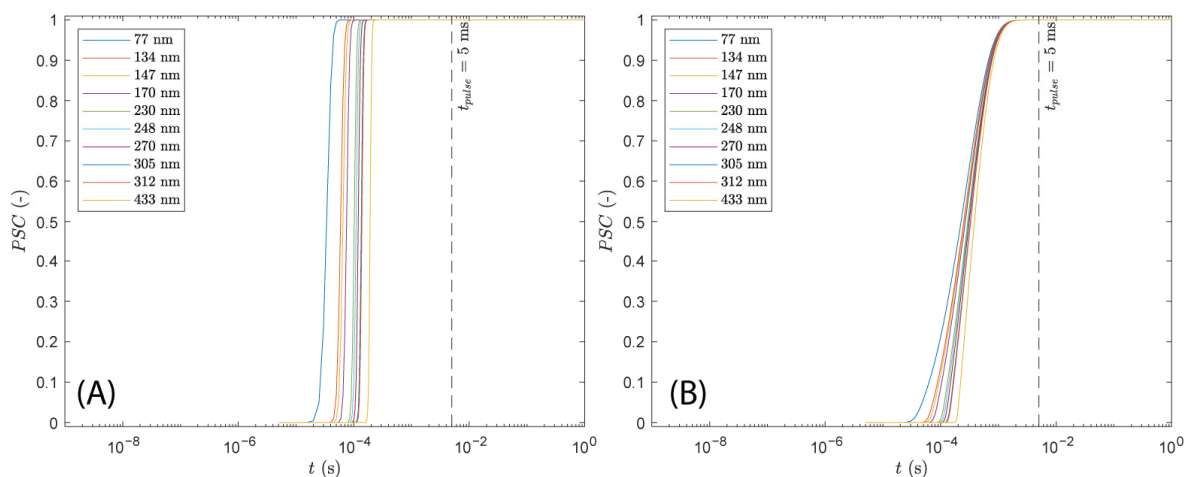

Figure 20. Evolution of $PSC(t)$ for different (B_L, B_R) ranging from 77 nm to 433 nm (corresponding to concentrations ranging from 2500 μg/mL to 15 μg/mL) for a 5 ms pulse at an electric field intensity of 0.6 kV/cm (Table 1 for C2C12 cells): (**A**) without free energy barrier and (**B**) with free energy barrier. Dashed lines represent the time at which the 5 ms pulse ends.

For the case with the free energy barrier, $PSC(t)$ begins to rise before pulse termination at $t = 5$ ms for (B_L, B_R) raning from 77 nm to 433 nm (representing 2500 μg/mL to 15 μg/mL pDNA solution concentration, respectively) (Figure 20B). The time at which $PSC(t)$ begins to rise depends on (B_L, B_R), and the rate of the rise in $PSC(t)$ is slower compared the case without the free energy barrier. For a 5 ms pulse at an electric field intensity of 0.6 kV/cm, the electrophoresis acts for a sufficient amount of time to ensure that $PSC(t)$ reaches a final

value of 1 before pulse termination for all (B_L, B_R) tested. This is unlike the case for a 100 μs pulse with the free energy barrier, where $PSC(t)$ could not attain a final value of 1 for the range of (B_L, B_R) tested, even though twice as strong of an electric field, with an intensity of 1.25 kV/cm, was applied.

The results in Figure 20 indicate that irrespective of the presence of free energy barrier, $PSC(t)$ reaches a final value of 1 before the 5 ms pulse termination for all (B_L, B_R) tested, indicating that GET should not depend on the concentration for these pulse parameters.

We can further calculate the Peclet number as $Pe = \frac{\mu E t_p}{\sqrt{2D t_{bp}}} = 7.95$; considering $t_p = 5$ ms, time between pulses $t_{bp} = 1$ s, and $E = 0.6$ kV/cm. $Pe = 7.95$ indicates that electrophoresis dominates diffusion during the phase (pulse + post pulse), and individual pulses cannot be inferred in isolation. However, the pulse duration is long enough to ensure that $PSC(t)$ reaches a final value of 1 before pulse termination for both – with and without the free energy barrier. So, even though the model does not account for multiple pulses since $P(X, t) = 0$ in $X \in [B_L, B_R]$ before the onset of the next pulse, subsequent pulses can be thought to add more pDNA molecules to the cell membrane.

4. Discussion

Electroporation with long pulses in vitro and in vivo is a well-established and efficient method for GET [55,66]. Most often, a train of pulses in the range of few to several tens of millisecond is used, although even shorter, i.e., 100–500 μs, pulses are used. With expanding the use of GET from in vitro to in vivo, the need to avoid pain and undesirable muscle contractions emerged. It was also suggested that electrochemical reactions could negatively affect GET efficiency [27–33]. The approval of cell therapies, where cells are transfected ex vivo, further strengthen the need to reduce electrochemical reactions during treatment because, usually, the number of available cells is low; consequently, it is important that most of the cells survive the treatment. Currently, when GET is performed ex vivo, the high voltage required for electroporation poses risks of cytotoxicity and loss of cytoplasmic content, which can adversely affect GET efficiency [67].

The use of shorter pulses in GET provides a potential mitigation of the above-mentioned drawbacks of long pulses, but the HF-BP and nanosecond pulse range remains poorly explored. Currently, there are only a few studies reporting the use of HF-BP and nanosecond pulses for GET [15,40,41]. Therefore, the aim of this study was to further explore the nanosecond range of pulse durations and HF-BP pulses. We aimed to find optimal parameters for GET with 200 ns and 500 ns pulses in two different cell lines and compare efficiency and expression dynamics of different pulse durations, up to 5 ms, including HF-BP. Since the electrophoretic effect of electric pulses on pDNA in GET is considered important, we also developed a theoretical framework of the diffusive and electrophoretic movement of pDNA during different pulse protocols and compared the results to those obtained experimentally.

4.1. Cell Membrane Permeabilization and Cell Survival

For GET, it is critical to use pulse parameters which achieve cell membrane permeabilization and at the same time maintain high cell survival. It was postulated that membrane permeabilization is prerequisite for successful GET. GET, however, is a complex process comprised of several consecutive steps, with cell membrane permeabilization alone not being a guarantee for successful GET [1,55]. Nevertheless, cell membrane permeabilization was first determined by using PI. Because the electric field at the intersection of the permeabilization and survival curves is not necessarily optimal also for GET, we also determined GET efficiency at slightly larger and slightly lower electric fields. With all tested pulse protocols, we were able to determine the optimal electric field for GET, which usually resulted in around 80% cell membrane permeabilization and higher than 60% cell survival. As expected, using longer pulses and/or higher numbers of applied pulses, cell membrane permeabilization was reached at lower electric fields [48,68]. The optimal electric field for GET was similar for both cell lines (Supplementary Tables S3 and S4). We electroporated

cells in suspension, which means they are of similar round shape, their size does not differ significantly (Table 1), and they are evenly distributed between electrodes, which all leads to a similar electric field needed for having the majority of cells permeabilized [69].

4.2. Effect of pDNA Concentration on Overall Gene Electrotransfer

The high concentration of pDNA can have a negative effect on cell survival [16] and consequently on GET efficiency, but it is also needed to obtain GET with nanosecond and HF-BP pulses [15,49]. Pathogen-associated molecular patterns that are associated with pDNA, for example, unmethylated CpG motifs in pDNA, can be recognized by TLR9 and can induce an innate immune response in tissue, which can lead to apoptosis activation [70,71]. pDNA concentrations used in our experiments were higher than concentrations usually used in in vitro experiments, which are most often between 10 and 100 µg/mL [14,72–75]. On the other hand, it has been shown that pDNA concentration affects GET efficiency and that, with higher pDNA concentration, efficient GET can also be achieved with shorter pulses [15,16,25,76]. The effect of the pDNA concentration was observed in our experiments, where a decreasing pDNA concentration led to a significant decrease in the overall GET. This was especially observed in 1306 fibroblasts, where, at pDNA concentrations up to 100 µg/mL, the overall GET was higher with 8×100 µs, HF-BP, and 8×5 ms pulses compared to 500 ns and 200 ns pulses, whereas, at 500 µg/mL of pDNA, there was no significant difference in the overall GET between different pulse protocols. Interestingly, this was not observed in C2C12 myoblasts where the overall GET rose with increasing pDNA concentration for all pulse protocols. At the highest pDNA concentration (500 µg/mL), the overall GET was, however, still significantly higher with longer pulse protocols (8×100 µs and 8×5 ms), where electrophoresis acts for a longer period of time compared to shorter pulse protocols (HF-BP, 500 ns, and 200 ns) (Figure 5). Difference in overall GET between two cell lines confirms that the efficiency of GET does not depend solely on parameters of applied pulses. GET is a multistep process including various intracellular mechanisms (cell membrane repair mechanism, DNA sensors activation, endocytic pathways, cytoskeleton reorganization) which can differ between cell lines [77,78].

Contrary to our previous results on a CHO cell line [15], in C2C12 myoblasts and 1306 fibroblasts, we observed some decrease in cell survival with increasing pDNA concentration, however, not for all pulse protocols. With 8×5 ms pulses, we did not observe a decrease in cell survival with increasing pDNA concentrations (in both cell lines). In addition, in C2C12 myoblasts, pDNA concentration did not have an effect on cell survival after GET with the HF-BP, 100×500 ns, and 25×200 ns pulse protocols. A decrease in cell survival with 250 µg/mL of pDNA was only observed in 1306 fibroblasts after the 8×100 µs pulse protocol; with other pulse protocols, decreased survival was observed only with the highest pDNA concentration, 500 µg/mL (Figure 4). Our results are similar to [79], where the authors observed decreased cell survival with pDNA concentrations higher than 400 µg/mL. However, the decrease in cell survival in our experiments was not high enough to cause a drop in the overall GET at 500 µg/mL of pDNA. These and our previous results [15] show that decreases in cell survival following GET with high pDNA concentration seem to be cell-line-dependent. pDNA by itself was not toxic to cells, as observed before [15,80]. High pDNA concentration could trigger a decrease in cell survival in different steps of GET. We have shown previously that higher pDNA concentration leads to larger pDNA aggregates formed on cell membrane [15] during pulse delivery, which could slow down or obstruct cell membrane repair. Furthermore, high pDNA concentration in endosomes or cytoplasm could activate endosomal and/or cytoplasmic DNA sensors which can induce programmed cell death [81]. Finally, cell death could be triggered by high number of pDNA copies in nucleus or by the high number of transgenes being produced [82].

4.3. Gene Electrotransfer Using Different Plasmid Sizes

Since pDNA size is reported to have an influence on GET efficiency, we compared GET, cell survival, and overall GET with a 4.7 kb and a 3.5 kb pDNA having the same CMV promoter and both encoding GFP. We did not observe any difference in GET and cell survival between different pDNA sizes. Interestingly, smaller pDNA led to higher overall GET only when using the 8×100 µs pulse protocol in both cell lines. For other pulse protocols, we did not observe a significant increase in the overall GET with smaller pDNA, although the copy number of smaller pDNA was 1.34 times higher compared to the larger pDNA, as we used the same concentration of pDNA (500 µg/mL) (Figure 6). Similarly, it was previously shown that GFP knockdown with pDNA sizes from 1.9 to 4.3 kb was equally efficient when the same moles of pDNA were used applying 2×30 ms pulses [83]. Our results show that smaller pDNA did not have a strong effect on overall GET, which is contrary to observations by [41], where they report higher sub-microsecond high-frequency GET with smaller pDNA. Reducing pDNA size also improved GET efficiency in other studies [84,85]. The difference in the size of the pDNA used in our study was only 25%, which might be the reason why we did not observe a significant increase in overall GET efficiency with smaller pDNA.

Interestingly, when comparing MFI of GFP-positive cells transfected with pDNA of different sizes in C2C12 myoblasts, a significantly higher MFI with smaller pDNA was observed after GET with the 200 ns, 500 ns, and HF-BP pulses. On the contrary, in 1306 fibroblasts, a higher MFI with smaller pDNA was observed after GET with 8×100 µs and 8×5 ms (Figure 7) pulses. This means that in C2C12 myoblasts, shorter pulses enabled more copies of smaller pDNA to reach the nucleus. With longer pulses, the MFIs after GET with both pDNA sizes were comparable. The situation seems to be reversed in 1306 fibroblasts, where longer pulses enabled more copies of smaller pDNA to reach the nucleus. This suggests that not only cell line and pDNA size but also pulse parameters influence the degree of transgene expression.

4.4. Effect of Pulse Parameters on Overall Gene Electrotransfer

We achieved GET in both cell lines with all pulse protocols, but with variable efficiency (Figure 8). Differences in GET efficiency between different cell lines have been reported before [86–88] and are still not well understood. It has been suggested that differences in GET efficiency can be the consequence of various biophysical factors such as the fluidity of the cell membrane or biological parameters such as different mechanisms that are present or activated in cells and the ability of cells to recover after the delivery of electric pulses [89,90]. If the difference would be the consequence of different cell membrane composition or fluidity or induced transmembrane voltage, then we would expect to also observe the difference in cell membrane permeabilization. Since permeabilization and survival curves were similar for both cell lines, the difference in GET efficiency is more likely the consequence of the difference in the presence and degree of activity of intrinsic cellular mechanisms and pathways. Furthermore, in in vitro experiments, the composition of the electroporation medium can also influence GET efficiency [91–93]. The GET of each cell line in our experiments was performed in their recommended growth medium. For C2C12 myoblasts, this was DMEM, and for 1306 fibroblasts, this was EMEM. They are both variations of basic medium used for primary and diploid cultures, but DMEM has a higher concentration of amino acids and vitamins compared to EMEM. DMEM also contains iron in the form of ferric sulfate, which is absent in EMEM [94].

We performed GET in growth medium, which is more like in vivo extracellular fluid compared to other buffers used for GET. Growth medium is highly conductive, which results in high currents and increased electrochemical reactions such as electrolysis, the generation of radicals, and the release of metal ions from the electrodes during pulse delivery [28,95]. It was shown previously that short, i.e., nanosecond, pulses and bipolar pulses decrease metal release from electrodes compared to longer pulses [29,35,48,96]. Furthermore, high medium conductivity also results in high currents, leading to heating

and temperature increases in the sample during pulse delivery. The temperature increase is more pronounced when longer or more pulses are applied [35]. In our experiments, the temperature of the sample never exceeded 32 °C, meaning that thermal effects were negligible (Supplementary Table S5).

In addition to achieving a higher percentage of transfected cells in 1306 fibroblasts, the MFI of the GFP-positive cells was higher (Figure 9). Fluorescence intensity is reported to be dependent on the number of pDNA copies inside the cell that have reached the cell nucleus and have been successfully transcribed and translated into fluorescent proteins [97,98]. In this respect, this could mean that the higher number of pDNA copies was transferred to 1306 fibroblasts during pulse delivery compared to C2C12 myoblasts. Other factors, such as the availability and degree of activity of the cellular machinery for transcription and translation, also affect production of proteins from transfected pDNA [97,98]. Based on this, higher GET efficiency in 1306 fibroblasts could also mean that the rate of pDNA transcription and translation into fluorescent protein is higher in 1306 fibroblasts compared to C2C12 myoblasts.

4.5. Time Dynamics of pDNA Expression

Measurements of pDNA expression every 8 h over a six-day period (Figures 10 and 11) show that the onsets of GFP expression (both percentage of GFP-positive cells and their MFI) are comparable for the 200 ns, HF-BP, 8 × 100 µs, and 8 × 5 ms pulse protocols but depend greatly on the cell line. Similar time dynamics of the GET and MFI for all pulse durations in one cell line suggest that all pulse protocols triggered the same mechanisms responsible for pDNA translocation through the cytoplasm to the cell nucleus.

In C2C12 myoblasts, the GFP-positive cells and their MFI reached a peak soon after GET and then declined steadily, falling below 10% for all four pulse durations at day 6. Similar time dynamics were observed for human mesenchymal stem cells [86]. On the contrary, in 1306 fibroblasts, peaks of the maximum GFP-positive cells and their MFI were broad and not very pronounced. After reaching a peak, the percentage of GFP-positive cells started to decrease slowly. On day 6 after GET with all pulse durations, around half of the cells were still GFP-positive (Figures 10 and 11). Differences in time dynamics and duration of transgene expression after GET between cell lines have been reported previously [99]. Differences in curves for the GET and MFI for all pulse protocols between cell lines suggest that mechanisms of pDNA translocation through the cytoplasm to the cell nucleus and the duration of the transcription of pDNA are most probably different in different cell lines.

The lower percentage of GFP-positive cells and their lower MFIs in C2C12 myoblasts could be a consequence of the higher number or degree of activation of DNA sensors in this cell line, which could trigger pDNA degradation to a larger extent compared to 1306 fibroblasts. During GET, pDNA could activate endosomal DNA sensors during translocation to the nucleus with endocytosis mediated pathways or cytoplasmic DNA sensors by entering the cell through cell membrane defects caused during pulse delivery. Additionally, cytosolic DNA sensors might be triggered by pDNA released to cytosol after endosomal escape. It was already shown that GET with pDNA led to the upregulation of several proposed cytosolic DNA sensors in different tumor cell types [78,100] and also in C2C12 myoblasts [82]. Other reasons for the observed decrease in transgene expression over time in C2C12 myoblasts could be the loss of the pDNA through the nuclear pores, loss of the pDNA at each mitosis, de novo pDNA methylation preventing pDNA transcription, or pDNA degradation by endonucleases [80].

We continuously observed differences in the overall GET and MFI between the two cell lines studied. These differences might be the consequence of variations in cell membrane composition [101], endocytic pathways specific to certain cell lines, or the degree of activation of endocytic pathways [102,103], as well as the presence of cytosolic nucleases [104].

Our results show that MFI of GFP-positive cells is more unpredictable and unrepeatable than the percentage of GFP-positive cells. The MFI of 1306 fibroblasts in our experiments with increasing pDNA concentration (Figure 3D) was much lower than the

MFI of 1306 fibroblasts transfected with the same concentration (500 µg/mL) of pDNA and with the same pulse protocols in the experiments of time dynamics of pDNA expression (Figure 11B). At the same time, the GET efficiency in both experiments was comparable with the same pulse protocols. Contrarily, in C2C12 myoblasts, the MFI was comparable in both experiments, but GET after 8×5 ms was much lower in the experiments of the time dynamics of the pDNA expression (Figure 10A) compared to the experiments with increasing pDNA concentration (Figure 3A). It was shown previously that the time after cell passage at which cells are exposed to electric pulses affects GET efficiency. The GET and MFI of all plasmid concentrations differed significantly when comparing cells transfected 24 h and 48 h after passage. The GET and MFI were higher in cells which were transfected 24 h after passage compared to cells transfected 48 h after passage. Observed differences in the transfection efficiency of the cells passaged at different times before the experiment could be the consequence of the differences in cell cycle phases at which GET was performed [79]. Biological factors, such as cell growth phase, which determine cell shape, size, and, probably most important, composition, and the integrity of the nuclear envelope play an important role in cell response to electric pulse delivery and the ability to repair damage after pulse delivery. During cell ageing, the cell membrane composition changes due to the increase in the total amount of proteins and cholesterol, potentially affecting cell membrane permeabilization [18,105]. In our experiments, we used cells 2–4 days after cell passage for GET, so this could be the reason for differences observed in GET and MFI of GFP-positive cells [79].

4.6. Modeling the Probability of pDNA Cell Membrane Contact during GET

From results of modeling the probability of pDNA cell membrane contact during GET, it can be inferred that the process of a pDNA molecule reaching the cell membrane and being absorbed by it is mediated by diffusion for 200 ns, 500 ns pulse and HF-BP pulses, whereas for the 100 µs and 5 ms pulse, the process is mediated by electrophoresis. As done in the results section, one can define a Peclet number as: $Pe = \frac{\mu E t_p}{\sqrt{2D t_{bp}}}$, where t_p is the pulse duration, t_{bp} is the duration between pulses, E is the electric field intensity, μ is the electrophoretic mobility and D is the diffusion coefficient. Alternatively, the time between pulses can be inferred as the frequency (f, Hz), in which case $Pe = \frac{\mu E t_p}{\sqrt{2D/f}}$. The values of Pe used in experiments, and mentioned in the results, are given again in Table 2. Such a Pe gives the relative contributions of electrophoresis and diffusion during the single phase of pulse/burst. Inferring the role of electrophoresis for different types of pulses used (ns, HF-BP, µs, and ms) using this parameter helps to correctly identify the role electrophoresis and diffusion as inferred from the model results.

Table 2. Values of Pe for various experimental conditions for C2C12 cells.

	200 ns	**500 ns**	**HF-BP**	**100 µs**	**5 ms**
Frequency, f (Hz)	10.00	10.00	1.00	1.00	1.00
t_{bp} (s)	0.10	0.10	1.00	1.00	1.00
t_p (s)	2×10^{-7}	5×10^{-7}	2×10^{-6}	1×10^{-4}	5×10^{-3}
E (kV/cm)	15.80	4.10	1.25	1.25	0.60
Pe	0.03	0.02	0.01	0.33	7.95

$Pe \ll 1$ for the 200 ns, 500 ns, and HF-BP pulses indicates the dominant role of diffusion in bringing the pDNA molecule to the cell membrane. For the 100 µs pulse, $Pe = 0.33$ or $Pe \sim 1$, indicating that neither diffusion nor electrophoresis dominates the process of pDNA coming in contact with the cell membrane. From the model results of the 100 µs pulse, we saw that $PSC(t)$ begins to rise sharply before $t = 100$ µs, for both–with and without the free energy barrier. It could be possible that for the range of (B_L, B_R) tested from 77 nm to 433 nm corresponding to concentrations from 2500 µg/mL

to 15 µg/mL, the pDNA molecule was close to the cell membrane, and electrophoresis played the dominant role in bringing the pDNA molecules to the cell membrane On further reducing the concentration to <15 µg/mL, one might find that electrophoresis is insufficient to bring the pDNA molecule close to the cell membrane. As already seen for (B_L, B_R) = 433 nm, corresponding to 15 µg/mL (Figure 18A,B), $PSC(t)$ begins to rise very close to pulse termination (dotted line in Figure 18A,B). Therefore, one can argue that for (B_L, B_R) > 433 nm (or concentrations < 15 µg/mL), electrophoresis will be insufficient to bring the pDNA molecule to the cell membrane, and the process will have to partly rely on diffusion, indicating the dominance of neither. For the 5 ms pulse, Pe = 7.95 indicates the dominant role of electrophoresis in bringing the pDNA molecule close to the cell membrane. This is also seen from Figure 20A,B, where $PSC(t)$ begins to rise and attains a value of 1 much before pulse termination for both—with and without the free energy barrier, indicating electrophoresis as the dominant mechanism.

For 200 ns, 500 ns, and HF-BP, the electric field acts for a short duration, which is not sufficient to drive the pDNA molecule to the cell membrane through electrophoresis. The pDNA molecule thus diffuses to the cell membrane, and the distance (l) that the pDNA molecule travels by diffusion variers with time as $l^2 \sim Dt$. Therefore, normalizing the time in Figure 13A,C for nanosecond pulses and in Figure 15A for HF-BP pulses with l^2 should collapse the curves for different domain lengths $l = (B_L, B_R)$ ranging from 77 nm to 433 nm (corresponding concentration ranging from 2500 µg/mL to 15 µg/mL). The normalization (and the corresponding collapse) is shown in Figure 21A for the 200 ns pulse, in Figure 21C for the 500 ns pulse, and in Figure 21E for the HF-BP pulses for the case without the free energy barrier. This collapse further indicates that the process for pDNA reaching the cell membrane in the absence of a free energy barrier is purely diffusive for 200 ns, 500 ns, and HF-BP pulses.

For the case with the free energy barrier for 200 ns, 500 ns, and HF-BP pulses (Figures 13B,D and 15B), normalizing the time with l^2 does not produce a good collapse. Rather, normalizing with l collapses all the curves onto a single master curve (Figure 21B,D,F). Such a collapse with l indicates that the process for 200 ns, 500 ns, and HF-BP pulses with the free energy barrier is not entirely diffusive.

For 100 µs and 5 ms pulses without the free energy barrier, the process of pDNA reaching the cell membrane is electrophoretic for (B_L, B_R) ranging from 77 nm to 433 nm (corresponding concentration ranging from 2500 µg/mL to 15 µg/mL). The electrophoretic distance traveled by the pDNA molecule in the presence of an electric field is given by $l = \mu Et$; therefore, normalizing the curves with l in Figures 18A and 20A should collapse them into a single master curve. The collapse is shown as $PSC(t)$ vs. t/l in Figure 21G for the 100 µs pulse and in Figure 21I for the 5 ms pulse. This indicates that the process by which the pDNA molecule establishes contact with the cell membrane in the absence of the free energy barrier is driven by electrophoresis for 100 µs and 5 ms pulses.

For 100 µs and 5 ms pulses, in the case when the free energy barrier is present, we can follow the same process of normalizing the curves in Figures 18B and 20B by l and check the collapse. This is shown in Figure 21H,J for the 100 µs and 5 ms pulse, respectively. As can be seen from these figures, the collapse for times t when $PSC(t)$ begins to rise is good; however, for later times or far larger $PSC(t)$, the collapse is not satisfactory. This indicates that in the presence of free energy barrier, the process by which the pDNA molecule moves close to the cell membrane (since that is when $PSC(t)$ begins to rise) is driven by electrophoresis. However, the process of a pDNA molecule coming into contact with the cell membrane by overcoming the free energy barrier is not entirely electrophoretic. It is observed from Figure 20B that $PSC(t)$ is already collapsed for late times (i.e., for $PSC(t)$ close to 1) without normalizing, implying that $PSC(t)$ is independent of $l = (B_L, B_R)$ for the range of l tested between 77 nm and 433 nm.
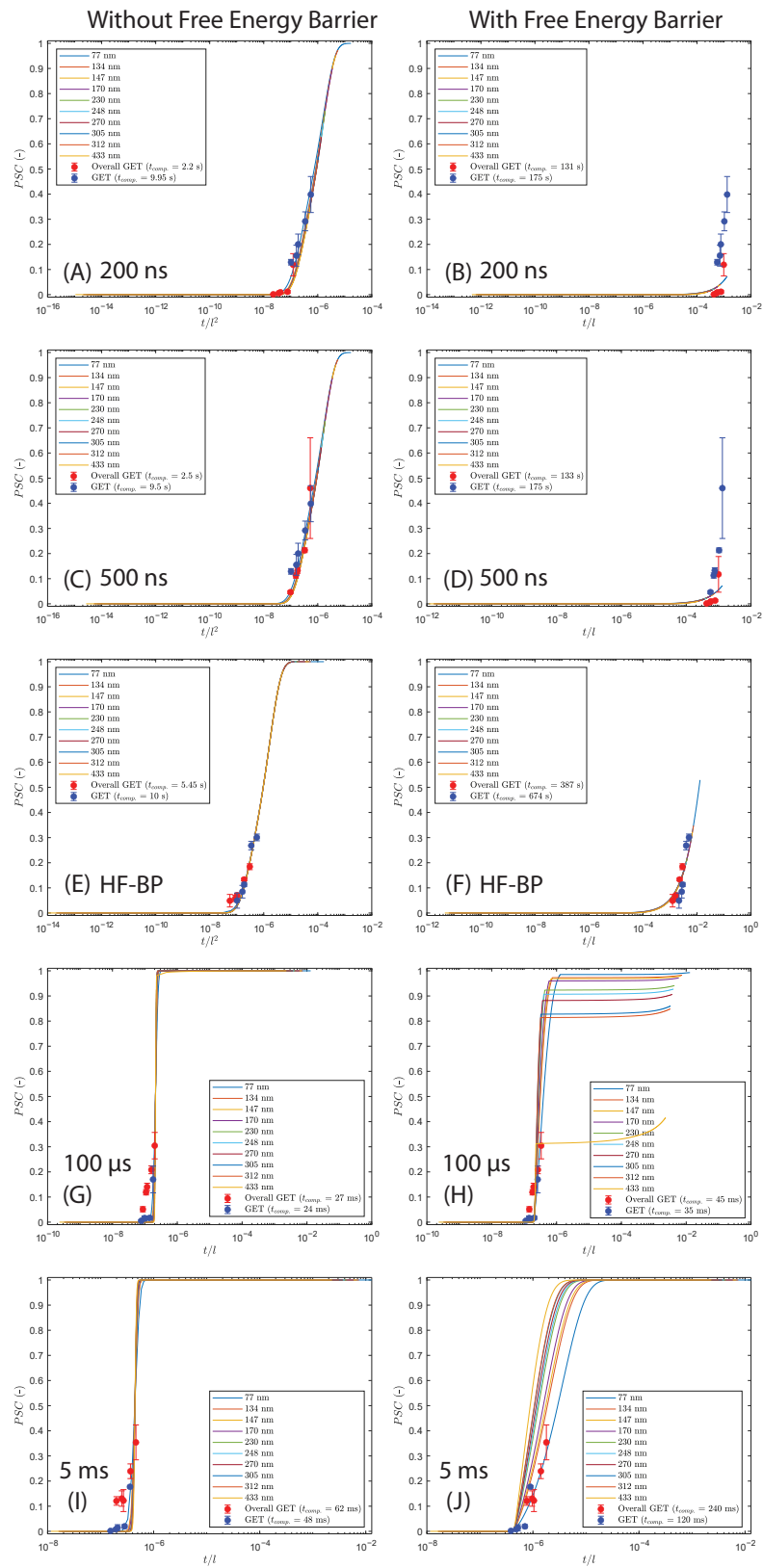
Figure 21. (**A**) Results for 200 ns pulse in Figure 13A plotted as $PSC(t)$ vs. t/l^2; (**B**) Results for 200 ns pulse in Figure 13B plotted as $PSC(t)$ vs. t/l; (**C**) Results for 500 ns pulse in Figure 13C plotted as $PSC(t)$ vs. t/l^2; (**D**) Results for 500 ns pulse in Figure 13D plotted as $PSC(t)$ vs. t/l; (**E**) Results for HF-BP pulses in Figure 15A plotted as $PSC(t)$ vs. t/l^2; (**F**) Results for HF-BP pulses in Figure 15B

plotted as $PSC(t)$ vs. t/l; (**G**) Results for 100 μs pulse in Figure 18A plotted as $PSC(t)$ vs. t/l; (**H**) Results for 100 μs pulse in Figure 18B plotted as $PSC(t)$ vs. t/l; (**I**) Results for 5 ms pulse in Figure 20A plotted as $PSC(t)$ vs. t/l; (**J**) Results for 5 ms pulse in Figure 20B plotted as $PSC(t)$ vs. t/l. Also shown as dots are Overall GET (Figure 5) and GET (Figure 3) for C2C12 cells plotted against $t_{competent}/l^2$ or against $t_{competent}/l$, where l for the corresponding concentration was taken as R_{DNA} from Supplementary Table S1 and $t_{competent}$ was determined by fitting Overall GET/GET to $PSC(t)$ for $l = 77$ nm.

Also shown in Figure 21A–J are the results for overall GET and GET for the respective pulse parameters. Overall GET (Figure 5) and GET (Figure 3) for C2C12 myoblasts are plotted against $t_{competent}/l$ or against $t_{competent}/l^2$. Values of l for the respective concentrations are taken from R_{DNA} from Supplementary Table S1. $t_{competent}$ is taken to be the time for which the cell membrane remains competent to accept/absorb the incoming pDNA molecule. $t_{competent}$ was determined by varying $t_{competent}$ and minimizing the root mean squared error (RMSE) between Overall GET/GET vs. $t_{competent}/l^2$ and $PSC(t)$ vs. t/l^2 (at $l = 77$ nm) in Figure 21A,C,E. For Figure 21B,D,F,G–J, $t_{competent}$ was determined by varying $t_{competent}$ and minimizing the root mean squared error (RMSE) between Overall GET/GET vs. $t_{competent}/l$ and $PSC(t)$ vs. t/l (at $l = 77$ nm). $l = 77$ nm was chosen since the curves are collapsed for various values of l, and fitting to $l = 77$ nm would imply fitting to all the collapsed curves. The best fit values are given in the legends in Figure 21A–J against their respective Overall GET and GET.

It should be noted that this exercise of plotting Overall GET/GET vs. $t_{competent}/l^2$ or $t_{competent}/l$ along with $PSC(t)$ vs. t/l^2 or t/l should not be considered as a direct one-to-one comparison between the model and the experiment. Such an exercise is only performed to place the experiments within the context of the model. Overall GET and GET cannot be directly compared to $PSC(t)$, as overall GET and GET represent efficiencies which also include downstream processes of pDNA translocation across the cell membrane, migration through the cytoplasm, entering the nucleus, transcription, translation, and protein expression. $PSC(t)$, on the other hand, only represents the probability of pDNA establishing contact with the cell membrane. However, in a first approximation, only those cells on which pDNA molecules have established contact with the cell membrane can be expected to be transfected. Therefore, $PSC(t)$ can be considered as an upper limit of transfection efficiency. Moreover, different durations of pulses (short nanosecond pulses, HF-BP, or long micro- and millisecond pulses) can permeabilize the cell membrane in different ways. This can in turn result in the cell membrane being competent in different ways to absorb the pDNA molecule for different durations of pulses. Different durations of pulses can also alter the free energy barrier between the pDNA and the cell membrane, further influencing the results. Different types of cells themselves can be sensitive in different ways to permeabilization by the pulses, yielding different transfection efficiencies, as seen in Figure 3 for C2C12 myoblasts and 1306 fibroblasts. The models based on $PSC(t)$ do not account for such parameters and differences. An experimental observable that can perhaps be better compared to the $PSC(t)$ could therefore be the fraction of cells forming pDNA aggregates on the cell membrane [21,56].

From the fitting parameters of $t_{competent}$ in Figure 21A–J, it can be observed that $t_{competent}$ for 200 ns, 500 ns, and HF-BP, where the process is diffusive, is much larger than $t_{competent}$ for 100 μs and 5 ms pulses, where the process is mainly electrophoretic. Absolute values $t_{competent}$ cannot be considered, as $t_{competent}/l$ or $t_{competent}/l^2$ are not non-dimensional; however, from fitting, $t_{competent}$ for 200 ns, 500 ns, and HF-BP is around two orders of magnitude larger than $t_{competent}$ for 100 μs and 5 ms pulses. Furthermore, adding a free energy barrier between the pDNA and the cell membrane shifts the rise in $PSC(t)$ vs. t/l^2 or t/l to the right, indicating that it is harder for the pDNA molecule to be absorbed by the cell membrane in the presence of free energy. One can then argue that the cell membrane needs to be competent for a longer amount of time in the presence of a free energy barrier to absorb the incoming pDNA molecule. As a result, larger $t_{competent}$ was

observed for the cases with free energy barrier (Figure 21B,D,F,H,J) compared to the cases without free energy barrier (Figure 21A,C,E,G,I).

To determine the time it takes for the pDNA molecule to reach the cell membrane by diffusion or by electrophoresis, some estimates can be considered. The time it takes for the pDNA molecule to reach the cell membrane at a distance l by diffusion is given by $t = l^2/2D$ (for 200 ns, 500 ns, and HF-BP pulses), whereas time it takes for the pDNA molecule to reach the cell membrane at distance l by electrophoresis is given by $t = l/\mu E$ (for 100 µs and 5 ms pulse). These estimates are given in Figure 22 for l ranging from 77 nm to 433 nm, corresponding to concentrations ranging from 2500 µg/mL to 15 µg/mL. E is taken as 0.6 kV/cm for the 5 ms pulse and 1.25 kV/cm for the 100 µs pulse. One can observe that the time it takes for pDNA to reach the cell membrane by diffusion varies from around $O(1)$ ms (for l = 77 nm, 2500 µg/mL) to around $O(100)$ ms (for l = 433 nm, 15 µg/mL). For electrophoresis, the time it takes to reach the cell membrane varies from around $O(0.01)$ ms (for l = 77 nm, 2500 µg/mL) to $O(0.1)$ ms (for l = 433 nm, 15 µg/mL). It can be inferred that the cell membrane should be competent for at least $O(100)$ ms, i.e., $t_{competent} \sim 100$ ms, for transfection by 200 ns, 500 ns, and HF-BP pulses, whereas the cell membrane should be competent for at least $O(0.1)$ ms, i.e., $t_{competent} \sim 100$ µs, for transfection by 100 µs and 5 ms pulses. There is a 2–3 orders of magnitude difference in $t_{competent}$ for 200 ns, 500 ns, and HF-BP and $t_{competent}$ for 100 µs and 5 ms pulses, as also inferred from the fitting parameters in Figure 21.
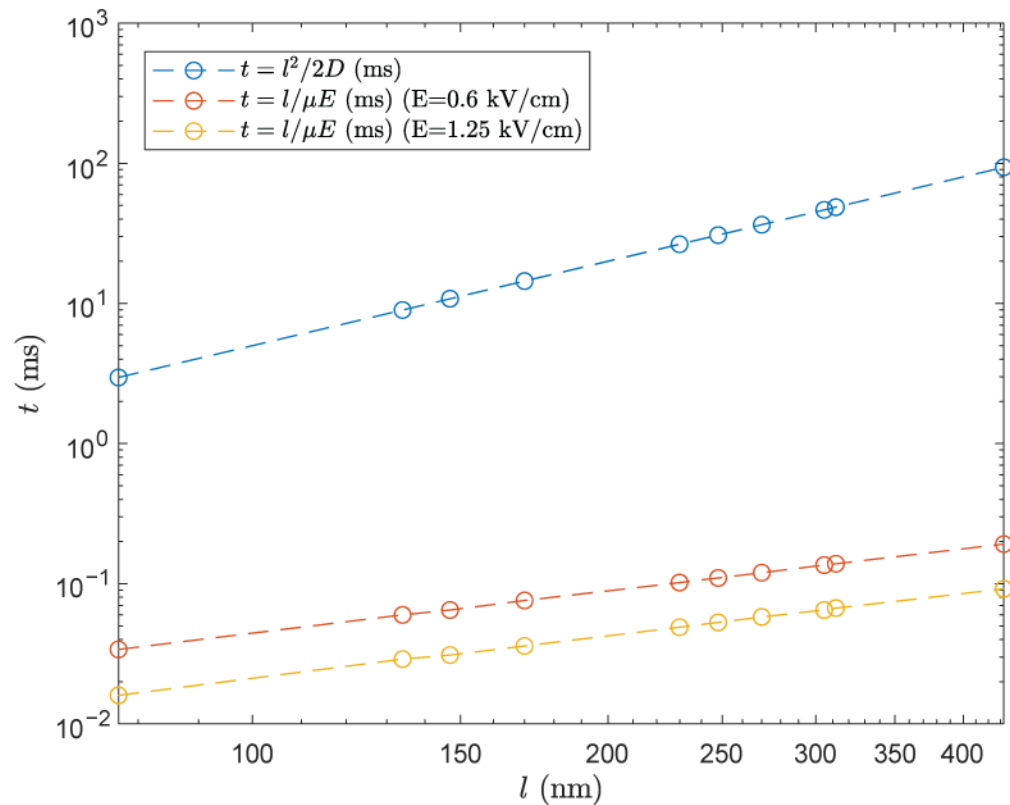

Figure 22. Time it takes for a pDNA molecule to cover a distance by diffusion and by electrophoresis. l ranges from 77 nm too 433 nm, corresponding to concentrations ranging from 2500 µg/mL to 15 µg/mL.

One can also observe from Figure 21 that for very large values of t/l or t/l^2, $PSC(t)$ reaches a final value of 1, and the results should not depend on l (or concentration). That is, if the cell membrane is able to absorb the pDNA molecule for a very large amount of time, then irrespective of l (or concentration), the pDNA molecule will have an equally high probability of reaching the cell membrane. Since we see a concentration dependence

for 200 ns, 500 ns, and HF-BP pulses, one can argue that $t_{competent}$ is around $O(1-100)$ ms, since this the amount of time it takes for the pDNA to reach the cell membrane by diffusion (Figure 22). The time it takes for the pDNA to reach the cell membrane by electrophoresis is $O(0.01-0.1)$ ms (Figure 22). For a large $t_{competent}$ of around $O(1-100)$ ms, we should not observe a concentration dependence for 100 µs and 5 ms pulses. However, since we do observe a concentration dependence for Overall GET and GET for 100 µs and 5 ms pulses, it could be that the $t_{competent}$ is different—and shorter (around $O(0.01-0.1)$ ms)—for these pulses. It has been observed experimentally that the cell membrane remains permeable for a longer amount of time with ns pulses compared to µs and ms pulses [48].

Recently, 300 ns pulses have been successfully used for GET [106]. However, 100 pulses were used at a pulse repetition frequency of 1 MHz. This high frequency of pulse repetition, or the corresponding short duration between successive pulses, could imply that the cumulative effect of 100 pulses at 1 MHz pulse repetition frequency is equivalent to a single pulse of duration 100 µs. To test this, Equation (4) was solved for 100 pulses of duration 300 ns and an electric field intensity of 7 kV/cm at a pulse repetition frequency of 1 MHz and a pDNA cell membrane distance of 170 nm (corresponding to 250 µg/mL, Supplementary Table S1), similar to the conditions used in [106]. The evolution of $P(X,t)$ is shown in Figure 23 for pulse numbers 1, 5, 10, 20, and 30. From Figure 23A, it can be seen that during the first pulse, the peak shifts towards the right due to electrophoresis (until 300 ns) and also spreads only slightly due to diffusion. After the cessation of first pulse, the peak stays at the same place, and the distribution spreads only slightly due to diffusion from 300 ns to 1 µs. During the second pulse, this peak is then further driven to the right by electrophoresis, spreading only slightly by diffusion. After the end of the second pulse, the distribution spreads only slightly by diffusion, until the time the third pulse acts and the process repeats (see Figure 23B for pulse number 5). By the 10th pulse, the peak of the distribution has already migrated a distance greater than 50 nm towards the right, spreading only slightly by diffusion (as seen by a broadening of $P(X,t)$ and a decrease in the maximum value of $P(X,t)$) (Figure 23C). By pulse number 20 (starting at $t = 19$ µs), the peak of the distribution has already drifted to the right by $\sim$150 nm by electrophoresis indicating a non negligible $PSC(t)$ by $t \sim$19 µs (Figure 23D,F). Figure 23E, corresponding to the 30th pulse (or $t = 29$ µs), indicates that the pDNA molecule has already been absorbed at the cell membrane as $P(X,t) = 0$ in $X \in [B_L, B_R]$ by $t = 29$ µs. This is further evident from Figure 23F, which shows that $PSC(t)$ has risen sharply and reached a final value of 1 before $t \sim 30$ µs.

The results in Figure 23 corresponding to the high frequency of 1 MHz differ from the results of Figure 12 corresponding to the low frequency of 10 Hz. In both cases, electrophoresis drives the peak of $P(X,t)$ towards the right (cell membrane) during the pulse while spreading it only slightly by diffusion. Once the pulse ends, the distribution of $P(X,t)$ is allowed to spread by diffusion. For the low frequency of 10 Hz case, the time between the subsequent pulses or the time allowed for the distribution to relax by diffusion is significantly higher ($t \sim 100$ ms). This large time allows the spread of $P(X,t)$ by diffusion and flattens it out in a way that enough flux of $P(X,t)$ can be collected at the cell membrane and $PSC(t)$ starts to rise by diffusion. However, for the high frequency of 1 MHz, the time between subsequent pulses or the time allowed for the distribution to relax by diffusion is small, corresponding to $t < 1$ µs. This time is too small for the distribution of $P(X,t)$ to spread by diffusion and reach the cell membrane. Soon after, the next pulse acts on the pDNA molecule driving the still narrow $P(X,t)$ distribution to the right. Cumulatively, this is how $P(X,t)$ is driven to the right by electrophoresis; if enough pulses are delivered (in this case $\sim$20), the pDNA molecule reaches the cell membrane by electrophoresis, as seen by the early and sharp rise in $PSC(t)$.
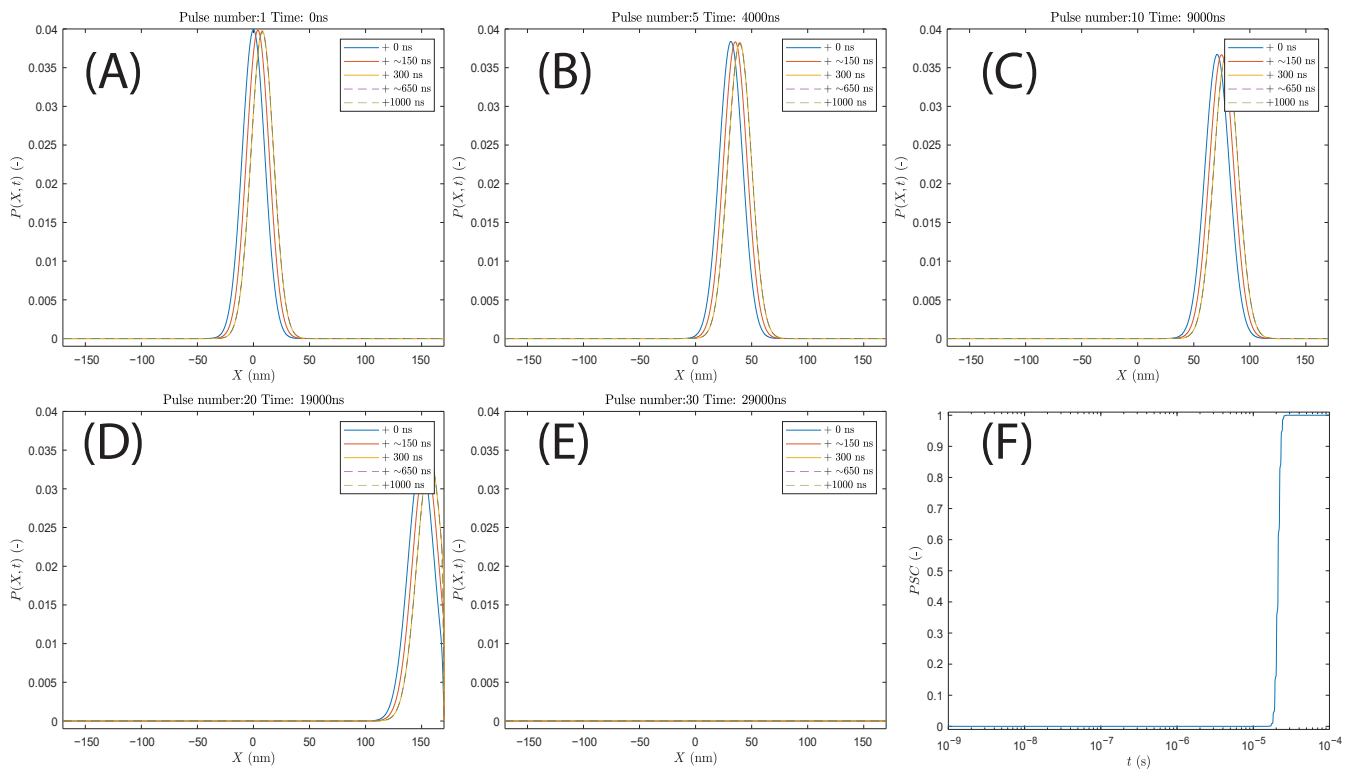
Figure 23. (**A–E**) Evolution of $P(X, t)$ without free energy barrier (Equation (4)) for 100 pulses of 300 ns and 7 kV/cm applied at a high frequency of 1 MHz and for a pDNA and cell membrane distance of 170 nm (corresponding to 250 µg/mL). The pulse numbers for each pulse and corresponding time are shown on top of (**A–E**). Solid lines indicate the during pulse $P(X, t)$ and dotted lines represent after pulse $P(X, t)$. (**F**) Evolution of $PSC(t)$ without free energy barrier.

The process of high-frequency ns pulses can also be analyzed from the point of view of Peclet number defined as $Pe = \frac{\mu E t_p}{\sqrt{2D/f}}$. For experimental conditions in [106], $t_p = 300$ ns, $E = 7$ kV/cm, and $f = 1$ MHz, which gives $Pe = 5.57$, indicating that electrophoresis is dominating the transport of pDNA to the cell membrane, and multiple pulses at such a high pulse repetition frequency can be thought of as a single long pulse providing the electrophoresis. For the experimental conditions in this work, $t_p = 200$ ns, $E = 15.8$ kV/cm, $f = 10$ Hz, and $Pe = 0.03$ (see Table 2), indicating that the pDNA molecule reaches the cell membrane predominantly by diffusion. Thus, the Peclet number defined as $Pe = \frac{\mu E t_p}{\sqrt{2D/f}}$ can be used as useful parameter to infer the role of electrophoresis and diffusion for a variety of pulses used in this work and in [106].

5. Conclusions

In summary, we showed that GET can also be achieved with nanosecond pulses (with low pulse repetition rate, i.e., 10 Hz) in addition to widely used millisecond and microsecond pulses and previously shown HF-BP pulses. GET efficiency depends on pDNA concentration, cell line, and pulse parameters. In our experiments, smaller pDNA did not significantly improve GET efficiency, but it had an effect on the degree of transgene expression. We showed that the time dynamics of transgene expression are comparable between millisecond, microsecond, HF-BP, and nanosecond pulses but differ greatly between the two cell lines. A simple mathematical model of the probability of pDNA and cell membrane contact during GET shows that pDNA migration for nanosecond (at low repetition frequency) and HF-BP pulses is dominated by diffusion, and for micro- and millisecond pulses, the process is dominated by electrophoresis. A Peclet (*Pe*) number has been defined that can be used to infer the role of diffusion and electrophoresis in a wide

variety of pulsing conditions. However, for the process of pDNA molecules coming into contact with the cell membrane in the presence of a strong free energy barrier close to the cell membrane, the role of diffusion and electrophoresis cannot be isolated as effectively. Nevertheless, the migration of pDNA close to the cell membrane can still be inferred based on electrophoresis and diffusion. The developed model and modeling results can provide valuable guidance for further experiments and interpretations of results obtained by various pulse protocols.

Supplementary Materials: The following supporting information can be downloaded at: https://www.mdpi.com/article/10.3390/app12168237/s1, Figure S1: Schematic of distribution of pDNA molecules and cells in suspension; Figure S2: Comparison of permeabilization and survival curves of C2C12 myoblast and 1306 fibroblasts with 200 ns pulses and 10 Hz pulse repetition rate; Figure S3: Comparison of permeabilization and survival curves of C2C12 myoblast and 1306 fibroblasts with 500 ns pulses and 10 Hz pulse repetition rate; Figure S4: Comparison of MFI of permeabilized C2C12 myoblast and 1306 fibroblasts; Figure S5: Comparison of permeabilization, survival curves, and MFI of C2C12 myoblast and 1306 fibroblasts with 8×100 μs and 8×5 ms pulses; Figure S6: Comparison of permeabilization, survival curves, and MFI of C2C12 myoblast and 1306 fibroblasts with HF-BP pulses; Table S1: Various estimates of the distance between a pDNA molecule and the nearest cell membrane (R_{DNA}); Table S2: Various estimates of the distance between a DNA molecule and the nearest cell membrane and between two pDNA molecules; Table S3: Nanosecond, HF-BP, micro and millisecond pulse protocols with which the best overall GET with 500 μg/mL of pEGFP-N1 was achieved in C2C12 myoblasts; Table S4: Nanosecond, HF-BP, micro and millisecond pulse protocols with which the best overall GET with 500 μg/mL of pEGFP-N1 was achieved in 1306 fibroblasts; Table S5: Maximum temperature increases of the cell sample during pulse delivery. References [107,108] are cited in the supplementary materials.

Institutional Review Board Statement: Not applicable.

Informed Consent Statement: Not applicable.

Data Availability Statement: Data are available from the corresponding author on request.

Conflicts of Interest: The authors declare no conflict of interest. The funders had no role in the design of the study, in the collection, analyses or interpretation of data; in the writing of the manuscript, or in the decision to publish the results.

References

1. Rosazza, C.; Haberl Meglic, S.; Zumbusch, A.; Rols, M.-P.; Miklavcic, D. Gene Electrotransfer: A Mechanistic Perspective. *Curr. Gene Ther.* **2016**, *16*, 98–129. [CrossRef] [PubMed]
2. Sokołowska, E.; Błachnio-Zabielska, A.U. A Critical Review of Electroporation as a Plasmid Delivery System in Mouse Skeletal Muscle. *Int. J. Mol. Sci.* **2019**, *20*, 2776. [CrossRef] [PubMed]

3. Fajrial, A.K.; He, Q.Q.; Wirusanti, N.I.; Slansky, J.E.; Ding, X. A Review of Emerging Physical Transfection Methods for CRISPR/Cas9-Mediated Gene Editing. *Theranostics* **2020**, *10*, 5532–5549. [CrossRef] [PubMed]

4. Folegatti, P.M.; Bittaye, M.; Flaxman, A.; Lopez, F.R.; Bellamy, D.; Kupke, A.; Mair, C.; Makinson, R.; Sheridan, J.; Rohde, C.; et al. Safety and Immunogenicity of a Candidate Middle East Respiratory Syndrome Coronavirus Viral-Vectored Vaccine: A Dose-Escalation, Open-Label, Non-Randomised, Uncontrolled, Phase 1 Trial. *Lancet Infect. Dis.* **2020**, *20*, 816–826. [CrossRef]

5. Morrow, M.P.; Kraynyak, K.A.; Sylvester, A.J.; Shen, X.; Amante, D.; Sakata, L.; Parker, L.; Yan, J.; Boyer, J.; Roh, C.; et al. Augmentation of Cellular and Humoral Immune Responses to HPV16 and HPV18 E6 and E7 Antigens by VGX-3100. *Mol. Ther. Oncolytics* **2016**, *3*, 16025. [CrossRef] [PubMed]

6. Topol, E.J. Messenger RNA Vaccines against SARS-CoV-2. *Cell* **2021**, *184*, 1401. [CrossRef] [PubMed]

7. Algazi, A.P.; Twitty, C.G.; Tsai, K.K.; Le, M.; Pierce, R.; Browning, E.; Hermiz, R.; Canton, D.A.; Bannavong, D.; Oglesby, A.; et al. Phase II Trial of IL-12 Plasmid Transfection and PD-1 Blockade in Immunologically Quiescent Melanoma. *Clin. Cancer Res.* **2020**, *26*, 2827–2837. [CrossRef] [PubMed]

8. Bhatia, S.; Longino, N.V.; Miller, N.J.; Kulikauskas, R.; Iyer, J.G.; Ibrani, D.; Blom, A.; Byrd, D.R.; Parvathaneni, U.; Twitty, C.G.; et al. Intratumoral Delivery of Plasmid IL12 via Electroporation Leads to Regression of Injected and Noninjected Tumors in Merkel Cell Carcinoma. *Clin. Cancer Res.* **2020**, *26*, 598–607. [CrossRef] [PubMed]

9. Heller, R.; Heller, L.C. Gene Electrotransfer Clinical Trials. *Adv. Genet.* **2015**, *89*, 235–262. [CrossRef]

10. Geboers, B.; Scheffer, H.J.; Graybill, P.M.; Ruarus, A.H.; Nieuwenhuizen, S.; Puijk, R.S.; Van Den Tol, P.M.; Davalos, R.V.; Rubinsky, B.; De Gruijl, T.D.; et al. *High-Voltage Electrical Pulses in Oncology: Irreversible Electroporation, Electrochemotherapy, Gene Electrotransfer, Electrofusion, and Electroimmunotherapy*; Radiological Society of North America (RSNA): Oak Brook, IL, USA, 2020; Volume 295, pp. 254–272.

11. Alzubi, J.; Lock, D.; Rhiel, M.; Schmitz, S.; Wild, S.; Mussolino, C.; Hildenbeutel, M.; Brandes, C.; Rositzka, J.; Lennartz, S.; et al. Automated Generation of Gene-Edited CAR T Cells at Clinical Scale. *Mol. Ther. Methods Clin. Dev.* **2021**, *20*, 379–388. [CrossRef]

12. Mingozzi, F.; High, K.A. Immune Responses to AAV in Clinical Trials. *Curr. Gene Ther.* **2011**, *11*, 321–330. [CrossRef] [PubMed]

13. Stewart, M.P.; Sharei, A.; Ding, X.; Sahay, G.; Langer, R.; Jensen, K.F. In Vitro and Ex Vivo Strategies for Intracellular Delivery. *Nature* **2016**, *538*, 183–192. [CrossRef] [PubMed]

14. Haberl, S.; Kandušer, M.; Flisar, K.; Hodžić, D.; Bregar, V.B.; Miklavčič, D.; Escoffre, J.M.; Rols, M.P.; Pavlin, M. Effect of Different Parameters Used for in Vitro Gene Electrotransfer on Gene Expression Efficiency, Cell Viability and Visualization of Plasmid DNA at the Membrane Level. *J. Gene Med.* **2013**, *15*, 169–181. [CrossRef]

15. Potočnik, T.; Miklavčič, D.; Maček Lebar, A. Gene Transfer by Electroporation with High Frequency Bipolar Pulses in Vitro. *Bioelectrochemistry* **2021**, *140*, 107803. [CrossRef] [PubMed]

16. Chopra, S.; Ruzgys, P.; Maciulevičius, M.; Jakutavičiute, M.; Šatka, S. Investigation of Plasmid DNA Delivery and Cell Viability Dynamics for Optimal Cell Electrotransfection in Vitro. *Appl. Sci.* **2020**, *10*, 6070. [CrossRef]

17. Gehl, J.; Mir, L.M. Determination of Optimal Parameters for in Vivo Gene Transfer by Electroporation, Using a Rapid in Vivo Test for Cell Permeabilization. *Biochem. Biophys. Res. Commun.* **1999**, *261*, 377–380. [CrossRef]

18. Young, J.L.; Dean, D.A. Electroporation-Mediated Gene Delivery. *Adv. Genet.* **2015**, *89*, 49–88. [CrossRef]

19. Čemažar, M.; Jarm, T.; Miklavčič, D.; Lebar, A.M.; Ihan, A.; Kopitar, N.A.; Serša, G. Effect of Electric-Field Intensity on Electropermeabilization and Electrosensitivity of Various Tumor-Cell Lines in vitro. *Electro Magn.* **1998**, *17*, 263–272. [CrossRef]

20. Faurie, C.; Rebersek, M.; Golzio, M.; Kanduser, M.; Escoffre, J.M.; Pavlin, M.; Teissie, J.; Miklavcic, D.; Rols, M.P. Electro-Mediated Gene Transfer and Expression Are Controlled by the Life-Time of DNA/Membrane Complex Formation. *J. Gene Med.* **2010**, *12*, 117–125. [CrossRef]

21. Sachdev, S.; Feijoo Moreira, S.; Keehnen, Y.; Rems, L.; Kreutzer, M.T.; Boukany, P.E. DNA-Membrane Complex Formation during Electroporation Is DNA Size-Dependent. *Biochim. Biophys. Acta Biomembr.* **2020**, *1862*, 183089. [CrossRef]

22. Wu, M.; Yuan, F. Membrane Binding of Plasmid DNA and Endocytic Pathways Are Involved in Electrotransfection of Mammalian Cells. *PLoS ONE* **2011**, *6*, e20923. [CrossRef] [PubMed]

23. Wang, L.; Miller, S.E.; Yuan, F. Ultrastructural Analysis of Vesicular Transport in Electrotransfection. *Microsc. Microanal.* **2018**, *24*, 553–563. [CrossRef] [PubMed]

24. Rosazza, C.; Deschout, H.; Buntz, A.; Braeckmans, K.; Rols, M.P.; Zumbusch, A. Endocytosis and Endosomal Trafficking of DNA After Gene Electrotransfer In Vitro. *Mol. Ther. Nucleic Acids* **2016**, *5*, e286. [CrossRef] [PubMed]

25. Pavlin, M.; Flisar, K.; Kandušer, M. The Role of Electrophoresis in Gene Electrotransfer. *J. Membr. Biol.* **2010**, *236*, 75–79. [CrossRef] [PubMed]

26. André, F.M.; Gehl, J.; Sersa, G.; Préat, V.; Hojman, P.; Eriksen, J.; Golzio, M.; Cemazar, M.; Pavselj, N.; Rols, M.P.; et al. Efficiency of High- and Low-Voltage Pulse Combinations for Gene Electrotransfer in Muscle, Liver, Tumor, and Skin. *Hum. Gene Ther.* **2008**, *19*, 1261–1271. [CrossRef]

27. Sano, M.B.; Fan, R.E.; Cheng, K.; Saenz, Y.; Sonn, G.A.; Hwang, G.L.; Xing, L. Reduction of Muscle Contractions during Irreversible Electroporation Therapy Using High-Frequency Bursts of Alternating Polarity Pulses: A Laboratory Investigation in an Ex Vivo Swine Model. *J. Vasc. Interv. Radiol.* **2018**, *29*, 893–898.e4. [CrossRef]

28. Chafai, D.E.; Mehle, A.; Tilmatine, A.; Maouche, B.; Miklavčič, D. Assessment of the Electrochemical Effects of Pulsed Electric Fields in a Biological Cell Suspension. *Bioelectrochemistry* **2015**, *106*, 249–257. [CrossRef]

29. Vižintin, A.; Vidmar, J.; Ščančar, J.; Miklavčič, D. Effect of Interphase and Interpulse Delay in High-Frequency Irreversible Electroporation Pulses on Cell Survival, Membrane Permeabilization and Electrode Material Release. *Bioelectrochemistry* **2020**, *134*, 107523. [CrossRef]

30. Klein, N.; Guenther, E.; Botea, F.; Pautov, M.; Dima, S.; Tomescu, D.; Popescu, M.; Ivorra, A.; Stehling, M.; Popescu, I. The Combination of Electroporation and Electrolysis (E2) Employing Different Electrode Arrays for Ablation of Large Tissue Volumes. *PLoS ONE* **2019**, *14*, e0221393. [CrossRef]

31. Maglietti, F.; Michinski, S.; Olaiz, N.; Castro, M.; Suárez, C.; Marshall, G. The Role of Ph Fronts in Tissue Electroporation Based Treatments. *PLoS ONE* **2013**, *8*, e80167. [CrossRef]

32. Olaiz, N.; Signori, E.; Maglietti, F.; Soba, A.; Suárez, C.; Turjanski, P.; Michinski, S.; Marshall, G. Tissue Damage Modeling in Gene Electrotransfer: The Role of PH. *Bioelectrochemistry* **2014**, *100*, 105–111. [CrossRef] [PubMed]

33. Turjanski, P.; Olaiz, N.; Maglietti, F.; Michinski, S.; Suárez, C.; Molina, F.V.; Marshall, G. The Role of PH Fronts in Reversible Electroporation. *PLoS ONE* **2011**, *6*, e17303. [CrossRef] [PubMed]

34. Sano, M.B.; Arena, C.B.; Bittleman, K.R.; Dewitt, M.R.; Cho, H.J.; Szot, C.S.; Saur, D.; Cissell, J.M.; Robertson, J.; Lee, Y.W.; et al. Bursts of Bipolar Microsecond Pulses Inhibit Tumor Growth. *Sci. Rep.* **2015**, *5*, 14999. [CrossRef]

35. Mahnič-Kalamiza, S.; Miklavčič, D. Scratching the Electrode Surface: Insights into a High-Voltage Pulsed-Field Application from in Vitro & in Silico Studies in Indifferent Fluid. *Electrochim. Acta* **2020**, *363*, 137187. [CrossRef]

36. Yao, C.; Dong, S.; Zhao, Y.; Lv, Y.; Liu, H.; Gong, L.; Ma, J.; Wang, H.; Sun, Y. Bipolar Microsecond Pulses and Insulated Needle Electrodes for Reducing Muscle Contractions during Irreversible Electroporation. *IEEE Trans. Biomed. Eng.* **2017**, *64*, 2924–2937. [CrossRef]

37. Mercadal, B.; Arena, C.B.; Davalos, R.V.; Ivorra, A. Avoiding Nerve Stimulation in Irreversible Electroporation: A Numerical Modeling Study. *Phys. Med. Biol.* **2017**, *62*, 8060–8079. [CrossRef]

38. Aycock, K.N.; Zhao, Y.; Lorenzo, M.F.; Davalos, R.V. A Theoretical Argument for Extended Interpulse Delays in Therapeutic High-Frequency Irreversible Electroporation Treatments. *IEEE Trans. Biomed. Eng.* **2021**, *68*, 1999–2010. [CrossRef]

39. Cvetkoska, A.; Maček-Lebar, A.; Trdina, P.; Miklavčič, D.; Reberšek, M. Muscle Contractions and Pain Sensation Accompanying High-Frequency Electroporation Pulses. *Sci. Rep.* **2022**, *12*, 8019. [CrossRef] [PubMed]

40. Ruzgys, P.; Novickij, V.; Novickij, J.; Šatkauskas, S. Nanosecond Range Electric Pulse Application as a Non-Viral Gene Delivery Method: Proof of Concept. *Sci. Rep.* **2018**, *8*, 15502. [CrossRef]

41. Novickij, V.; Balevičiūtė, A.; Ruzgys, P.; Šatkauskas, S.; Novickij, J.; Zinkevičienė, A.; Girkontaitė, I. Sub-Microsecond Electrotransfection Using New Modality of High Frequency Electroporation. *Bioelectrochemistry* **2020**, *136*, 107594. [CrossRef]

42. Chang, A.Y.; Liu, X.; Tian, H.; Hua, L.; Yang, Z.; Wang, S. Microfluidic Electroporation Coupling Pulses of Nanoseconds and Milliseconds to Facilitate Rapid Uptake and Enhanced Expression of DNA in Cell Therapy. *Sci. Rep.* **2020**, *10*, 6061. [CrossRef]

43. Thompson, G.L.; Roth, C.C.; Kuipers, M.A.; Tolstykh, G.P.; Beier, H.T.; Ibey, B.L. Permeabilization of the Nuclear Envelope Following Nanosecond Pulsed Electric Field Exposure. *Biochem. Biophys. Res. Commun.* **2016**, *470*, 35–40. [CrossRef]

44. Batista Napotnik, T.; Reberšek, M.; Vernier, P.T.; Mali, B.; Miklavčič, D. Effects of High Voltage Nanosecond Electric Pulses on Eucaryotic Cells (in Vitro): A Systematic Review. *Bioelectrochemistry* **2016**, *110*, 1–12. [CrossRef]

45. Beebe, S.J.; Blackmore, P.F.; White, J.; Joshi, R.P.; Schoenbach, K.H. Nanosecond Pulsed Electric Fields Modulate Cell Function through Intracellular Signal Transduction Mechanisms. *Physiol. Meas.* **2004**, *25*, 1077–1093. [CrossRef]

46. Chopinet, L.; Batista-Napotnik, T.; Montigny, A.; Rebersek, M.; Teissié, J.; Rols, M.P.; Miklavčič, D. Nanosecond Electric Pulse Effects on Gene Expression. *J. Membr. Biol.* **2013**, *246*, 851–859. [CrossRef] [PubMed]

47. Guo, S.; Jackson, D.L.; Burcus, N.I.; Chen, Y.J.; Xiao, S.; Heller, R. Gene Electrotransfer Enhanced by Nanosecond Pulsed Electric Fields. *Mol. Ther. Methods Clin. Dev.* **2014**, *1*, 14043. [CrossRef] [PubMed]

48. Vižintin, A.; Marković, S.; Ščančar, J.; Miklavčič, D. Electroporation with Nanosecond Pulses and Bleomycin or Cisplatin Results in Efficient Cell Kill and Low Metal Release from Electrodes. *Bioelectrochemistry* **2021**, *140*, 107798. [CrossRef]

49. Novickij, V.; Balevičiute, A.; Malysko, V.; Želvys, A.; Radzevičiute, E.; Kos, B.; Zinkeviciene, A.; Miklavčič, D.; Novickij, J.; Girkontaite, I. Effects of Time Delay between Unipolar Pulses in High Frequency Nano-Electrochemotherapy. *IEEE Trans. Biomed. Eng.* **2022**, *69*, 1726–1732. [CrossRef]

50. Schoenbach, K.H.; Beebe, S.J.; Buescher, E.S. Intracellular Effect of Ultrashort Electrical Pulses. *Bioelectromagnetics* **2001**, *22*, 440–448. [CrossRef] [PubMed]

51. Tekle, E.; Oubrahim, H.; Dzekunov, S.M.; Kolb, J.F.; Schoenbach, K.H.; Chock, P.B. Selective Field Effects on Intracellular Vacuoles and Vesicle Membranes with Nanosecond Electric Pulses. *Biophys. J.* **2005**, *89*, 274–284. [CrossRef] [PubMed]

52. Napotnik, T.B.; Wu, Y.H.; Gundersen, M.A.; Miklavčič, D.; Vernier, P.T. Nanosecond Electric Pulses Cause Mitochondrial Membrane Permeabilization in Jurkat Cells. *Bioelectromagnetics* **2012**, *33*, 257–264. [CrossRef] [PubMed]

53. Vernier, P.T.; Sun, Y.; Marcu, L.; Salemi, S.; Craft, C.M.; Gundersen, M.A. Calcium Bursts Induced by Nanosecond Electric Pulses. *Biochem. Biophys. Res. Commun.* **2003**, *310*, 286–295. [CrossRef] [PubMed]

54. Ford, W.E.; Ren, W.; Blackmore, P.F.; Schoenbach, K.H.; Beebe, S.J. Nanosecond Pulsed Electric Fields Stimulate Apoptosis without Release of Pro-Apoptotic Factors from Mitochondria in B16f10 Melanoma. *Arch. Biochem. Biophys.* **2010**, *497*, 82–89. [CrossRef] [PubMed]

55. Sachdev, S.; Potočnik, T.; Rems, L.; Miklavčič, D. Revisiting the Role of Pulsed Electric Fields in Overcoming the Barriers to in Vivo Gene Electrotransfer. *Bioelectrochemistry* **2022**, *144*, 107994. [CrossRef] [PubMed]

56. Golzio, M.; Teissié, J.; Rols, M.P. Direct Visualization at the Single-Cell Level of Electrically Mediated Gene Delivery. *Proc. Natl. Acad. Sci. USA* **2002**, *99*, 1292–1297. [CrossRef] [PubMed]

57. Muthukumar, M. Polymer Translocation. Murugappan. Available online: https://books.google.si/books?hl=sl&lr=&id=PcuT-ibRtRIC&oi=fnd&pg=PP1&dq=Muthukumar,+Murugappan.+Polymer+translocation.+CRC+press,+2016.&ots=K0bz9eAsWT&sig=LYEClwUyYngqBXZ5CsyHdcy3Wjc&redir_esc=y#v=onepage&q=Muthukumar%2C (accessed on 9 June 2022).

58. Yu, M.; Tan, W.; Lin, H. A Stochastic Model for DNA Translocation through an Electropore. *Biochim. Biophys. Acta Biomembr.* **2012**, *1818*, 2494–2501. [CrossRef] [PubMed]

59. Sachdev, S.; Muralidharan, A.; Choudhary, D.K.; Perrier, D.L.; Rems, L.; Kreutzer, M.T.; Boukany, P.E. DNA Translocation to Giant Unilamellar Vesicles during Electroporation Is Independent of DNA Size. *Soft Matter* **2019**, *15*, 9187–9194. [CrossRef] [PubMed]

60. Sweeney, D.C.; Reberšek, M.; Dermol, J.; Rems, L.; Miklavčič, D.; Davalos, R.V. Quantification of Cell Membrane Permeability Induced by Monopolar and High-Frequency Bipolar Bursts of Electrical Pulses. *Biochim. Biophys. Acta Biomembr.* **2016**, *1858*, 2689–2698. [CrossRef]

61. Bosnjak, M.; Lorente, B.C.; Pogacar, Z.; Makovsek, V.; Cemazar, M. Different Incubation Times of Cells after Gene Electrotransfer in Fetal Bovine Serum Affect Cell Viability, but Not Transfection Efficiency. *J. Membr. Biol.* **2014**, *247*, 421–428. [CrossRef] [PubMed]

62. Delteil, C.; Teissié, J.; Rols, M.P. Effect of Serum on in Vitro Electrically Mediated Gene Delivery and Expression in Mammalian Cells. *Biochim. Biophys. Acta Biomembr.* **2000**, *1467*, 362–368. [CrossRef]

63. Antipina, A.Y.; Gurtovenko, A.A. Molecular-Level Insight into the Interactions of DNA with Phospholipid Bilayers: Barriers and Triggers. *RSC Adv.* **2016**, *6*, 36425–36432. [CrossRef]

64. Stellwagen, N.C.; Gelfi, C.; Righetti, P.G. The Free Solution Mobility of DMA. Available online: https://onlinelibrary.wiley.com/doi/epdf/10.1002/%28SICI%291097-0282%28199711%2942%3A6%3C687%3A%3AAID-BIP7%3E3.0.CO%3B2-Q (accessed on 9 June 2022).

65. Portet, T.; Favard, C.; Teissié, J.; Dean, D.S.; Rols, M.P. Insights into the Mechanisms of Electromediated Gene Delivery and Application to the Loading of Giant Vesicles with Negatively Charged Macromolecules. *Soft Matter* **2011**, *7*, 3872–3881. [CrossRef]

66. Potter, H.; Heller, R. Transfection by Electroporation. *Curr. Protoc. Mol. Biol.* **2018**, *2018*, 9.3.1–9.3.13. [CrossRef] [PubMed]

67. Atsavapranee, E.S.; Billingsley, M.M.; Mitchell, M.J. Delivery Technologies for T Cell Gene Editing: Applications in Cancer Immunotherapy. *EBioMedicine* **2021**, *67*, 103354. [CrossRef] [PubMed]

68. Pucihar, G.; Krmelj, J.; Reberšek, M.; Napotnik, T.B.; Miklavčič, D. Equivalent Pulse Parameters for Electroporation. *IEEE Trans. Biomed. Eng.* **2011**, *58*, 3279–3288. [CrossRef] [PubMed]

69. Vera-Tizatl, C.E.; Talamás-Rohana, P.; Vera-Hernández, A.; Leija-Salas, L.; Rodríguez-Cuevas, S.A.; Chávez-Munguía, B.; Vera-Tizatl, A.L. Cell Morphology Impact on the Set-up of Electroporation Protocols for in-Suspension and Adhered Breast Cancer Cells. *Electromagn. Biol. Med.* **2020**, *39*, 323–339. [CrossRef] [PubMed]

70. Harris, E.; Elmer, J.J. Optimization of Electroporation and Other Non-Viral Gene Delivery Strategies for T Cells. *Biotechnol. Prog.* **2021**, *37*, e3066. [CrossRef] [PubMed]

71. Michieletto, D.; Lusic, M.; Marenduzzo, D.; Orlandini, E. Physical Principles of Retroviral Integration in the Human Genome. *Nat. Commun.* **2019**, *10*, 575. [CrossRef] [PubMed]

72. Pavlin, M.; Kandušer, M. New Insights into the Mechanisms of Gene Electrotransfer—Experimental and Theoretical Analysis. *Sci. Rep.* **2015**, *5*, 9132. [CrossRef] [PubMed]

73. Zhang, Z.; Qiu, S.; Zhang, X.; Chen, W. Optimized DNA Electroporation for Primary Human T Cell Engineering. *BMC Biotechnol.* **2018**, *18*, 4. [CrossRef]

74. Yu, L.; Reynaud, F.; Falk, J.; Spencer, A.; Di Ding, Y.; Baumlé, V.; Lu, R.; Castellani, V.; Yuan, C.; Rudkin, B.B. Highly Efficient Method for Gene Delivery into Mouse Dorsal Root Ganglia Neurons. *Front. Mol. Neurosci.* **2015**, *8*, 2. [CrossRef] [PubMed]

75. Markowicz, S.; Niedzielska, J.; Kruszewski, M.; Ołdak, T.; Gajkowska, A.; Machaj, E.K.; Kurzak, H.; Pojda, Z. Nonviral Transfection of Human Umbilical Cord Blood Dendritic Cells Is Feasible, but the Yield of Dendritic Cells with Transgene Expression Limits the Application of This Method in Cancer Immunotherapy. *Acta Biochim. Pol.* **2006**, *53*, 203–211. [CrossRef] [PubMed]

76. Kandušer, M.; Miklavčič, D.; Pavlin, M. Mechanisms Involved in Gene Electrotransfer Using High- and Low-Voltage Pulses—An in Vitro Study. *Bioelectrochemistry* **2009**, *74*, 265–271. [CrossRef] [PubMed]

77. Frandsen, S.K.; McNeil, A.K.; Novak, I.; McNeil, P.L.; Gehl, J. Difference in Membrane Repair Capacity Between Cancer Cell Lines and a Normal Cell Line. *J. Membr. Biol.* **2016**, *249*, 569–576. [CrossRef] [PubMed]

78. Znidar, K.; Bosnjak, M.; Cemazar, M.; Heller, L.C. Cytosolic DNA Sensor Upregulation Accompanies DNA Electrotransfer in B16.F10 Melanoma Cells. *Mol. Ther. Nucleic Acids* **2016**, *5*, e322. [CrossRef] [PubMed]

79. Chopra, S.; Ruzgys, P.; Maciulevičius, M.; Šatkauskas, S. Effect of Cell Passage Time on the Electrotransfection Efficiency. *Biol. Bull.* **2020**, *47*, 441–447. [CrossRef]

80. Lesueur, L.L.; Mir, L.M.; André, F.M. Overcoming the Specific Toxicity of Large Plasmids Electrotransfer in Primary Cells In Vitro. *Mol. Ther. Nucleic Acids* **2016**, *5*, e291. [CrossRef] [PubMed]

81. Zahid, A.; Ismail, H.; Li, B.; Jin, T. Molecular and Structural Basis of DNA Sensors in Antiviral Innate Immunity. *Front. Immunol.* **2020**, *11*, 3094. [CrossRef] [PubMed]

82. Semenova, N.; Bosnjak, M.; Markelc, B.; Znidar, K.; Cemazar, M.; Heller, L. Multiple Cytosolic DNA Sensors Bind Plasmid DNA after Transfection. *Nucleic Acids Res.* **2019**, *47*, 10235–10246. [CrossRef] [PubMed]

83. Hornstein, B.D.; Roman, D.; Arévalo-Soliz, L.M.; Engevik, M.A.; Zechiedrich, L. Effects of Circular DNA Length on Transfection Efficiency by Electroporation into HeLa Cells. *PLoS ONE* **2016**, *11*, e0167537. [CrossRef] [PubMed]
84. Molnar, M.J.; Gilbert, R.; Lu, Y.; Liu, A.B.; Guo, A.; Larochelle, N.; Lochmuller, H.; Petrof, B.J.; Nalbantoglu, J.; Karpati, G. Factors Influencing the Efficacy, Longevity, and Safety of Electroporation-Assisted Plasmid-Based Gene Transfer into Mouse Muscles. *Mol. Ther.* **2004**, *10*, 447–455. [CrossRef] [PubMed]
85. Ribeiro, S.; Mairhofer, J.; Madeira, C.; Diogo, M.M.; Lobato Da Silva, C.; Monteiro, G.; Grabherr, R.; Cabral, J.M. Plasmid DNA Size Does Affect Nonviral Gene Delivery Efficiency in Stem Cells. *Cell. Reprogram.* **2012**, *14*, 130–137. [CrossRef]
86. Smirnikhina, S.A.; Lavrov, A.V.; Bochkov, N.P. Dynamics of Elimination of Plasmids and Expression of VEGF121 Gene Transfected into Human Mesenchymal Stem Cells by Different Methods. *Bull. Exp. Biol. Med.* **2011**, *151*, 121–125. [CrossRef] [PubMed]
87. Čegovnik, U.; Novaković, S. Setting Optimal Parameters for in Vitro Electrotransfection of B16F1, SA1, LPB, SCK, L929 and CHO Cells Using Predefined Exponentially Decaying Electric Pulses. *Bioelectrochemistry* **2004**, *62*, 73–82. [CrossRef]
88. Bodwell, J.; Swift, F.; Richardson, J. Long Duration Electroporation for Achieving High Level Expression of Glucocorticoid Receptors in Mammalian Cell Lines. *J. Steroid Biochem. Mol. Biol.* **1999**, *68*, 77–82. [CrossRef]
89. Tsong, T.Y. Electroporation of Cell Membranes. *Biophys. J.* **1991**, *60*, 297–306. [CrossRef]
90. Kotnik, T.; Rems, L.; Tarek, M.; Miklavcic, D. Membrane Electroporation and Electropermeabilization: Mechanisms and Models. *Annu. Rev. Biophys.* **2019**, *48*, 63–91. [CrossRef] [PubMed]
91. Sherba, J.J.; Hogquist, S.; Lin, H.; Shan, J.W.; Shreiber, D.I.; Zahn, J.D. The Effects of Electroporation Buffer Composition on Cell Viability and Electro-Transfection Efficiency. *Sci. Rep.* **2020**, *10*, 3053. [CrossRef]
92. Haberl, S.; Miklavčič, D.; Pavlin, M. Effect of Mg Ions on Efficiency of Gene Electrotransfer and on Cell Electropermeabilization. *Bioelectrochemistry* **2010**, *79*, 265–271. [CrossRef]
93. Potočnik, T.; Miklavčič, D.; Maček Lebar, A. Effect of Electroporation and Recovery Medium PH on Cell Membrane Permeabilization, Cell Survival and Gene Transfer Efficiency in Vitro. *Bioelectrochemistry* **2019**, *130*, 107342. [CrossRef]
94. Arora, M. Cell Culture Media: A Review. *Mater. Methods* **2013**, *3*, 24. [CrossRef]
95. Saulis, G.; Rodaitė-Riševičienė, R.; Dainauskaitė, V.S.; Saulė, R. Electrochemical Processes during High-Voltage Electric Pulses and Their Importance in Food Processing Technology. *Adv. Food Biotechnol.* **2015**, *35*, 575–591. [CrossRef]
96. Kotnik, T.; Miklavčič, D.; Mir, L.M. Cell Membrane Electropermeabilization by Symmetrical Bipolar Rectangular Pulses: Part II. Reduced Electrolytic Contamination. *Bioelectrochemistry* **2001**, *54*, 91–95. [CrossRef]
97. Cohen, R.N.; van der Aa, M.A.E.M.; Macaraeg, N.; Lee, A.P.; Szoka, F.C. Quantification of Plasmid DNA Copies in the Nucleus after Lipoplex and Polyplex Transfection. *J. Control. Release* **2009**, *135*, 166–174. [CrossRef]
98. Tsai, Y.C.; Tsai, T.H.; Chang, C.P.; Chen, S.F.; Lee, Y.M.; Shyue, S.K. Linear Correlation between Average Fluorescence Intensity of Green Fluorescent Protein and the Multiplicity of Infection of Recombinant Adenovirus. *J. Biomed. Sci.* **2015**, *22*, 31. [CrossRef]
99. Chicaybam, L.; Barcelos, C.; Peixoto, B.; Carneiro, M.; Limia, C.G.; Redondo, P.; Lira, C.; Paraguassú-Braga, F.; De Vasconcelos, Z.F.M.; Barros, L.; et al. An Efficient Electroporation Protocol for the Genetic Modification of Mammalian Cells. *Front. Bioeng. Biotechnol.* **2017**, *4*, 99. [CrossRef]
100. Znidar, K.; Bosnjak, M.; Semenova, N.; Pakhomova, O.; Heller, L.; Cemazar, M. Tumor Cell Death after Electrotransfer of Plasmid DNA Is Associated with Cytosolic DNA Sensor Upregulation. *Oncotarget* **2018**, *9*, 18665–18681. [CrossRef]
101. Rosazza, C.; Phez, E.; Escoffre, J.M.; Cézanne, L.; Zumbusch, A.; Rols, M.P. Cholesterol Implications in Plasmid DNA Electrotransfer: Evidence for the Involvement of Endocytotic Pathways. *Int. J. Pharm.* **2012**, *423*, 134–143. [CrossRef]
102. Mao, M.; Wang, L.; Chang, C.C.; Rothenberg, K.E.; Huang, J.; Wang, Y.; Hoffman, B.D.; Liton, P.B.; Yuan, F. Involvement of a Rac1-Dependent Macropinocytosis Pathway in Plasmid DNA Delivery by Electrotransfection. *Mol. Ther.* **2017**, *25*, 803–815. [CrossRef]
103. Chang, C.C.; Wu, M.; Yuan, F. Role of Specific Endocytic Pathways in Electrotransfection of Cells. *Mol. Ther. Methods Clin. Dev.* **2014**, *1*, 14058. [CrossRef]
104. Cervia, L.D.; Chang, C.C.; Wang, L.; Yuan, F. Distinct Effects of Endosomal Escape and Inhibition of Endosomal Trafficking on Gene Delivery via Electrotransfection. *PLoS ONE* **2017**, *12*, e0171699. [CrossRef] [PubMed]
105. Cervia, L.D.; Chang, C.C.; Wang, L.; Mao, M.; Yuan, F. Enhancing Electrotransfection Efficiency through Improvement in Nuclear Entry of Plasmid DNA. *Mol. Ther. Nucleic Acids* **2018**, *11*, 263–271. [CrossRef] [PubMed]
106. Radzevičiūtė, E.; Malyško-Ptašinskė, V.; Novickij, J.; Novickij, V.; Girkontaitė, I. Transfection by Electroporation of Cancer and Primary Cells Using Nanosecond and Microsecond Electric Fields. *Pharmaceutics* **2022**, *14*, 1239. [CrossRef] [PubMed]
107. Robertson, R.M.; Smith, D.E. Self-Diffusion of Entangled Linear and Circular DNA Molecules: Dependence on Length and Concentration. *Macromolecules* **2007**, *40*, 3373–3377. [CrossRef]
108. Robertson, R.M.; Laib, S.; Smith, D.E. Diffusion of Isolated DNA Molecules: Dependence on Length and Topology. *Proc. Natl. Acad. Sci. USA* **2006**, *103*, 7310–7314. [CrossRef] [PubMed]